Functionalization of Cotton Fabric by Metal and Metal Oxides Nanoparticles for Antibacterial and UV-Radiation Protection Applications

Tariku Bayisa Bedasa

A Dissertation Submitted to

Department of Applied Chemistry

School of Applied Natural Science

Presented in Partial Fulfillment of the Requirement for the Degree of

Doctor of Philosophy in Materials Chemistry

Office of Graduate Studies

Adama Science and Technology University

May, 2024

Adama, Ethiopia

Functionalization of Cotton Fabric by Metal and Metal Oxides Nanoparticles for Antibacterial and UV-Radiation Protection Applications

Tariku Bayisa Bedasa

Major Supervisor: Prof. Neeraj Kumar Gupta

Co-Supervisor: Dr. Gemechu Deressa (Assoc. Prof)

A Dissertation Submitted in Partial Fulfillment of the Requirements for the Degree of Doctor of Philosophy in Materials Chemistry

Department of Applied Chemistry

School of Applied Natural Science

Office of Graduate Studies

Adama Science and Technology University

May, 2024

Adama, Ethiopia

Declaration

I declare that this Ph.D. dissertation, "**Functionalization of Cotton Fabric by Metal and Metal Oxides Nanoparticles for Antibacterial and UV-Radiation Protection Applications**," is my original work. That is, it has not been submitted for the award of any academic degree, diploma, or certificate in any other university. All sources of materials used for this thesis have been duly acknowledged through citation.

_____	_____	_____
Name of the student	Signature	Date

ACKNOWLEDGEMENT

This Dissertation appears in its current form due to the assistance and guidance of several people and Institutions. I would therefore like to offer my sincere thanks to all of them.

I sincerely thank my supervisor, advisor, and mentor, Professor Neeraj K. Gupta, for his continuous support in my Ph.D. study and related research, patience, motivation, and critical comments. I thank him for all the opportunities I was given to conduct my research and further my dissertation.

I sincerely thank Gemechu Deressa (Assoc. Prof), my co-supervisor, for his generous support during my research.

I am deeply grateful to Dr. Lemma Teshoma for his contribution to material characterization.

I want to offer my special thanks to Professors Saidur Rahman and Kim Han Tan (Sunway University, Malaysia) for their assistance in the characterization of materials and unwavering support and belief in me.

I want to extend my sincere thanks to Professor Sundaramurthy Anandhakumar (SRM Institute of Science and Technology, India), Professor Ashish Kapoor (Harcourt Butler Technical University, India), and Miss Sakshi Bajhal (SRM Institute of Science and Technology, India) for their support in materials characterization and antibacterial activity and for providing invaluable feedback.

I want to thank the Applied Chemistry Department of Adama Science and Technology University staff who have contributed to the success of my Ph.D. study: Dr. Aschalew Taddese, Dr. Deferu Negera, Mr. Guta, and Mr. Lammi. I also thank Mr. Leta Guta for his assistance with the antibacterial activity work. I want to thank my friend and colleague Zerihun Feyissa (Ph.D), who has made a huge contribution to the success of my Ph.D. I want to acknowledge my close friend, Mr. Hailu Guluma, who has contributed significantly and closely followed my Ph.D. work.

I am grateful and indebted to my wife, Ayisha Muhidin, for the unreserved support and encouragement she offered me throughout my Ph.D. study.

Tariku Bayisa

Adama

Ethiopia.

Table of Contents

List of Tables

List of Figures

List of Acronyms and Abbreviations

AATCC	American Association of Textile Chemists and Colorists
AMR	Antimicrobial resistance
AmCot	Amine-modified cotton fabric
AS/NZS	Australian/New Zealand Standard
ASTM	American Society for Testing and Materials
ATR	Attenuated total reflectance
ATRP	Atom transfer radical polymerization
CFU	Colony forming unit
CDC	Center for Disease Control
DAEC	Diffusely adherent *E. coli*
EAEC	Enteroaggregative *E. coli*
EDTA	Ethyl diamine tetra acetic acid
EDX	Energy dispersive X-ray spectrophotometry
EIEC	Enteroinvasive *E.coli*
EPEC	Enteropathogeni*c E. Coli*
ETEC	*Enterotoxigenic E. coli*
FTIR	Fourier transform infrared spectrophotometry
GLASS	Global Antimicrobial Resistance and Use Surveillance System
GRAS	Generally recognized as safe
HAI	Hospital acquired infections
ICU	Intensive care unit

LMICs	Low and middle-income countries
MDR	Multi-drug resistance
MHB	Mueller Hinton Broth
MRSA	Methicillin-resistant *Staphylococcus aureus*
NP	Nanoparticle
NCPs	Nanocomposites
OECD	Organization for Economic Cooperation and Development
PPE	Personal protective equipment
ROS	Reactive oxygen species
SDS	Sodium dodecyl sulfate
SEM	Scanning electron microscopy
SPS	Surface plasma resonance
STEC	Shiga toxin-producing
TEM	Transmission electron microscopy
TIP	Titanium isopropoxide
UV-DRS	Ultraviolet-visible diffuse reflectance spectrophotometry
UPF	Ultraviolet protection factor
UVR	Ultra-violet radiation
WHO	World Health Organization
XDR	Extremely drug resistant
XRD	X-ray diffraction
XPS	X-ray photoelectron spectroscopy
ZOI	Zone of inhibition

Abstract

This study aimed to produce wash durable antibacterial, and UV-protective cotton fabrics by first modifying cotton fabric (Cot). The cotton fabrics were modified by covalently linking L-methionine (Am), used as the binder, via esterification and then functionalizing the modified cotton fabrics (AmCot) with silver (Ag), copper oxide (CuO), zinc oxide (ZnO), and titanium dioxide (TiO_2) nanoparticles (NPs) and Ag-CuO, Ag-ZnO, Ag-TiO_2 and CuO-TiO_2 bimetallic nanocomposites (NCPs) to take advantage of their possible synergistic antibacterial and UV-protective properties.. Nitrate salts of Ag, Cu, and ZnO and titanium isopropoxide (TIP) were reduced by $NaBH_4$ in situ to form the NPs and NCPs onto the surface of AmCot. Fourier transform infrared (FTIR) and micro-Raman spectroscopy confirmed Am's chemical modification of the cotton fabrics. X-ray diffraction (XRD) revealed the crystallographic structure and the average crystalline size of Ag, CuO, TiO_2, and ZnO NPs in AmCot+Ag, AmCot+CuO, AmCot+TiO_2, and AmCot+ZnO which were 30.10, 18.13, 30.12 and 14.88 nm respectively. The average crystalline size of Ag NPs in AmCot+Ag-CuO, AmCot+Ag-ZnO, and AmCot+Ag-TiO_2 were 30.34, 27.24, and 16.85 nm, respectively. The average crystalline size of CuO, ZnO, and TiO_2 NPs in AmCot+Ag-CuO, AmCot+Ag-ZnO, and AmCot+Ag-TiO_2 were 11.75, 9.16, and 22.50 nm, respectively. The AmCot+CuO-TiO_2 yielded CuO and TiO_2 NPs with average crystalline sizes of 18.09 and 32.05 nm, respectively. X-ray photoelectron spectroscopy (XPS) further supported the ATR-FTIR and XRD results. Scanning electron microscopy (SEM) showed the distribution of the NPs and NCPs on the fibers of functionalized amine-modified cotton, and energy-dispersive X-ray (EDX) mapping of sulfur (S), oxygen (O), and nitrogen (N) supported the esterification reaction between Am and Cot. The mapping further supported the evidence of Ag, CuO, ZnO, and TiO_2 NPs on the respective functionalized AmCot. The ultraviolet protection factor (UPF) examined by UV-vis diffuse reflectance spectroscopy (UV-DRS) was 7.54, 27.76, 58.5, 26.5, and 16.97 for AmCot, AmCot+Ag, AmCot+CuO, AmCot+TiO_2 and AmCot+ZnO, respectively. AmCot+Ag-CuO, AmCot+Ag-ZnO, AmCot+Ag-TiO_2, and AmCot+CuO-TiO_2 had UPF values of 36.21, 48.2, 28.5, and 26.5, respectively. The results showed that the functionalization of AmCot by the NPs and NCPs resulted in good UV protection. The NP and NCP functionalized AMCot antibacterial activity, water absorbability, and vapor permeability were also analyzed. AmCot did not show any antibacterial activity, whereas the NP and the NCP functionalized fabrics showed excellent antibacterial activity against Gram-negativee (E. coli and P. aeruginosa) *and Gram-positive* (*S. aureus and S. pyogenes*) *bacteria species with excellent wash durability of up to 50 wash cycles. The largest zone of inhibition (ZOI) was reported for AmCot+Ag-ZnO and AmCot+Ag-CuO. For AmCot+Ag-ZnO against E. coli and S. aureus, the ZOI was 22.6± 0.6 and 21.7 ± 0.1 before washing and 21.1 ± 0.2 and 18.5 ± 0.2 after 50 washing cycles respectively. The ZOI of AmCot+Ag-CuO against E. coli and S. aureus was 22.1 ± 0.8 and 19.6 ± 0.8 before washing, and 20.3 ± 0.4 and 18.8 ± 0.7 after 50 washing cycles, respectively. Moreover, the change in water absorption and vapor permeability properties after functionalization was within 10%, which is acceptable regarding important properties and comfort.*

Keywords: Cotton fabric, L-methionine esterification, nanoparticles, nanocomposite particles, antibacterial activity, wash durability

CHAPTER 1

Introduction

1.1 Background of the Study

Nosocomial infections are called hospital-acquired infections (HAIs), which in clinical terms are recognized as a disease caused by microbes that affect the patient because of hospitalization or the hospital workforce due to their activity in the hospitals, regardless of signs of the illness emerging while the infected person is in the hospital. HAIs are the foremost health and financial problems worldwide (Perelshtein *et al*., 2015) and one of the significant reasons for mortality in hospitals worldwide (Alagarasan *et al*., 2021). Due to the overall problem of bacterial contagion in general and specifically in hospitals, comprehensive research is being conducted on how to produce antibacterial textiles in the industry (Arendsen *et al*., 2019). The economic impression of such infections overcomes the present health improvements by increasing the average hospital days per patient. HAIs are related to increased impute death, longer hospital days, and health care expenses acquired by patients and health care services (Perelshtein *et al*., 2015). Preventing nosocomial disease transmission is stimulating due to the large size of sick and immune-compromised populations and enormously transitional communities. An infection is conceived as HAI if it appears within 48 hours of a patient's hospitalization or 30 days of discharge. *Escherichia coli (E. coli), Pseudomonas aeruginosa (P. aeruginosa), Staphylococcus aureus (S. aureus), Legionella and Mycobacterium tuberculosis* are the primary pathogenic organisms that cause HAIs (Haque *et al*., 2018). Due to the continuous use of antibiotics over the past two decades, there has been a prevalence of genetically decisive multidrug-resistant (MDR) and highly multidrug-resistant (XDR) bacteria that are a cause of life-threatening infections (Tabah *et al*., 2012).

According to WHO (2020), HAIs are more recurrent in low-income countries than in high-income countries. Accordingly, in terms of trends, it has been shown that the prevalence of health-related infectious diseases varies between 5% and 19% in low- and middle-income countries. In low-income countries, the number of infected patients treated in intensive care units (ICU) increased from 4% to 88%, with overall infections occurring approximately threefold higher than in developed countries (Haque *et al*., 2018). Even in developed countries like Germany and the USA, the frequent infections related to using ICU devices, which are most

widely used for newborns, are prevalent. However, these devices are used at higher percentages in low-income countries because of the frequent infections associated with central lines, ventilators, and other invasive devices (Haque *et al*., 2018). Among hospital-born babies in low-income countries, HAIs are thought to account for four to 50% - 60% of all infant deaths. Furthermore, surgical site infections are the most common infections in the patient population in resource-constrained countries. It affects 67% of surgical patients, and its frequency is about nine times higher than in developed countries (Mengesha *et al*., 2014).

Wound infections are predominantly caused by *S. aureus, E. coli, P. aeruginosa, and Enterococci*. It is an essential issue for healthcare professionals, not only because of the increasing trauma experienced by patients but also because of the pressure on financial resources and the growing demand for cost-effective management in the healthcare system (Mohammed *et al.*, 2017). With the growth of antibiotic resistance in the prevalent resistant strains of microorganisms, there is a significant need to produce a novel pharmacotherapy for severe infection caused by Gram-positive and Gram-negativee bacterial species. Preparing antibacterial agents on a soft substrate is one of the novel pharmacotherapies being investigated for reducing both Gram-negativee and Gram-positive bacterial species. In recent years, many significant research efforts have been made to produce antibacterial agents on various materials such as textiles and medical devices (Morris & Murray, 2020).

In the textile industry, a new revolution in technologies that may add particular functions and features to fabrics has created opportunities for the textile sector to be widely employed in the healthcare sector (Raut *et al*., 2010). Textiles comprising natural and synthetic fibers and their blends are commonly used materials in healthcare sectors, and cotton fabric-based textiles must not transfer microbes to people admitted to hospitals for medical care and hospital workers (Kurtz *et al*., 2008). However, the growth of pathogens on non-functionalized cotton fabric textiles, specifically those made from natural fibers, can be viewed in terms of a sizeable sensor surface part and the facility for adequate growth conditions, namely temperature, oxygen, humidity, and nutrients (Fijan and Turk, 2012). The growing of microbes has an adverse burden on cotton fabric and the carrier since it causes the biological degradation of textile materials, and their spread is hazardous to people's health (Fijan and Turk, 2012). Unless functionalized with antibacterial chemicals, all textiles have the potential to grow bacteria and serve as a source

of infection. In pathogen transmission, such textile materials play a critical part in the concatenation of infection caused by pathogenic microorganisms such as bacteria, fungi, and viruses and are significantly involved in providing a conducive environment for the propagation of infection outbreaks. (Sasahara *et al*., 2011; Fijan and Turk, 2012).

Curative textiles are an expanding and growing field in the textile industry. They represent engineered and finished structures for medical purposes. The usage of medical fabrics in the workplace has advanced for various reasons, ranging from a specific yarn suture to multidimensional fused structures for varied uses. The global price of the medical textile market, valued at USD 12.2 billion in 2018, will reach USD 18.5 billion by 2025 (Akter *et al*., 2014).

Nanotechnology is an effective method for developing functional materials that can turn textiles into high-performance and value-added goods. Metal and metal oxide NP-based functional textiles have recently gained popularity. Incorporating metal and metal oxide NPs in textiles provides multifunctional properties, including UV-protection, self-cleaning, electrical conductivity, antimicrobial, antistatic, anti-wrinkle, and flame-retardant properties, without compromising the textile's inherent characteristics. Nanotechnology introduced "Nano finishing," a new area of textile finishing in which nano-sized materials of suitable size exhibit unique properties without affecting the natural characteristics of fabric. The first nanotechnology in textiles was called Nano-tex and was founded by a company in Burlington, USA (Abou *et al*., 2022). The factors that make the development of bacterial resistance difficult and cause the spectrum of antibacterial activity to expand are that metal-based NPs possess a non-specific mechanism of bacterial toxicity. Due to their well-known antibacterial activities toward Gram-positive and Gram-negativee harmful bacteria, NPs are proposed as the best alternatives over traditional antibiotics to overcome bacterial resistance (Sportelli *et al*., 2020). Nanomaterials-finished textiles are becoming increasingly popular and are being considered as medical textiles. Nano finishing, nanocoating, nanofiber, and nanocomposites are the essential nanotechnology-fabricated textile materials used to functionalize the cotton fabric with nanomaterials (NMs). The nano-finishing process employs colloid mixtures or ultrafine dispersions of NMs to the fabrics to enhance specific functionalities. This process results in more durability owing to the high surface area-to-volume ratio and homogenous distribution of

particles onto the fabric. In a nanocoating, a thin layer with a thickness of about 100 nm is applied to a surface to advance specific properties or introduce new properties such as color fastness, flame retardancy, water/oil impermeability, wrinkle resistance, and antimicrobial properties (Khatami *et al*., 2018). Nanofiber is a fiber with a nanometer range in diameter and properties of high surface area to volume ratio, large porosity, and minor pore size. Due to these properties, nanofiber is used in several applications. Nanocomposite fibers are another type of nanotechnology-produced textile materials that can be formed by distributing nano-sized materials (fillers, metal oxide, metal, carbon nanotube) in a fiber matrix for various applications such as antibacterial activity, UV-radiation protection, electrical conductivity, excellent strength, ductility, and lightweight properties (Sivaranjana *et al.*,2021).

Silver nanoparticles (Ag NPs) are characterized by their excellent antimicrobial activities. However, weak fixation onto cotton fabric surfaces often results in undesired silver loss from antibacterial fabric surfaces, decreasing antibacterial durability and further leading to environmental and health pollution (Zhou *et al*., 2018).

Copper oxide nanoparticles (CuO NPs) are an II-VI group element. It has appropriate semiconducting properties directly associated with its band gap, which is ~ 1.74 eV at standard conditions, and CuO is categorized under p-type conductivity. Because of their harmlessness and biocompatibility with mammalian cells, CuO NPs are suitable modifiers for fibers (El-nahhal *et al*., 2022). CuO NPs exhibit excellent properties in inhibiting bacterial growth, and their availability makes them a more appropriate choice material for functionalizing the surface of substrates.

Zinc oxide nanoparticles (ZnO NPs) are an N-type semiconductor with a band gap of (3.37 eV) and high exciton binding energy (60 meV) at room temperature. ZnO NPs are widely used for their antibacterial and UV-blocking properties because they are an N-type semiconductor with a band gap of approximately 3.37 eV, high excitation binding energy of approximately 60 meV, and the ability to form very reactive species that kill microbes (Salat *et al*., 2018).

Titanium dioxide nanoparticles (TiO_2 NPs) are N-type semiconductors with two prominent phase structures, rutile and anatase. Under UV radiation, TiO_2 in water and air can produce electrons (e^-) and holes (h^+) and produce highly chemically active free radicals such as (HO) and (O_2), which are accountable for killing microorganisms (Verma *et al*., 2022).

Metal and metal oxide NPs, on the other hand, lack affinity with cotton fibers because both the fibers and NPs have negatively charged surfaces because of the existence of $^{-}$OH groups. Therefore, the effective immobilization of metal and metal oxide NPs onto the fabric surface is essential. Several strategies have been established over the previous decade to replace the conventional clothes used in the health sector with medical clothes functionalized with NMs in the same manner; improving the adherence of metal and metal oxide NPs to fiber surfaces was part of such sort of research efforts (Granados *et al.*, 2021; Zhang *et al*., 2016). Different reagents were investigated to improve the leachability of the NPs bound on the surface of the fabric. However, a polymer binder has been extensively researched. For example, carboxymethyl chitosan (Xu *et al*., 2017), L-cysteine (Xu *et al*., 2019), and starch (El-Nahhal *et al*., 2020) were found to be highly effective at binding metal and metal oxide NPs to cotton fabric. They are renewable resources that have been extensively researched due to their biocompatibility and biodegradability. Fixation of NPs onto cotton fabric is crucial because it improves the wash durability of the textile, thereby enhancing the performance of NP-finished textiles against the laundry regime. Searching for the most effective and biocompatible polymeric binder's gets attention since they coalesce different functional groups within a single polymer chain to achieve dual activities simultaneously, binding to the cotton fabric and immobilizing the NPs. Therefore, such types of binders should be investigated for immobilizing NPs, providing durable antibacterial and UV-radiation protection properties in fabrics, improving the economics of the process, and mitigating any suspected environmental pollution resulting from undesired discharge of NPs into the environment.

In this study, potential binder L-methionine, an essential amino acid for the human body, was used for surface modification and further immobilization of NPs and NCPs onto the surface of the cotton fabric. Since L-methionine comprises a carboxylic group that can modify the surface of cotton by esterification reaction with the hydroxyl groups of cotton. Further, the three electron donor atoms in the structure can form coordination bonds with metal NPs. Thus, this research focused on modifying the cotton surface with L-methionine and immobilizing metal and metal oxide NPs to improve performance, particularly antibacterial wash durability and UV–radiation protection properties.

1.2 Statement of the Problem

Deaths from infections due to drug resistance are currently predicted to be ten million annually, and the cost estimates are as high as US$100 trillion worldwide by 2050 (O'Neill, 2016). Even though many initiatives have been taken in the last few years, the world has failed to mitigate the increasing antimicrobial resistance (AMR) to currently available antibiotics due to the misuse and overuse of existing antimicrobials. AMR is becoming an inevitable phenomenon that is undermining the efficacy of essential primary and modern drugs and is affecting people from birth to death. AMR is a silent pandemic here to stay (Rochford *et al*., 2018).

In some countries such as Australia, Belgium, Czech Republic, Denmark, Estonia, and Finland, particularly members of the Organization for Economic Cooperation and Development (OECD), approximately 35% of human infections are already resistant to antibiotics available on the market (da Silva *et al*., 2020). This problem is paramount in low- and middle-income countries (LMICs), where resistance rates increased to 80 - 90% for some antibiotic bacteria (da Silva *et al*., 2020). In low-income countries like Ethiopia, HAIs are critical health problems and cause many people to die. These are severe problems in health centres like hospitals, especially in surgical rooms, where contamination with extremely infectious microbes most likely occurs. It is also a common practice that antibiotics can be acquired without a prescription by physicians, which leads to the appropriation of antibiotics by the people, thus causing the appearance and spread of antibacterial resistance (Mohammed *et al*., 2017). The frequency of bacterial load and their resistance to conventional antibiotic therapy were assessed by numerous researchers at healthcare facilities located in Addis -Ababa (Tikur Ambessa and Yekatit 12 specialized hospitals) (Kalayu *et al*., 2019; Gutema *et al*., 2018), Jimma (Jimma University medical center) (Ali *et al*., 2018), Harar (Hiwot Fana specialized hospital) (Tolera, M., *et al*., 2018) and Mekelle (Ayder Teaching and Referral hospital) (Mengesha, *et al*., 2014). All studies showed that hospital-acquired infections in all hospitals were alerting, and the investigation warned that antibiotic resistance should be a substantial concern for Ethiopia.

Future hospitals will replace traditional fabric-based textiles such as bed sheets, doctor aprons, pajamas, curtains, and pillow covers with antimicrobial textiles. To effectively incorporate all these applications, the antimicrobial properties of the functionalized cotton fabric-based textiles should be durable enough to resist regime washing cycles. The washing carried out in hospitals

is expected to be aggressive and conducted at high temperatures to maintain acceptable levels of hygiene. UV light is a known human carcinogen that causes basal cell carcinoma (BCC) and squamous cell carcinoma (SCC). These malignancies frequently occur on sun-exposed parts of the skin. Fortunately, when detected and treated early, many common skin tumors are typically curable. Regarding these problems, several efforts have been made to develop approaches for integrating antimicrobial and UV-Protective agents in the manufacture of fabrics that could efficiently prevent the growth and spread of bacterial infections. Therefore, innovative approaches should be investigated in creating novel technologies for embedding antibacterial and UV protection chemicals in fabrics, demonstrating high antibacterial and UV protection efficiency, durability, and low release into the environment. This study focused on nanoengineered metal and metal oxide NPs, a technology platform for improving existing cotton fabric performance, particularly broad-spectrum antibacterial activity and UV-radiation protection properties.

1.3 Objectives of the Study

1.3.1 General Objective

The general objective of this study is to functionalize cotton fabric with metal and metal oxide NPs for antibacterial activity and UV-radiation protection applications.

1.3.2 Specific Objectives

- ✓ to modify the surface of the cotton fabrics with L-methionine as a binder
- ✓ to perform *in-situ* functionalization of cotton fabric with single component metal and metal oxide of Ag, CuO, TiO_2, and ZnO NPs
- ✓ to carry out an *in-situ* functionalization of cotton fabric with binary NPs of Ag-CuO, Ag-ZnO, Ag-TiO_2, and CuO-TiO_2- (NCPs)
- ✓ to characterize the pristine, modified, and functionalized cotton fabric for their chemical composition, morphology, phase structure, and physical properties such as water absorption and water vapor permeability
- ✓ to determine the Ultra-Violet Protection Factor (UPF) value of amine-modified cotton fabric and amine-modified cotton fabric functionalized with NPs and NCPs

- ✓ to evaluate (qualitative and semi-quantitative) bactericidal activity of the functionalized cotton fabric against Gram-negativee bacteria *(E. coli* and *P. aeruginosa)* and Gram-positive bacteria (*S. aureus and S. pyogenes)*
- ✓ to evaluate the wash cycle durability of functionalized cotton fabric vis-a-vis the retention of the NPs vis-a-vis bactericidal efficacy

1.4 Significance of the Study

In Ethiopia, raw cotton is produced, and the country also participates in its exports. According to the Central Statistical Agency of Ethiopia, the country's annual production of raw cotton is approximately 120,000 tons, and small-scale farmers produce a large amount of the cotton. The average production of cotton fabric in Ethiopia from 2000-2018 is 33842.11 metric tons, according to the report by (Zeleke *et al*., 2019)According to information from the Global Agricultural Information Network (USDA, 2019), production increased to 57000 metric tons during 2019/2020 due to thriving textile industrial parks in different parts of the country.

This study aimed to produce cotton fabrics functionalized with metal and metal oxide NPs having antibacterial durability and UV-radiation protection properties. The L-methionine-modified cotton fabric was functionalized with single and bimetallic NPs and NCPs. Efforts were made to improve the antibacterial wash durability of the functionalized fabrics by immobilizing the NPs by binding them to the cotton surface and further improving the efficiency through the synergistic properties of the NCPs. The study's outcome is that functionalized fabrics show excellent antibacterial activity after 50 washing cycles and have potential UV-radiation protection properties. Therefore, if Ag, CuO, ZnO, and TiO_2 NPs alone or in combination were optimally deposited from their respective commercially available precursors and immobilized onto the cotton fabrics, such fabrics could be viable opportunities to reduce the complex problems associated with HAIs in domestic and medical care settings along with UV-radiation protection. Ethiopia's industrial parks that process textiles and textile-related materials provide the best opportunity for developing smart textiles in response to health sector demand based on this research's output. In addition to the health sector, functionalized cotton fabric with tuneable qualities has significant value in manufacturing military clothes. Thus, the relevant government departments should apply such research outputs to expand their technology in making smart military apparel. This research thus contributed significantly to knowledge and

information on the preparation and characterization of fabrics for wash-durable antibacterial and UV-radiation protection. Such progress is within the general approach to reducing the occurrence of HAIs in clinical settings using practical antimicrobial hospital textiles.

CHAPTER 2

Literature Review

2.1 Textiles

Textile is an umbrella word that includes fiber-based materials such as fibers, yarns, filaments, threads, and different fabrics. Textiles have been used extensively to make clothing for thousands of years. However, natural textiles, particularly those made from cellulose and protein fibers, are very vulnerable to the growth and transmission of pathogenic microorganisms (Butola, 2018). The natural properties of textiles, such as porosity and moisture affinity, could be favorable for microbes to induce foul odors, skin allergies, cross-infections in hospitals, and even textile degradation and deterioration (Markovi *et al.*, 2020). Textiles offer advantages such as biodegradability, softness, affinity to skin, and sweat absorption. Due to these advantages, materials have been commonly used in medical and healthcare applications (Shaheen *et al.*, 2018). Medical textiles are among the fastest growing areas of the technical textiles sector of the textile industry, aimed to manufacture products such as personal protective equipment (PPE), bandages, and dressings for various applications such as wound healing, compression and bandage garments and implant fabrics (Morris & Murray, 2020). Fabrication of antimicrobial textiles is among the hotspot areas in the textile industry. Several chemicals were applied to impart antimicrobial properties to textiles, including cation-forming agents such as quaternary ammonium salts, triclosan, inorganic metals, and metal oxides (Ag, ZnO, Cu, CuO, etc), halogen-based oxidizing agents, aldehydes, and peroxy compounds, derivatives of amine and antimicrobial dyes to naturally consequent antimicrobials (Zhang *et al*., 2016).

2.2 Cotton Fabric and its Inherent Properties

Because of its softness, breathability, safety, affordability, performance during renewal, and ease of mass production, cotton is the most popular natural textile fabric (Wu *et al*., 2019). The principal constituent of cotton fabric is cellulose, a polysaccharide with a linear chain of β - (1-4)-bonded D-glucose units. The hydroxyl group (OH) on each glucose unit is divided into three kinds: the primary hydroxyl groups on C-6 and secondary hydroxyl groups on C-2 and C-3. The hydroxyl groups cause broad hydrogen bonds between the glucose units of cellulose, responsible for chemical reactivity with a wide range of chemicals (Zhang *et al*., 2016). Different forms of chemical reactions, such as esterification, reduction, and oxidation with the

hydroxyl groups, have been employed to impart new functionalities like water repellence, antimicrobial activity, flame retardancy, and UV protection onto cotton fabrics. Figure 1 shows the raw cotton fabric and the chemical structure of the cotton fabric.

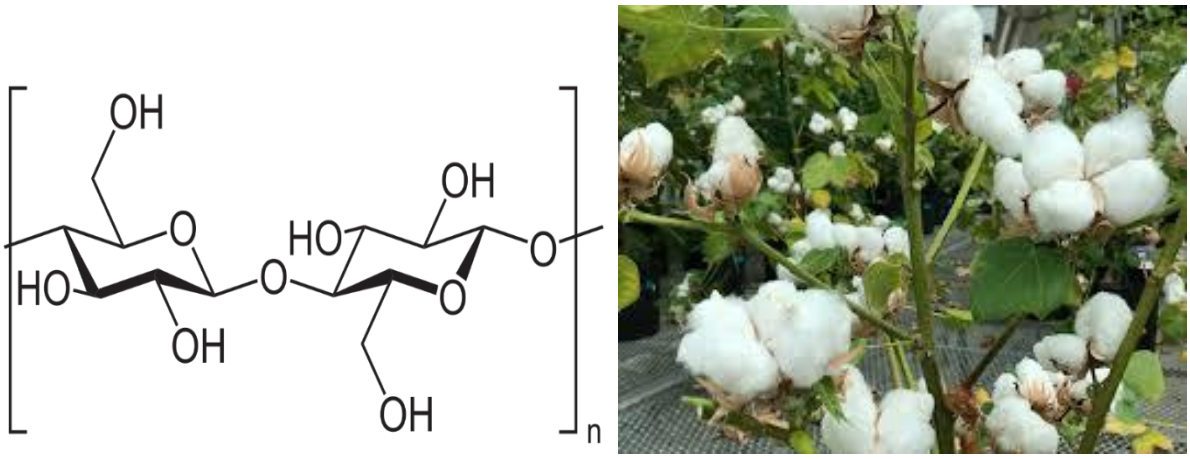

Figure 1. Chemical structure of cotton fabric (https://thecounter.org/fda-approves-genetically-modified-cotton-human-consumption/).

The cellulose component of raw cotton fiber ranges from 89 to 95%. Figure 1 shows that cellulose is a ß-D-glucose polymer with a specific arrangement. A repeating unit of cellulose known as cellobiose comprises two beta-glucose molecules connected at their C-1 and C-4. This results in a nearly flat linear polymer chain appropriate for fiber production (Wu *et al*., 2018).

Cotton fabric-based textiles have many benefits, including being biodegradable, hydrophilic, biocompatible, soft, attractive to the skin, and sweat assimilation. Because of these benefits, cotton products have been widely employed in various applications, including the medical and healthcare fields (Shaheen *et al.*, 2018).

Textile fabrics improved with chemical finishes via various finishing techniques exhibit several functionalities, such as antimicrobial activity, UV protection, and self-cleaning behavior (Zahid *et al*., 2018; Sivaranjana *et al*., 2021; Shao *et al*., 2017). However, cotton fabric-based textiles are the vital medium for the growth of microbes such as bacteria and fungi because the temperature, moisture, and nutrients on the fabric surface encounter the necessities for their growth and reproduction (Hassabo *et al*., 2019). In a medical setting, microbial infections dwelling on the fiber surface can cause unpleasant odors, color degradation, allergic reactions, and fiber breakdown, resulting in diseases. Consequently, the creation of antimicrobial fabrics has caught the interest of many academics, and the market for such textiles is expanding quickly

(Zhang *et al.*, 2016). Hence, the antibacterial finishing of textile materials becomes critical to meet the extraordinary demands and pressing needs for functionalized textile goods that can provide better and long-lasting protection for both the textile user and the substrate itself.

2.3 Hospital Acquired Infections (HAIs)

Hospital-acquired infections (HAIs), also known as nosocomial infections, are the most common adverse occurrence during hospitalization and are the cause of prolonged hospitalizations, increased medical expenses, and significant mortality and morbidity (Labi *et al.*, 2018; Perelshtein *et al.*, 2015). Bacterial infections attributed to nosocomial Gram-positive and Gram-negativee bacterial species significantly threaten patients' health in healthcare facilities, including hospitals, and result in potent mortality. Based on environmental conditions like temperature and humidity and high and low cell count, many bacterial strains persist on cotton for different periods, for example, *E. coli* (45 days), *Enterococcus spp*. (90 days), *P. aeruginosa* (up to eight weeks), *S. aureus* (eight weeks), *K. pneumoniae* (up to eight weeks), and *S. pyogenes* (near to 46 days) (Kampf, 2020). Other species with a high starting cell count, on the other hand, can only live for brief periods at room temperature, for example, *N. gonorrhoeae* and *S. marcescens* (~ three days), and *B. fragilis*, *B. cepacia* and *C. diphtheriae* (all ~ 2 days). A low inoculum of approximately 100 colony-forming units was found for numerous species with distinct survival periods of 2 hours (*Acinetobacter spp.*) or less than 1 hour (*E. coli*, *P. mirabilis*, *P. aeruginosa*, and S. *marcescens*). Higher air humidity was related to the more prolonged existence of *E. coli*, whereas the survival period of *S. aureus* and *S. pyogenes* was improved in less air humidity conditions (Kampf, 2020). Bacteria are present in all chronic wounds; however, this does not necessarily imply that the wound is infected or that bacteria have slowed wound healing. Wound healing is hampered when the number of bacteria reaches critical colonization and progresses to infection. For healing to occur, wounds must have a regular and sufficient influx of oxygen, nutrients, enzymes, and cells. Non-viable tissue blocks the movement of cells required to form granulation tissue, emphasizing the significance of wound debridement as a primary intervention. Edema or exudates also inhibit cell migration and leukocyte bactericidal activity (Sood *et al.*, 2014).

Open wounds are caused by the breakdown of skin and subcutaneous layer integrity, which results in noticeable surface bleeding. Germs can swiftly travel to deeper layers of the skin,

enter the lymph nodes, and disperse throughout the body. As a result, all scars should be cleaned and properly covered, and the coating should be repaired. Proper wound coating helps limit bleeding, reduces blood absorption and secretion contamination, and speeds wound healing (Khatami *et al*., 2018).

Various Gram-positive and Gram-negativee bacteria involve the progress of contamination and colonization by entering and populating the wound over time (Daeschlein, 2013). Bacterial bioburden refers to the metabolic demands the bacteria make on the tissue, including toxic by-products, competition for nearby nutrients and oxygen, and harmful effects of the host inflammatory response. Microbials in chronic wounds are known to develop biofilms impenetrable to most systematic and topical antimicrobials (Daeschlein, 2013).

The findings of Gutema *et al.* (2018) have revealed that a large variety of infections were treated in large hospitals in Ethiopia. Many surgical infections were discovered and treated in the hospitals despite comprehensive prophylaxis (antibiotics) prescribing. According to the study, the top 5 most common include pneumonia (26.6%), surgical site infections (21.5%), neutropenic fever (6.9%), sepsis (6.4%), and urinary tract infections (4.7%). Many reasons contribute to HAIs, including reduced patient immunity, multistep patient treatment, which leads to higher infections, the emergence of drug-resistant bacteria, and a lack of adherence to bacterial infection guidelines. Figure 2 indicates the different factors that cause HAIs. Tamire *et al.* (2021) have reported that methicillin-resistant *S. aureus* (MRSA) is the significant cause of HAI among patients admitted to Tikur-Ambessa specialized hospital. According to the study conducted in Dessie Referral Hospital, *E. coli* is reported as the primary cause of hospital-acquired urinary tract infections (Adugna *et al.*, 2021). HAIs can result from a variety of sources. Figure 2 depicts multiple causes of HAIs.

Figure 2. Different causes responsible for HAIs (Deshmukh *et al.*, 2019).

Personal hygiene, such as cleaning hands, gloves for hands, face masks, and working attire, has minimized the spread of pathogens from patient to caregiver. HAIs are spread from patient to community through different mechanisms such as individual patients, food, contaminated surfaces, hospital staff, air, and water.

Preventing infections in hospitals necessitates a multifaceted surveillance approach that considers numerous factors. Personal hygiene, such as hand washing, hand gloves, masks, working clothing, shoes, and disinfection of hospital equipment, has reduced the transmission of pathogens from patient to caregiver (Deshmukh *et al*., 2019). Furthermore, rising bacterial resistance significantly influences the health sector and exacerbates economic concerns. A wide range of policies have been implemented in the fight against HAIs, such as an infection control practitioner (Alamer *et al*., 2022), which is typically often assigned to undertake ongoing infection surveillance for specific wards, compute infection rates, and report these data to key personnel, provide staff education and training, respond to and implement outbreak control measures, and counsel on employee health issues. Hand hygiene, environmental cleanliness, leadership, and effective use of people protection equipment duties are the fundamental policies set by the Centers for Disease Control (CDC) to combat HAIs (Hughes, 2008). "Antimicrobial resistance threatens contemporary medicine and endangers millions of lives," said Dr. Tedros

Adhanom Ghebreyesus, WHO Director-General. Approximately 4.95 million deaths due to antimicrobial resistance were reported in 2019 (Irfan *et al*., 2022). GLASS (Global Antimicrobial Resistance and Use Surveillance System) 2022 report revealed that the global median AMR status of the two AMR sustainable development goal indicators, *E. coli* and MRSA, were 42% and 35%, respectively. In 2019, the six major pathogens causing resistance-related deaths (*E. coli, S. aureus, K. pneumoniae, Streptococcus pneumoniae (S. pneumoniae, Acinetobacter baumannii (A. pneumoniae), and P. aeruginosa were the* cause of 930,000 resistance-related deaths and ~3·5 million deaths caused by AMR (Irfan *et al*., 2022).

2.3.1 *Escherichia Coli (E. Coli)*

In microbiology, *E. coli* is the most widely investigated Gram-negativee bacteria species, roughly 1.1 - 1.48 µm long, and is typically found in the intestines of humans and animals. This species has primarily caused intestinal and extra-intestinal infections in humans and animals. The bacteria are a leading cause of bloodstream infections. Six major groups of intestinal pathogenic are identified *E. coli* (IPEC): enteropathogenic *E. coli* (EPEC), Shiga toxin-producing *E. coli* (STEC), enteroaggregative *E. coli* (EAEC), enterotoxigenic *E. coli* (ETEC), enteroinvasive *E. coli* (EIEC), and diffusely adherent *E. coli* (DAEC). *E. coli* strains are resistant to several drugs, causing HAIs through direct transmission, environmental pollution, or contamination of food and water sources (Toval *et al*., 2014).

2.3.2 *Pseudomonas aeruginosa (P. aeruginosa)*

P. aeruginosa is an aerobic, Gram-negativee, rod-like in shape, non-spore-forming bacterium that is actively mobile by the polar flagella and ranges in size from 1.5 to 3 µm in length x 0.5 µm in diameter. It is an entirely opportunistic nosocomial pathogen. Infections of *P. aeruginosa* typically affect hospitalized patients with weakened immune systems. For those with chronic lung diseases, this is very risky. It can colonize patients' intestinal tracts up to 50% of the time when critically ill, with about 30% being antibiotic-resistant strains (Zaborina *et al*., 2008). Despite the emergence of newer and the most potent antibiotics, infections caused by P. aeruginosa are still a principal responsible for mortality among critically ill and immuno-compromised infected people. Multidrug-resistant (MDR) species of the bacteria, described as resistant to the most common antibiotics such as ceftazidime, imipenem, gentamicin, or

ciprofloxacin, are regularly segregated from intensive care unit patients for a prolonged period (Tassios *et al*., 1997).

2.3.3 *Staphylococcus Aureus (S. Aureus)*

Staphylococcus is a Gram-positive bacterial species with diameters of 0.5 - 1.5 µm. They are distinguished by individual cocci, which divide into multiple planes to form irregular clusters of cocci that resemble grapes. *Staphylococci* are widespread, mostly found on the skin, skin glands, and mucous membranes of mammals and birds, but can cause infections under certain situations. *S. aureus* is the most pathogenic of ordinary members of the other genus, as it is known to cause many nosocomial infections. Resistant *S. aureus* (MRSA) has been reported to live on hospital substrates for up to 5 months. Methicillin-resistant isolates (β-lactam and other antibiotics) provide particularly significant problems for treatment and eradication control since they are a prevalent source of hospital and community-acquired illnesses (Leyland *et al*., 2016). The capacity of *S. aureus* to stick onto the extracellular matrix and the plasma proteins deposited on biomaterials has a dynamic impact on the pathogenesis of orthopedic-associated infections. Multiple adhesion proteins are present on the surface of *S. aureus*, but it is unknown how these proteins work together to form enduring bonds with the substrate. *S. aureus's* cell wall comprises multiple layers, but over half comprises a thick, solid peptidoglycan layer. A cytoplasmic membrane with a thin lipid layer surrounds the cytoplasm and is another cell wall component. In addition, 40% of the cell wall composition consists of two types of teichoic acid located in the cell wall and lipoteichoic acid of the cytoplasmic membrane embedded in the lipids class. Teichoic acids are responsible for transporting the substance. Most strains of *S. aureus* result in ailment in patients by forming an envelope composed of polysaccharides. Capsules protect microbes from parasitic cells and result in bacteremia in vivo. In addition, capsule plays a crucial role in forming bacterial biofilms, which are resistant to antibiotics (Rasheed *et al*., 2021)

2.3.4 *Streptococcus. Pyogenes (S. Pyogenes)*

Streptococcus strains are Gram-positive bacteria with a nutrient-demanding fermentative metabolism. They are generally visible as chains or pairs and oval to spherical. Several of these kinds form clusters. *S. pyogenes* (Group A *Streptococci*, GAS) is a Gram-positive bacterium that causes more than 517,000 fatalities annually and is one of the world's top 10 infectious

disease killers. Invasive infections that can be fatal and moderate pharyngitis are among the symptoms that GAS can induce (Walker *et al*., 2014). *S. pyogenes*, a multidrug-resistant (MDR) bacterium, has been linked to several illnesses and has been found to manufacture special enzymes that disrupt drugs more frequently than most other bacterial strains.

S. pyogenes results in various systemic and cutaneous infections, the most common source of acute pharyngitis. It is also a common pathogen of community infections, such as skin infections and pharyngitis. The pathogen is also an important causative agent of nosocomial infections, sometimes leading to fatal bacteremia. HAI because of *S. pyogenes* is more common in patients who have undergone surgical procedures or obstetric patients (Takahashi *et al*., 1998).

2.4 Nanotechnology in Textile Finishing

Nanotechnology is an innovative technology at the nanoscale that makes materials of at least one dimension smaller than 100 nanometers (nm). Nanoscale structures are mainly classified as NPs, such as metallic NPs, metal oxide NPs, nanowires, nanotubes like carbon nanotubes, nanolayers, and nanopores, such as aerogels. Manufacturing of nanomaterials (NMs) mainly depends on two basic approaches: the bottom-up method and the top-down method.

In the "bottom-up" approach, nanostructures are assembled from smaller starting materials such as atoms, molecules, or clusters. In the "top-down" methods, different nanoscale materials are formed from different bulk materials.

When materials are scaled down to the nanoscale, they exhibit different tunable properties than at the macroscale, opening new uses across various industries. The fundamental assumption is that as a substance's size is decreased to the nanoscale range, its mechanical, optical, and electrical properties might drastically change (Sahoo *et al*., 2007). Nanotechnology is an interesting emerging technology in the textile industry that can be used to produce various types of functionalized textiles. New finishes and new application approaches in materials present the influence of nanotechnology in textile finishing. Smooth, controllable, and highly functional chemical finishes have been made on the surface of textiles (Hassan *et al*., 2019). Nanotechnology is one of the prominent areas for research studies in developing super functional materials like fabrics with self-cleaning (Li *et al*., 2017), UV-protection (Porrawatkul *et al*., 2022), antimicrobial (Rodrigues *et al*., 2019; Wang X. *et al*., 2017) antistatic, soil and

stain repellent, water repellent, and fire retardant (An W *et al*., 2020). Textile is an excellent substrate for integrating NMs, electronics, and optical devices. Integrated materials and technologies provide a platform for responding to various stimuli, including mechanical, chemical, electrical, thermal, optical, and magnetic. Wearable gadgets may have sensors, data transmission, and computing components (Shaheen *et al*., 2021). Nanotechnology has also demonstrated enormous potential for improving the performance of current textiles in producing stains and wrinkle resistance, moisture retention, and release features (Jagadeeshan & Parsanathan, 2019). Figure 3 shows different functionalized textiles through the application of nanotechnology in the textile industry.

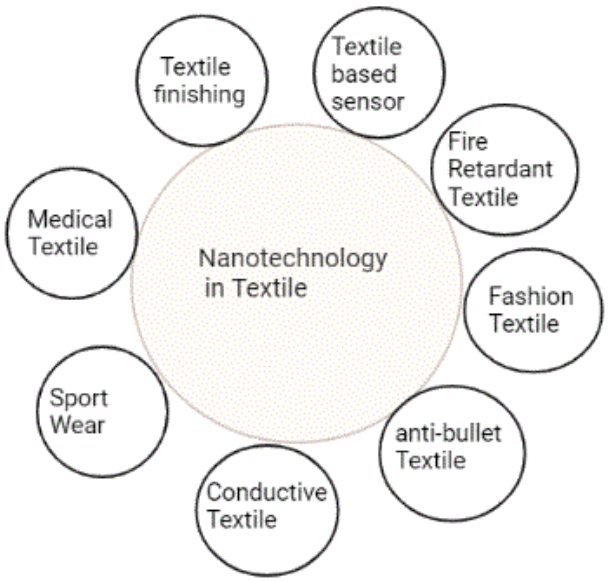

Figure 3. Nanotechnology used in different sectors of the textile industry.

Engineered materials should integrate effortlessly into fabrics, provide flexibility and comfort, and not cause allergic reactions. Because the deposited NPs on the surface of the textile have a significant surface area-to-volume ratio and a high surface energy, nanotechnology can provide materials with excellent durability, giving the textile greater affinity without compromising its feel or permeability. The two main concentrated nanotech research activities in the textile sector are improving textile materials' current functionality and performance and creating smart textiles with entirely new characteristics and functions (Raut *et al*., 2016).

2.5 Metal and Metal Oxide NPs

Metallic NPs are known as nano-sized metals with oxides ranging from 1-100 nm at least in one dimension (Jeevanandam *et al*., 2018). Due to their ultra-size and large surface area, they are characterized by outstanding chemical, optical, and electrical properties. Metal and metal oxide NPs have a wide range of applications, particularly in biomedical, energy, sensing, and photocatalytic applications. The size, structure, form, and distribution of the metal and metal oxide NPs affect their chemical and physical characteristics. Therefore, controlling the size and distribution of size is critical and always achieved by varying the synthesis methods and parameters such as reducing agents, reaction time, reaction temperature during synthesis, and stabilizers (Jagadeeshan and Parsanathan, 2019). Metal-oxide (MOx) NPs are among the most used NMs. MOx NPs display exceptional physical and chemical properties because of their nanoscale size and a high density of atoms or edge surface sites. MOx NPs are an attractive class and diverse form of NMs, widely used in various chemical, physical, and materials sciences applications.

Because of their size, crystal structure, and shape, metal and metal oxide NPs such as ZnO, TiO_2, CuO/Cu_2O, and Ag NPs are known for their inherent qualities. Their chemical, mechanical, electrical, structural, morphological, and optical properties can be changed as the size is reduced to the nanoscale. Such changes in the properties of NPs enable them to interact with cell biomolecules distinctively and make it easier for NPs to physically enter interior cellular structures (Rasmussen *et al*., 2010). Ag, a non-essential metal, is poisonous to bacteria with biocidal actions at deficient concentrations. In contrast, necessary metals like Cu and Zn, relevant to organisms' biochemistry, can also be fatal at a certain threshold (Paszkiewicz *et al*., 2016).

Recently, metal-based NPs have been widely explored for biomedical applications. Metal-based NPs are effective against pathogens identified as a priority for creating HAIs in addition to their broad surface area and selectivity for bacteria (Sánchez-López *et al.*, 2020). The most prevalent NPs made from inorganic substances are metal-based NPs, which offer a potential answer to the problem of antibiotic resistance. They display effectiveness against bacteria that have already gained resistance and use modes of action entirely different from those reported for

conventional antibiotics. However, they also target numerous biomolecules that hinder the development of resistant strains (Slavin *et al*., 2017).

Metallic NPs have dynamic properties when appropriate functional groups are fixed on their surfaces, allowing them to bind with ligands, polymers, antibodies, and drugs. A unique set of characteristics of metallic nanoparticles is their surface Plasmon resonance and optical properties (Venkatesh *et al*., 2019). NPs made of metal are frequently employed in engineering and the biomedical sciences. For medical and pharmaceutical applications (such as antibacterial, antifungal, antiviral, anti-amoebic, anti-cancer, anti-angiogenic, and anti-inflammatory medicines), Ag NPs, CuO NPs, TiO_2 NPs, and ZnO NPs' key characteristics are frequently exploited. These particles have been suggested as alternatives to conventional antibiotics to combat bacterial resistance because of their well-described antibacterial action against Gram-positive and Gram-negativee bacteria (Sánchez-López *et al*., 2020).

2.6 Durable Antibacterial Cotton Fabrics Coated with Metal and Metal Oxide NPs

2.6.1 Durable Antibacterial Cotton Fabric Coated with CuO NPs

CuO NPs are efficient toward a variety of Gram-positive and Gram-negativee bacteria, including S. *aureus*, *Bacillus subtilis* (*B. subtilis*), *E. coli*, *Micrococcus luteus* (*M. luteus*), and *K. pneumoniae,* as well as fungi, including *Aspergillus flavus*, *A. niger*, and *Candida albicans (*Zille *et al.*, 2014). However, CuO NPs bond poorly to cotton fibers, resulting in unsatisfactory laundry durability of antimicrobial fabrics (Xu *et al*., 2018). Several techniques have been utilized over the last decade to improve the adhering force of NPs to the fiber surface (Xu *et al*., 2017; Paszkiewick *et al*., 2016). Among these methods, the application of a binder has been extensively studied for binding on cotton fabric (Xu *et al*., 2017; Xu *et al*., 2018; El-Nahhal *et al.,* 2022; Radetić & Marković, 2019; Thampi *et al.*, 2015).

Sun *et al.*, (2018) reported on the atom transfer radical polymerization (ATRP) finishing procedures and electroless deposition methods to design and create robust antibacterial CuO NP coatings on cotton and polymeric substrates. CuO NPs with uniform distribution on the fiber surfaces of the substrate were obtained using the electroless method. They exhibited excellent antibacterial activity against *E. coli and S. aureus*, which was retained after 30 washing cycles due to strong binding forces between the deposited CuO NPs and substrates of polymer brushes

(Sun *et al.*, 2018). The diameter of the inhibitory zone grew as the deposition time of CuO NPs increased. The authors claimed that fibers with higher CuO NP content had better antibacterial activity, demonstrating that the CuO NP concentration influenced the antibacterial activity. The chemical reduction method is widely used for fabricating inorganic (metal and metal oxide) NPs for various applications. In this method, a metal precursor dissolved in a solvent is mixed with an appropriate reducing agent and a surfactant in a constantly stirring batch reactor under a controlled environment (Liu *et al*., 2006). CuO NPs were successfully synthesized and coated on the surface of cotton fabrics by the wet chemical method to impart functional properties such as antibacterial activity (Hasan, 2018). $Cu(NO_3)_2$ was hydrolyzed to $Cu(OH)_2$ with the help of NaOH, and soluble starch served as a reducing agent. The CuO NP particles were produced with sizes ranging from 60.0-75.0 nm. The resulting CuO NPs were applied onto cotton fabric using the pad dry cure method. The CuO NP-coated cotton fabric showed a 94.5% and 86.26% decrease toward *S. aureus and E. coli*, respectively. Figure 4 shows the SEM micrographs of the CuO NPs treated fabric at different magnifications. However, the antimicrobial activity of the treated cotton was reduced to zero after 20 wash cycles.

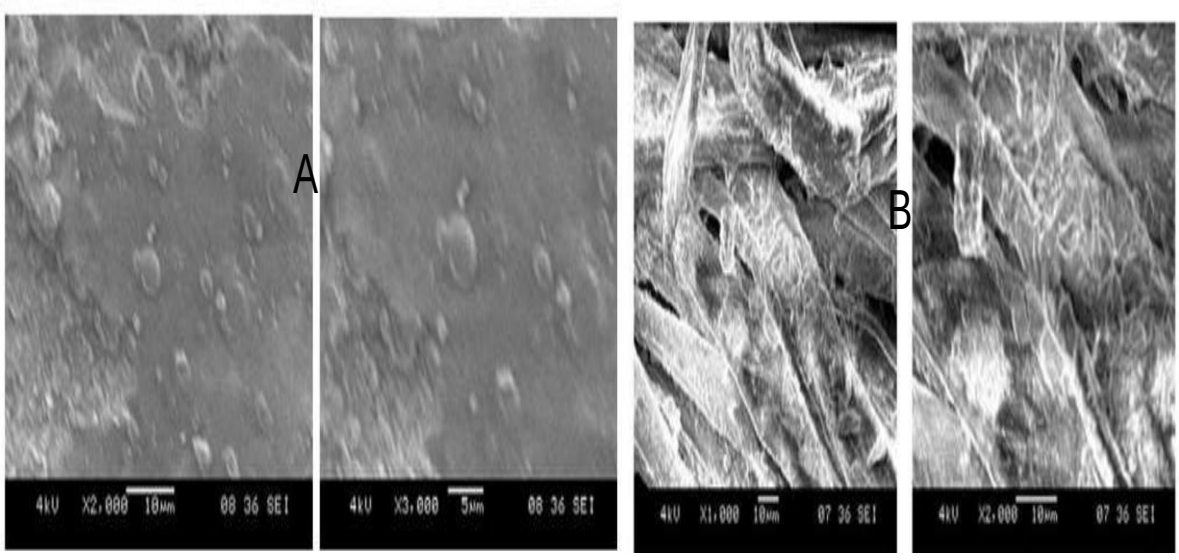

Figure 4. SEM micrographs (A) showing CuO NPs and (B) CuO NPs embedded in cotton fabrics (Hasan, 2018).

In this study, the padding conditions, such as roll temperature and the concentration of CuO NPs, were the main factors for optimization to get enhanced durable antibacterial CuO NPs embedded into the fabric. Despite the simple wet chemical method, researchers have

immobilized and deposited CuO NPs onto cotton fabrics for antibacterial activity using different techniques, such as spark discharge (Shahidi *et al*., 2017). In this work, nano-size particles were obtained with high antimicrobial activity toward *S. aureus* with the durability of 15 wash cycles. The results showed that a concentration of 100 ppm was enough to kill 10^6 CFU/mL of the bacteria.

Sonochemistry deposits various NMs (metals, metallic oxides, and semiconductors) on the surfaces of ceramics, cellulose, and polymer materials (Gedanken, 2004). In the Sonochemistry technique, molecules undergo a chemical reaction activated by applying powerful ultrasound radiation magnitude (20 kHz–10 MHz). The NP production is due to potent sonic radiation, which can break down the chemical bonds in the molecules of the precursors by creating, growing, and collapsing the bubbles.

Compared to other procedures, this method has shown the advantages of creating uniform distribution/ dispersion of NPs with a somewhat greater surface area, improved thermal stability, and phase purity. Sonochemistry has been employed to produce biocidal cotton bandages coated with nanocrystalline CuO NPs of 10-20 nm size that were homogeneously coated on the CuO–cotton bandage's surface, which had a composition of 1.50 wt.% CuO demonstrated activity for inhibiting the growth of *E. coli* bacteria (Abramov *et al.*, 2009). Additionally, the antibacterial activity of CuO NPs in binary and tertiary forms was studied in detail by (Reddy, 2017; Hassabo *et al*., 2019; Paul & Neogi, 2019; Sánchez-López *et al.*, 2020).

2.6.2 Durable Antimicrobial Cotton Fabric Coated with Ag NPs

Silver has become a primary medicinal therapeutic agent, primarily in infectious disorders, particularly clinical infections (Medici *et al*., 2019). Metallic Ag is the third metal known to have been utilized by the ancients, after Au and Cu. Over the millennia (as early as 4000 BC), Ag was utilized for various medical ailments, including empirical purposes, before it was discovered that bacteria were the agents causing illnesses (Cao & Liu, 2010). Ag NPs have astonishing antimicrobial effects. However, inadequate fixation onto the surface of cotton fibers often causes the leaching of Ag from antimicrobial-coated materials, reducing the antibacterial durability and becoming a source of environmental and health pollution (Zhou *et al*., 2018). Surface modification of cotton fabrics before *in-situ* impregnation with NPs is essential in

producing less leachable and stable nanocomposite antibacterial textiles. Different binders such as chitosan, carboxyl methyl, and other polymers (Xu e*t al.*, 2016; Wang *et al*., 2021; Zhu *et al*., 2021) have been explored for surface modification of cotton fabrics; among these, amino acids and derivatives of amino acids offer biocompatible and better adhesive properties (Yang *et al*., 2020).

Well-bound and dispersed Ag NPs on the cotton fabric surface were synthesized using sodium citrate and citric acid (CA) as stabilizing and binding agents, respectively (Wu *et al*., 2019). This work obtained the average NP size of 2.3 nm using the pad dry cure method. The antibacterial activity of the treated fabrics against *S. aureus* and *E. coli* was tested using the rotating flask method according to the GB/T 20944.3-2008 standard. The antibacterial durability of Ag-CA cotton fibers was maintained in the presence of a non-ionic detergent against successive launderings up to 50 wash cycles. According to the study, cotton fabric treated exclusively with CA had a bacterial reduction of 77.9% and 70.3% against *S. aureus* and *E. coli*, respectively, demonstrating that CA has antibacterial potential. Cotton fabrics loaded with Ag NPs demonstrated 99.9% bacterial reduction after 10 washing cycles, indicating that Ag NPs-CA cotton fabrics had excellent antibacterial action against *E. coli* and could effectively destroy germs. Figure 5 shows the scheme of the sequential grafting of CA, loading of Ag NPs, and the drying and curing process on the surface of cotton fabric (Wu *et al*., 2019).

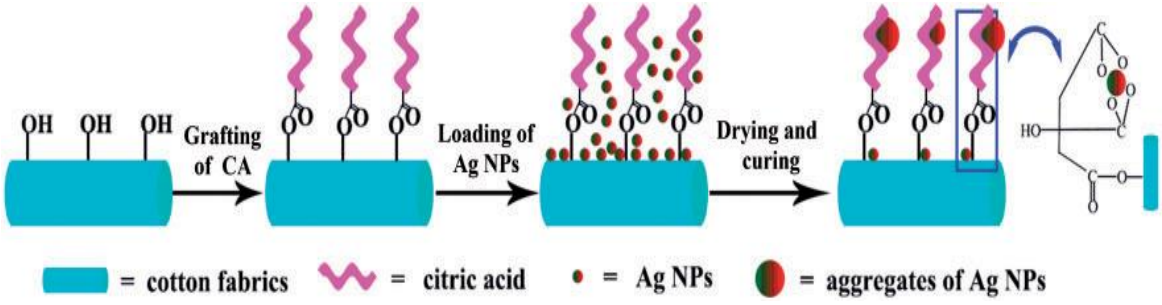

Figure 5. Scheme for preparing cotton fabrics infused with Ag-citric acid (CA) and the method by which Ag NPs are linked to the fabrics using CA (Wu *et al*., 2019).

The hydroxyl groups of cellulose first react with the carboxyl groups of CA. CA is grafted onto the cotton surfaces after the esterification reaction. In the second step, Ag NPs are loaded onto

the textiles by chelating Ag and oxygen (O) atoms derived from the esterified carboxylic groups of CA. Cotton samples were treated with a colloid solution of nano-Ag in concentrations of 100 and 200 ppm and an average particle size of 60 nm, which was then stabilized using 1, 2, 3, 4-butane tetracarboxylic acid (BTCA) (Montazer *et al*., 2012). The antibacterial activity of the treated samples was tested against *E. coli* and *S. aureus.* The carboxylic acid served as a crosslinking agent, forming bonds with cellulose. The reactions occurred via the esterification of hydroxyl groups on cellulose's three C- atoms (C1, C2, and C6). This phenomenon demonstrates surface charge formation, which contributed to the captivation and distribution of Ag NPs through the fibers. A lack of surface charge brought on the instability of absorbed particles. On the contrary, an overabundance of surface charge causes electrostatic repulsion and self-repulsion, which restrict critical uptake (King and Pierlot, 2009).

Multifunctional properties of textiles were developed by *in-situ* deposition of Ag NPs onto the surface of cotton fabrics via a simple green one-pot UV-reduction method (Rehan *et al*., 2017). This method synthesized Ag NPs with particle sizes ranging from 50-100 nm under UV radiation (320-400 nm). The Ag NP functionalized cotton fabrics demonstrated high protection against UV transmission (absorption of 65% in the UVA and UVB regions) and reduced *E. coli* by 99%. In addition to the described techniques, biogenic *ex-situ* and *in-situ* synthesis of Ag NPs as single NPs and in combination with other NPs onto cotton fabric is a more recent and actively engaged research by several researchers (Islam *et al*., 2018; Li *et al.*, 2017; Rodrigues *et al.*, 2019; Singh *et al.*, 2018).

2.6.3 Durable Antimicrobial Cotton Fabric Coated with TiO_2 NPs

TiO_2-NPs have gained much attention recently because of their appealing attributes, including electrical, UV absorption, brightness, and photocatalytic properties. The decomposition of organic pollutants and bacteria by nanostructured TiO_2 has been thought to produce multifunctional properties in the treated substrate, such as self-cleaning, air and water purification, and environmental sterilization (Martinez *et al*., 2010). These NPs have shown a pronounced significance in several applications due to their ability to absorb radiation. They are involved in forming positive electron-hole pairs that can degrade organic substrates (Ibrahim *et al*., 2018). Incorporating such metal oxide NPs into organic substrates like cellulose substrates has reportedly been envisioned for numerous uses in textiles and food packaging. Titanium-

based blends as biomaterials offer many benefits due to their superior mechanical and biological properties, such as lower modulus and excellent biocompatibility (Mohammad *et al*., 2021). Furthermore, TiO_2 NPs are chemically stable and inert and can constantly exhibit antimicrobial activity when the particles interact with light to produce superoxide and hydroxyl radicals (Liou, 2012).

TiO_2 NPs were successfully synthesized onto the surface of cotton fabric using titanium isopropoxide (TIP) as a precursor in the presence of urea nitrate as a peptizing agent (El-Naggar *et al*., 2016). The slow release of nitric acid resulted in the creation of TiO_2 NPs, which is the function of the concentration of urea nitrate (UN). Stable TiO_2 NPs with an average size of less than 50 nm and a spherical shape were successfully deposited on the surface of cotton fibers. The concentration of urea nitrate has a linear relationship with the number of NPs deposited depending on the amount of UN; the treated fabrics provided remarkable bacterial reduction with values reaching 95%. Furthermore, even after 20 washing cycles, the antibacterial performance of the TiO_2 NPs implanted cotton fabrics was outstanding.

Ibrahim *et al*., (2018) reported on the preparation of a multifunctional cellulosic substrate with TiO_2 NPs with an average size range of 8–15 nm from titanium tetraisopropoxide (TTIP) salts in the form of aqueous suspensions and ethanol as a reducing agent in the presence of CA/sodium hypophosphite as the binding agent. A concentration of 5 g L^{-1} of TiO2-NPs inhibited the growth of S. aureus in the presence of a reactive softener. The antibacterial action of TiO_2 NPs is often dependent on the active species generated in the presence of UV irradiation. Additionally, methods such as sol-gel (Galkina *et al*., 2014), casting (Montaser *et al*., 2019), electrochemical (Alamer *et al*., 2019), and co-precipitation *(*Stan *et al*., 2019) have been applied in the deposition of TiO_2 NPs synthesized from various precursors onto the surface of cotton fabrics to provide multifunctional textiles. Improvement in the fixation of NPs onto the surface of substrates, such as cotton, obtaining wash durability, and the synergistic antimicrobial effect of binary or tertiary NPs are the requirements for modification.

2.6.4 Durable Antimicrobial Cotton Fabrics Coated with ZnO NPs

At ambient temperature, zinc oxide is an n-type semiconductor with a band gap of 3.37 eV and a high excitation binding energy of 60 meV. ZnO NPs have antimicrobial activity, UV

absorption protection, photocatalytic activity, and piezoelectric capabilities. ZnO NPs are commonly used on textiles to provide antibacterial, photocatalytic, UV protection, self-cleaning, and wound healing properties. Several studies on the synthesis and application of ZnO NPs on various textile substrates have been discussed in the literature (Salem & Fouda, 2020; Singh *et al*., 2012). ZnO is an inorganic oxide frequently used in everyday life. The Food and Drug Administration lists ZnO as a generally recognized safe (GRAS) ingredient and is utilized as a food additive. Nanoscale ZnO has demonstrated antibacterial characteristics and potential applications in food preservation. ZnO NPs have been used in polymeric matrices to promote antimicrobial action and improve packaging qualities (Espitia *et al.*, 2012).

Using ultrasound irradiation techniques, ZnO NPs were successfully deposited onto cotton and cotton fabrics grafted with starch (El-Nahhal *et al*., 2020). Starched cotton was chosen as the substrate over the original cotton because starch is non-toxic and compatible with the cotton substrate. Starch is a modifying agent to improve cotton adhesion properties for improved ZnO NP deposition. At the same time, it reduces ZnO-NPs leaching from the cotton fabric surface while significantly increasing antibacterial activity. Further functionalization of ZnO NPs coated cotton sample with Ag NPs and curcumin, resulting in ZnO-Ag nanohybrid and Zn (II) curcumin complex coated cotton, was tested for antibacterial activity against *E. coli* and *S. aureus* bacterial strains (E-Nahhal *et al*., 2020). Figure 6 depicts using starch to perform two tasks simultaneously: improve cotton adherence and immobilize ZnO-NPs.

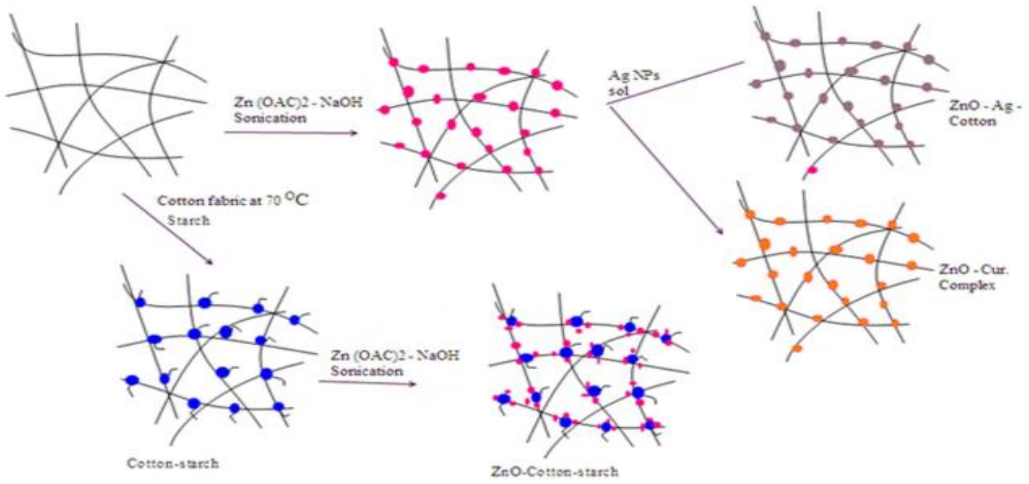

Figure 6. Scheme of deposition of ZnO-NPs, ZnO-Ag NC, and Zn (II) curcumin complex onto cotton fibers (El-Nahhal, *et al.*, 2020).

The sono-enzymatic in situ synthesis approach created long-lasting and effective antibacterial coatings on cotton textiles by depositing ZnO NPs and gallic acid (GA) in a single-step–laccase procedure (Salat *et al*., 2018). However, pre-activation of cellulose substrates was required to ensure acceptable NP durability on the surface. The simultaneous sonochemical deposition of ZnO NPs and the production of a bio-based adhesive generated by the enzymatic crosslinking of GA in which the NPs were embedded overcame this shortcoming. Even after 60 washing cycles at 75 °C hospital laundry regime, the ZnO NPs-GA coated materials maintained > 60% antibacterial activity. The high-resolution scanning electron microscopy micrographs of cotton fabrics coated with ZnO NPs before and after the removal of GA by numerous washing cycles, the initial amount of ZnO NPs deposited on the fabric (Figure 7a, b) using active laccase and in the absence of active enzyme are shown.

The enzymatically speeded-up crosslinking reaction of GA was predicted to improve the stability of ZnO NPs on the fabric and the durability of antibacterial activity. By enclosing the NPs in an in situ laccase-generated GA bio-adhesive, the GA would synergistically improve the antibacterial action of ZnO NPs and encourage their adherence to the fabric surface. The samples made with active laccase (Figure 7a) have a denser and more uniform NP coating on their surface than the cotton fabric coated with denatured laccase (corresponding to a non-enzymatic method) where the creation of a phenolic bioadhesive was unlikely (Figure 7c). After

10 washing cycles at 75 °C, the cloth treated with active laccase (Figure 7b) remained consistent and densely covered with NPs. The control sample, on the other hand, contained considerably fewer NPs (Figure 7d).

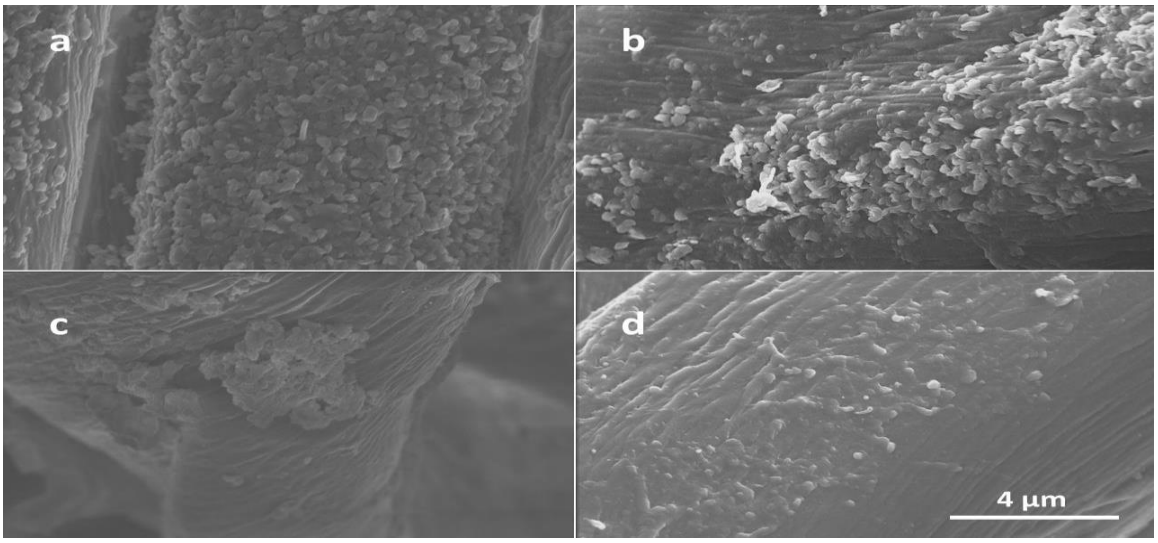

Figure 7. HR-SEM micrographs of cotton fabrics deposited with ZnO NPs and GA (a) before washing without Lacasse, (b) without Lacasse after 10 washing cycles, (c) in the presence of active Laccase before washing, and (d) with active Lacasse after 10 washing cycles (d). (Salat *et al.*, 2018).

ZnO-NPs deposited onto the surface of cotton fibers were acquired by immobilizing the NPs from $ZnSO_4.7H_2O$ precursors onto the cotton fibers via ultrasound irradiation. The NP formation mechanism probably encompassed three or four steps: the first interaction was between Zn^{2+} ions and surfactant; the second was the creation of stable $Zn(OH)_2$, which is absorbed onto the cotton surface; and the third was the transformation of $Zn(OH)_2$ to ZnO NPs by irradiation energy and finally washing to remove unreacted excess surfactant (El-Nahhal *et al.*, 2017). Figure 8 depicts the coating of cotton fiber with ZnO-NPs in the presence of SDS surfactant.

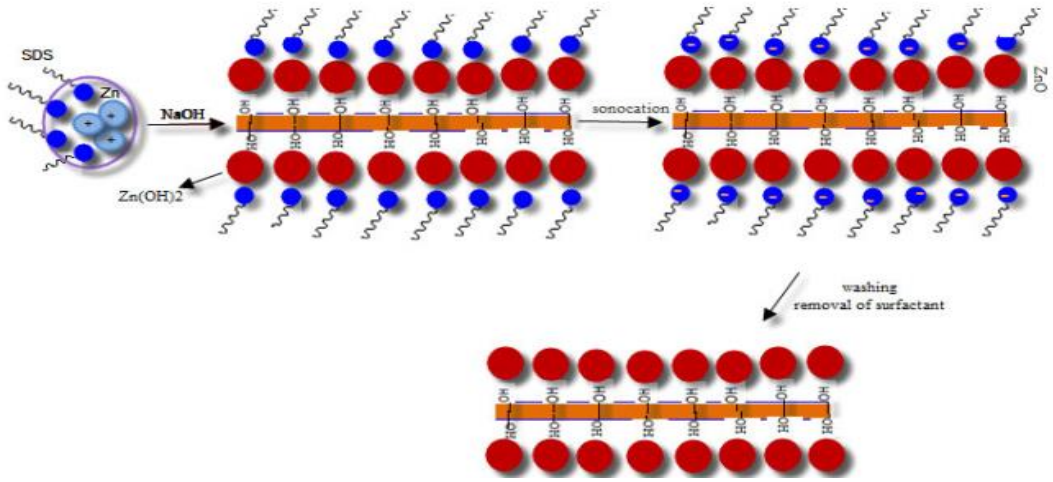

Figure 8. Ultrasound irradiation to prepare ZnO-cotton nanocomposites (El-Nahha *et al*., 2017).

The results showed that using surfactants, especially SDS, reduced the leaching of ZnO-NPs. The small size of the ZnO NPs with an average mean crystalline size of 8.00-12.8 nm upon using the surfactants is the main reason for decreasing the leaching of ZnO-NPs from the cotton substrate. Even after ten washing cycles, the durability of the ZnO-NPs coated fabric revealed a subsequent decline in ZnO-NPs leaching and a loss in antibacterial efficacy. Because of its smaller size, ZnO-SDS was the most effective surfactant in reducing antibacterial activity.

Different reports revealed that the functionalization of cotton fiber with ZnO NPs via the sonochemical technique (Perelshtein *et al*., 2015; Singh *et al*., 2012; Petkova *et al.,* 2016; Abramova *et al.,* 2013; Yusof *et al*., 2019). The antimicrobial activity of ZnO NPs coated sonochemically onto cotton fabrics varies based on the modifying agent used to activate the cellulose. Cotton fabrics coated via *in-situ* synthesis of ZnO NPs capped with date seed extract were designed to have multifunctional characteristics (El-Naggar *et al*., 2018). To obtain the bulk state, the produced ZnO NPs prefer to agglomerate. Following that, date seed extract would be critical in preserving these NPs in small nano size without agglomeration. The efficacy of date seed as a stabilizer is due to the presence of phenols, polysaccharides, and other components that are high in hydroxyl groups. Compared to uncapped ZnO nanoparticles, the ZnO nanoparticles capped with the extract exhibited a spherical shape, smaller nano size, and more uniform dispersion in the cotton structure, regardless of the substrate. The bacterial

reduction of date seed extract against *E. coli* is relatively low (26%), while the antibacterial reduction of tested samples of uncapped and capped ZnO NPs against *E. coli* is up to 85 and 99%, respectively (El-Naggar *et al*., 2018). Moreover, various techniques were applied in the *in-situ* immobilization of ZnO NPs into the surface of cotton fabrics, such as UV-irradiation (Ghayempour & Montazer, 2017), wet chemical (El-Nahhal *et al*., 2020) and precipitation (El-Nahhal *et al*., 2017).

2.6.5 Durable Antimicrobial Cotton Fabrics Coated with Bimetallic NCPs

To enhance the properties of nanoparticles (NPs), researchers have developed binary and tertiary nanocomposites (NCs). Aloe vera extract was used as a reducing agent to generate bimetallic NCs in cotton fabrics. First, aqueous solutions of $AgNO_3$ and $CuSO_4.5H_2O$ mixtures were prepared, and then cotton fabrics with infused Aloe vera leaf extracts (matrix) were kept in these metallic source solutions and stirred. The NC-infused cotton fabrics showed good antibacterial activity against *E. coli, Pseudomonas, Bacillus, Klebsiella, and Staphylococcus* cultures (Mamatha *et al.,* 2018). In another study, red sander extracts were used to reduce $CuSO_4.5H_2O$ and $AgNO_3$, with flavonoids and sugars of the extracts acting as reducing agents and other constituents as capping agents (Venkateswara *et al.,* 2019). Cotton fabrics were dipped in hyperbranched poly(amide-amine) (HBPAA) to encapsulate metal NPs, showing an excellent protective ability to prevent agglomeration and oxidation (Gao *et al*., 2020). $NaBH_4$ reduced $AgNO_3$, $HAuCl_4$, and H_2PtCl_6 to metal NPs in the polymer's presence. Then cotton fibers were impregnated to produce monolayered Ag-Au-Pt coated fabrics, probably due to electrostatic repulsion among positively charged NPs. Furthermore, the combination of Ag, Au, and Pt NPs yielded a positive potential and could aid in the self-assembly of cotton upon surface capping with HBPAA. The authors inferred that different metal NPs capped with the same functional polymer may inherit the chemical characteristics of the latter, and antibacterial activities were found *against E. coli and P. aeruginosa*.

TiO_2 has become the benchmark for promising applications such as antibacterial agents among metal oxides (Ibrahim *et al.,* 2017). In another work, a coating dispersion treated on textile fibers based on TiO_2 NPs and ZnO NPs was prepared through uniform dispersion of NPs in binder melamine tri-polyphosphate acrylate solution by ultrasonication. The superiority of TiO_2

NPs as an antibacterial agent was observed over ZnO NPs against *S. aureus* bacteria. However, when an equal mass ratio of TiO_2 NPs and ZnO NPs was used, the antagonistic effect was observed in the antibacterial effect as the inhibition zone was recorded (Attia *et al.,* 2017).

Inorganic bacterial agents are usually photocatalytic metal oxides that belong to semiconductor compounds. Among them, ZnO attracts the most attention because of its excellent biocompatibility. However, the photocatalytic antibacterial performance of ZnO can be reduced because of the high recombination rate of the electron-hole pair. One way to overcome these problems and promote the photocatalytic antibacterial activity of ZnO is doping with noble metals. On the other hand, Ag NPs are a gold-standard bacteriostatic agent. A study was conducted to enhance the antibacterial activity of ZnO using tri-component NCs of Ag, Cu, and ZnO deposited onto the cotton textile surface. This resulted in long-lasting antibacterial activity, protection against ultraviolet radiation, and the ability to conduct electricity. These metal and metal oxide NPs were synthesized using polymethylol and functionalized polyethylenimine compounds (Hassabo *et al.,* 2019). Ag/ZnO NPs were prepared from commercial ZnO NPs in the presence of 3-aminopropyltriethoxysilane, $AgNO_3$, and trisodium citrate solution as reductant and stabilizer. Then, an organic-inorganic hybrid was synthesized through radical polymerization of diallyl dimethyl ammonium chloride and an acyloxy silane coupling agent to form a pyrrolidinium-based polymer. Ag/ZnO nanoparticles were incorporated into this mixture. The cotton samples were immersed in the dispersion solution for paddling. Antibacterial activity against *S. aureus and E. coli*, durability, hydrophilicity, and air permeability were studied (Gao L. *et al.,* 2020). In cotton fabrics coated with Ag, TiO_2, and ZnO NPs, Ag NPs were synthesized from $AgNO_3$ with trisodium citrate, whereas TiO_2 NPs were prepared by mixing $TiCl_4$ and ammonium carbonate. Finally, ZnO NPs were obtained from $ZnCl_2$ and sodium hydroxide. They were first immersed in a beaker containing a polyurethane solution to coat the cotton fabrics with the synthesized nanoparticles. After that, the fabrics were immediately immersed in the ZnO NP solution and then in the beaker containing TiO_2 NPs. This process was repeated with the beaker containing Ag NPs solution. The optimum photocatalytic and antibacterial activities against *Salmonella typhi* and *Shigella* were observed in the decorated fabrics with Ag, ZnO, and TiO_2 (Ansari *et al.,* 2020).

An alternative method for producing antibacterial cotton fabrics involves attaching Ag NPs decorated with bismuth oxybromide (BiOBr) nanosheets to carboxymethyl cotton fabrics. To promote the nucleation of BiOBr, the cotton fabric was altered through an SN2 reaction of hydroxyl groups using chloroacetic acid and NaOH as a base, resulting in the formation of sodium carboxylates (carboxymethyl cotton fabrics, CCF). When this fabric was placed in a $Bi(NO_3)_3$ solution, $Bi_2O_2^+$ ions were absorbed by the carboxyl groups. Subsequently, immersion in a KBr solution triggered the reaction of bromide ions with $Bi_2O_2^+$ to produce BiOBr-CCF. Ag^+ ions from $AgNO_3$ were then absorbed by BiOBr-CCF and reduced by exposure to UV irradiation. This Ag/BiOBr-CCF showed a practical bacteriostatic effect against *E. coli and S. aureus* (Zhou *et al.,* 2020). In another study, *Streptomyces sp*, a marine bacterium, was used as both a reducing and stabilizing agent for the biosynthesis of Au NPs. After treating cotton fabrics with O^{2-} plasma, the fabrics were coated with a combination of Au NPs/ZnO NPs, which exhibited high antibacterial activity against *S. aureus and E. coli* and durability after 15 washes (Ibrahim *et al.,* 2016).

The antimicrobial efficacy of the formed NPs deposited onto cotton is promising in all fabrication methods. However, antibacterial wash durability is still challenging when making durable antibacterial cotton fabrics. NPs and NCPs leached off the surface of the cotton fabric unless a strong link was established between the surface of the cotton and the NPs and NCPs. Several chemical reagents, particularly polymeric compounds, were used to modify the fabric's surface before functionalization with NPs and NCPs.

Essential amino acids with electron-donating groups, such as L-methionine, are of interest for surface modification of cotton fabrics because of their non-toxicity to human cells, biocompatibility, and biodegradability. During surface modification, the amino acid carboxyl group reacts with the cellulose's hydroxyl group on the cotton fabric, adding donating groups to the surface of the cotton fabric. Figure 9 shows the schematic chemical reaction between the L-methionine and cotton fabric. Figure 9 shows that the amino acid (L-methionine) contains an S atom attached to the terminal methyl group. The presence of the S atom, in addition to the amine functional group, enhances a covalent bond that would be formed with the metal and metal oxide NPs.

L-methionine is covalently linked onto the surface of cotton fibers via an esterification reaction with the hydroxyl groups of cellulose using a facile finishing pad-dry cure process. Then, the metal and metal oxide NPs are synthesized and immobilized on the modified surface by the enhanced adhesive force of the L-methionine moieties.

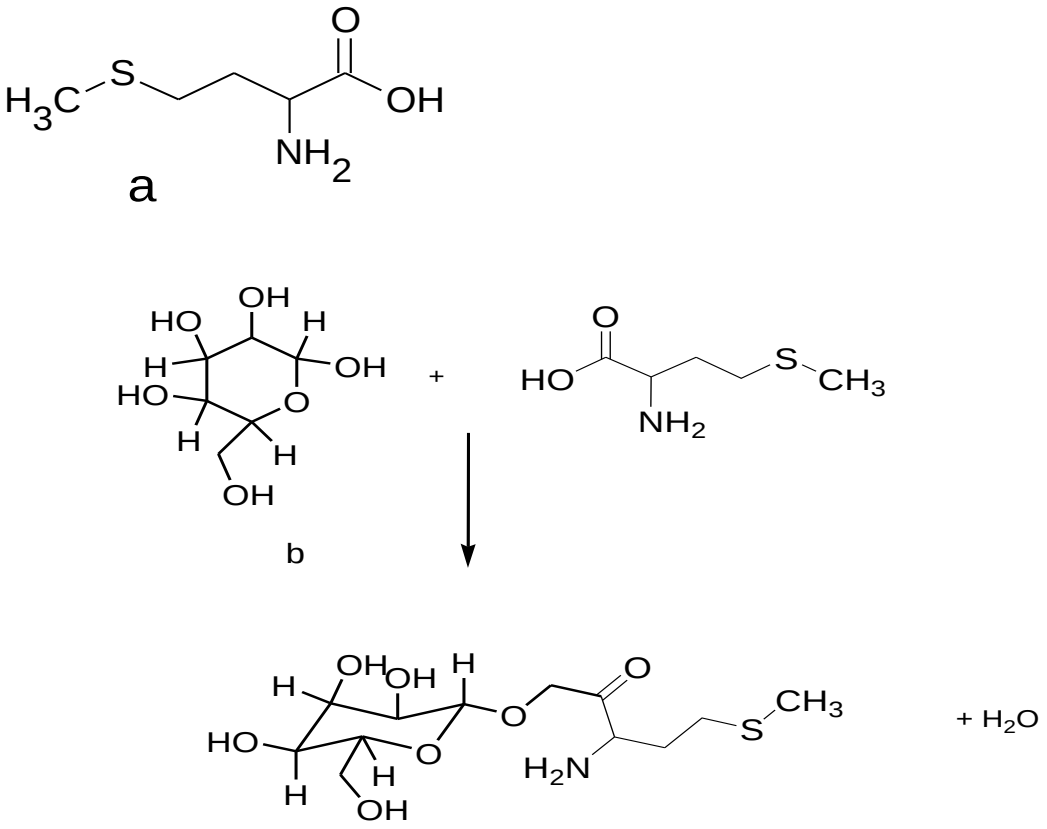

Figure 9. Modification of cotton by the amino acid L-methionine (a) chemical structure of L-methionine, and (b) esterification reaction between hydroxyl groups of the hypothetical cellulose monomer and carboxylic amino acid groups.

2.7 The Mechanism of Antibacterial Activity

The resistance of bacteria is currently a serious concern as a result of the widespread use of antibiotics for preventative or curative purposes without sufficient medical justification, the incorrect selection of alternate antimicrobials, and the frequent switching between antimicrobial therapies (Wang *et al.*, 2017).

The unceasing emergence of bacterial resistance has challenged the exploration community to advance novel antibiotic agents. Among the most encouraging novel antibiotic agents are metal

NPs, which have shown strong antibacterial activity in many studies (Slavin *et al.*, 2017). The main reason for considering NPs as an alternative to antibiotics is that they can effectively combat microbial drug resistance in certain situations. Metal NPs can also alter the metabolic activity of bacteria. Additionally, NPs have the ability to penetrate biofilms, offering a valuable approach to preventing biofilm development by inhibiting gene expression.

The cytoplasmic membrane and cell wall are degraded as part of the killing process because of the production of reactive oxygen species such as hydroxyl radicals and hydrogen peroxide. This mainly causes seepage of cellular contents, followed by cell lysis; subsequently, the organism may completely mineralize. Electrostatic attraction, van der Waals forces, receptor-ligand interactions, and hydrophobic interactions all contribute to the most effective killing when the organisms and the NPs are in close proximity (Tatlıdil *et al*., 2011). The ability of transition metal NPs to create ROS and their propensity to form intimate associations with biological components such as amino acids, DNA, and tissues are the two most significant factors contributing to their bactericidal action. The high atomic number of metal ions of non-essential transition metals, like Ag^{+} or $Zn^{2+,}$ can readily bind to SH groups, like cysteine. This can directly interfere with the function of specific enzymes or disrupt the S-S bridges necessary to maintain the integrity of folded proteins, negatively affecting the cell's metabolism and physiology. ROS production has a particularly negative impact on bacterial cells (Slavin *et al*., 2017).

Although the antimicrobial mechanisms of NPs are not fully known, the currently recognized processes include metal ion release, oxidative stress induction, and non-oxidative mechanisms. It is challenging for bacterial cells to develop NP resistance since the many simultaneous modes of exploitation against microorganisms would require multiple simultaneous gene alterations in the same bacterial cell (Wang L. *et al*., 2017).

One of the most crucial antibacterial defense mechanisms is oxidative stress brought on by reactive oxygen species (ROS) (Li *et al.*, 2015). Under UV irradiation, metal oxide NPs produce the ROS type's superoxide radical, hydroxyl radical, and singlet oxygen. The survival of *E. coli* cells in NP-containing aqueous suspensions under UV radiation was used to establish a quantitative correlation between oxidative stress and the antibacterial activity of NPs. A linear relationship was discovered between the average concentration of total ROS and the bacterial

survival rates. NP concentration is assumed to decline when the NPs are bound to the organic matrix in the culture broth and deteriorated cell components. Figure 10 shows the combined ROS production exposed to Ag NPs.

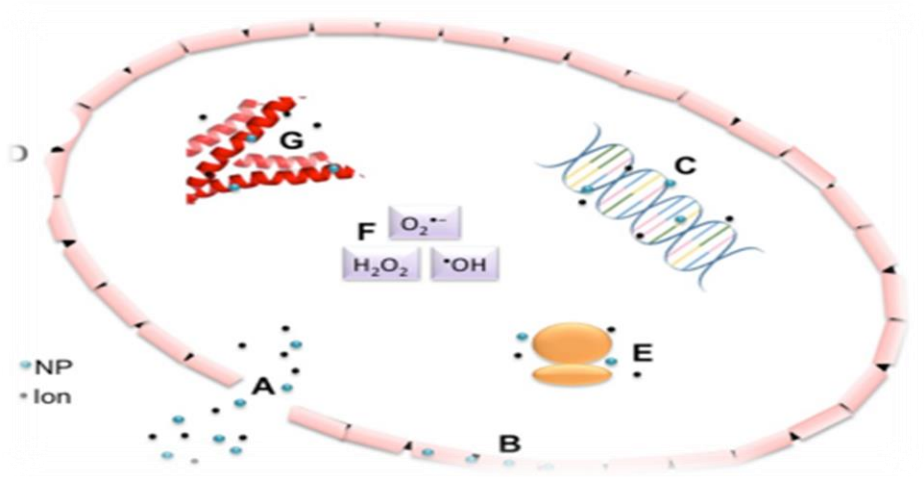

Figure 10. A scheme illustrating the mechanisms of Ag NPs while exposed to *E. coli* cells. (A) cell wall breakdown, allowing intracellular components to exit the cell, (B) Ag NPs penetrate the periplasmic space, starting the disintegration of the cytosol from the membrane, (C) DNA and Ag NPs interaction, (D) cell pits that develop upon exposure, (E) incorrect DNA function, ROS generation, protein suppression or malformation, and obstruction of appropriate ribosome function, (F) ROS produced, and (G) protein interaction, particularly with cysteine (Slavin *et al.*, 2017).

In Figure 10, the precise method by which destructive activity occurs is only speculated. Although explanation is challenging due to the numerous routes that appear to be simultaneously activated by NPs, this is also why NP exposure is so powerful. According to currently available studies, the main mechanisms underlying the antibacterial actions of NPs are generally as follows: 1) bacterial cell walls rupturing; 2) Production of Reactive oxygen species; 3) penetration into bacterial cell membrane; and 4) interplay with DNA and proteins as well as the production of intracellular antimicrobial effects. Bacterial cell membranes are highly conserved and, therefore, difficult to alter with only a couple of genetic alterations, which lessens the possibility of bacterial drug resistance. The creation of biofilms is hampered by the

rupture of bacterial membranes, which is a significant process because biofilms are essential for the emergence of bacterial resistance (Walker *et al.,* 2014).

2.8 UV-Protective Coated Cotton Fabric

Ultraviolet radiation is powerful, energetic, short-wavelength light. Three wavelength ranges of ultraviolet radiation, also known as UVR, can be distinguished: UVA (315–400 nm), UVB (280–315 nm), and UVC (100–290 nm). The UVC region, the most damaging region of UV rays for human health, is absorbed in the stratosphere by oxygen molecules in the ozone layer. However, UVA and UVB radiation reach the surface of the planet and result in severe health problems, including skin cancer, sunstroke, and photoaging (Attia *et al*., 2022). Consequently, it has drawn significant attention to UV penetration of fabrics due to the rising request in the market for light-protective garments that provide UV protection (Xin *et al.,* 2014). When UVA and UVB are exposed for an extended period to sensitive skin, they trigger a photoallergic reaction, resulting in wrinkles or a loss of flexibility in the outermost layer of the skin (Porrawatkul *et al*., 2022). A parameter used to assess a material's average level of protection, after which it may be examined under the spectrum, is the ultraviolet protection factor (UPF). According to the Australian/New Zealand Standard (AS/NZS 4399:1996), the UPF values are primarily measured in the 280–400 nm range using the following formula:

$$\frac{\sum_{280}^{400} \mathrm{E}\lambda \ \mathrm{x}\mathrm{S}\lambda \ \mathrm{x}\ \Delta\lambda}{\sum_{280}^{400} E\lambda \mathrm{x}\mathrm{T}\lambda \mathrm{x}\mathrm{S}\lambda \mathrm{X}\Delta\lambda}$$

Where,

Sλ ------ the spectral irradiation of the skin,

Eλ ---- the erythemal spectral effectiveness,

Tλ ----- is the spectral transmittance of the materials, and Δλ is related to increment wavelength in (nm)

The ultraviolet protection factor (UPF) of cotton fabrics treated with Ag NPs, TiO_2 NPs, and Ag/TiO_2 NPs was determined (El-Naggar *et al*., 2022). In this study, NPs were impregnated onto the fabric by the *ex-situ* method, and cotton fabrics coated with Ag NPs have minimal UPF ratings for UV radiation protection. Furthermore, the fabrics treated with TiO_2 NPs showed

higher UV protection ratings of 28.2 and 42.7 before washing. UV Protective properties of cotton fabric coated with carboxymethyl chitosan and Ag/TiO_2 NCPs were successfully prepared (Xu *et al*., 2021). The original fabric had a UPF value of less than 10.0, confirming that non-functionalized cotton fabric has insufficient UV protection. The UPF values of functionalized fabric with Ag/TiO_2 samples exceeded 79.0, indicating excellent UV protection after 50 laundry cycles. The durable and adequate UV protection demonstrated that the chitosan is uniformly spread on the fabric and binds the NPs to the cotton fabric.

In-situ synthesis of Ag NPs on cotton fabric surfaces was achieved by immersing the fabrics in an alcoholic $AgNO_3$ solution (concentrations varying from 100 to 500 ppm) and subjecting them to UV light (Rehan *et al.,* 2017). According to the report, the blank cotton fabric has good UV transmittance, while Ag NP cotton fabrics have poor transmission. UV transmittance diminishes when the Ag content of cotton fibers increases. Cotton fabrics treated with Ag NPs have reduced UV transmittance, particularly between 320 and 375 nm. The coated fabric provides good UV protection in the UVA spectrum. Integrating Ag NPs into cotton fabrics provides significant UV protection due to Plasmon resonance and efficient UV scattering due to their high refractive index (Gorenšek and Recelj, 2007). The effectiveness of TiO_2 as a UV absorber, which is highly influenced by the production process and additives used, was synthesized (Ibrahim *et al*., 2019). Uncoated cotton transmits a significant amount of UV light. Adding 10% TiO_2 to the fabric dramatically boosted UPF (UPF = 58.10). The concentration ratio of composite components influenced the UV protection capabilities of the synthesized Cu_2O/TiO_2 NCPs. Including Cu_2O enhances UV protection by increasing the absorption property of CuO/TiO_2 NCPs, ascribed to the crystalline structure of Cu_2O formed (Ibrahim *et al*., 2019 ; Badry *et al.,* 2023).

UV protection properties of the biosynthesized ZnO NPs were investigated (Fouda *et al.,* 2018; Xu and Cai, 2008). The recovered fungal biomass (protein-secreted fungus) was combined with Zinc acetate $Zn(CH_3CO_2)_2$ to form biosynthesized ZnO NPs with an average crystalline size of 10-45 nm. The treated cotton fabrics with ZnO NPs had a UPF value of 16.1, indicating good protection according to Australian/New Zealand Standard AS/NZS 4399:1996. Untreated fabrics had a lower UPF value of 4, indicating poor protection. UV-radiation protection was explored by applying *in-situ* synthesized ZnO NPs to cotton fabric using hexamethyltriethylene tetramine (HMTETA) without capping or immobilizing agents (Shaheen *et al.,* 2016). A 26.3

nm average crystalline size of ZnO NPs was synthesized, and the UPF value ranged from 15-22 depending on the amount of ZnO NP precursor applied.

Table 1 summarizes the UV-protection factor (UPF) of some selected cotton fabrics coated with various NMs.

Table 1: UPF values of cotton fabric treated with various NMs.

Sample code	**UPF Value**	**References**
Ag-ZnO treated cotton fabric	69.67	Porrawatkul *et al*., 2022
ZnO treated cotton fabric	37.67	Porrawatkul *et al.*, 2022
$BaTiO_3$ NPs embedded cotton fabric	73.48	Kumar *et al*., 2023
SiO_2/ZnO NP/ZnO nanorod hybrid treated cotton fabric	124.58	Kucuk and Ovecoglu, 2020
Ag/TiO_2 coated fabrics	56.39	Li *et al*., 2017
Ag NPs coated cotton fabric	34.09	Zhu *et al*., 2021
Biosynthesized ZnO NPs treated with cotton fabric	16.30	Fouda *et al*., 2018
Cu_2O/TiO_2 coated cotton fabric	102.04	Ibrahim *et al*., 2019
PA/ODA/TiO_2 Cotton fabric	2000	Abidi *et al*., 2009
Carboxymethyl Chitosan and Ag/TiO_2	79.0	Xu *et al*., 2021

CHAPTER 3

Materials and Methods

3.1 Chemicals and Apparatus

Handloom cotton fabrics were purchased from the local market in Adama, Ethiopia. Liquid detergent and surfactants were purchased from Bekas Chemicals Plc, Adama, Ethiopia. Urea ($CO(NH_2)_2$, 98% purity), nitric acid (HNO_3, 70% purity), hydrogen peroxide (H_2O_2, 60-70% purity), ethyl diamine tetra acetic acid (EDTA, 99% purity), hydrochloric acid (HCl, 37% purity), and ethanol,(CH_3CH_2OH, 97% purity) were all purchased from Sigma Aldrich. Silver nitrate ($AgNO_3$, 99% purity), sodium borohydride ($NaBH_4$, 99.99% purity), titanium isopropoxide ($Ti\{OCH(CH_3)_2\}_4$ 99.5% purity), and L-methionine ($C_5H_{11}NO_2S$, 98% purity) were all purchased from Sisco Research Laboratories Pvt. Ltd., India. Sodium hydroxide (NaOH, 99.99% purity), ammonia solution (NH_3, 35% purity), magnesium sulfate ($MgSO_4$, 99% purity), sodium carbonate (Na_2CO_3, 99.9% purity), glacial acetic acid (CH_3CO_2H, 99.7% purity), and zinc nitrate trihydrate ($Zn(NO_3)_2.3H_2O$, 99.99% purity), were purchased from Loba Chemie Pvt. Ltd., India, and copper nitrate trihydrate ($Cu(NO_3).3H_2O$, 99.5% purity) was purchased from Guangdong Guanghua Sci-Tech Co Ltd, China. All chemicals were used as received without further purification. Deionized water was used throughout the experimental work for solution preparation and cleaning. Apparatus such as different-size capacity borosilicate volumetric flasks, beakers, measuring cylinders, and micropipettes were also used. A magnetic stirrer, desiccator, pad roller, vacuum filter, ice bath, thermometer, and Petri dishes were also used during the experiments.

3.2 Cleaning of Cotton Fabrics and Surface Modification of Cotton Fabric by L-Methionine (Am)

The cotton fabrics were scoured and bleached to expose the OH groups of cellulose for the esterification reaction with L-methionine. The fabrics were scoured using 250 mL of 0.1 M of Na_2CO_3 and NaOH as the scouring agents and 25 mL of 0.01 M EDTA as the sequestering agent to remove fats, waxes, and any other impurities from the surface of the cotton fabrics. The scoured fabrics were then bleached using 100 mL of 15% H_2O_2 as a bleaching agent, washed with excess DI water, and dried in an oven at 80 ℃ for 30 min. The scoured and bleached fabrics were coded Cot. Following a reported method (Zhou *et al*., 2018), they were immersed

in 250 mL of 1.5% w/w aqueous L-methionine solution for 30 min at room temperature, pad rolled to ~90% wet pick up, and then oven heated at 180 °C for 5 min for thermal fixation. The modified fabrics were coded AmCot and cut into samples of 3.0 cm x 3.0 cm and 10.0 cm x 10 cm for evaluating the chemical, morphological, antibacterial activity, UV protection, and physical properties.

3.3 Functionalization of Surface Modified Fabrics (AmCot) by Metal and Metal Oxide NPs

AmCot was functionalized by in-situ synthesis and deposition of single NPs and binary component metal and metal oxide NCPs.

3.3.1 *In-Situ* Preparation and Immobilization of Ag NPs onto AmCot

In-situ preparation and immobilization of Ag NPs onto L-methionine-modified cotton fabric was adapted from a reported procedure (Zhou *et al.,* 2018)**.** AmCot fabrics were soaked in 250 mL aqueous $AgNO_3$ (0.045 M) and heated at 100 ℃ for 30 min. These fabrics were removed and soaked in 250 mL of an aqueous solution of 0.1 M $NaBH_4$ for 2 min to reduce $AgNO_3$ to Ag NPs at pH 5. The Ag NPs functionalized fabrics were then rinsed with DI water (100 mL x 3 times), oven-dried at 100 ℃ for 30 min, and then cured at 180 ℃ for 5 min. The functionalized fabrics were coded as AmCot+Ag.

3.3.2 In-Situ Preparation and Immobilization of CuO NPs onto AmCot

In-situ preparation and immobilization of CuO NPs onto AmCot fabrics were carried out according to a reported procedure (Zhao *et al.,* 2020)**.** AmCot fabrics were immersed in 100 mL of 0.12 M $Cu(NO_3)_2 \cdot 3H_2O$ aqueous solution and stirred for 15 min, after which 15 mL of 25% NH_3 solution was added dropwise to adjust the pH to approximately 9 and stirred for 30 min to facilitate the formation of Cu^{+2} ions due to the cupric ammonium complex. Subsequently, the fabrics were soaked in 0.5 M of 100 mL of aqueous NaOH solution for 5 min, rinsed with DI water, and added into 100 mL 0.05 M $NaBH_4$ aqueous alkaline solution for 15 min while stirring at 30 °C. Finally, the fabrics were thoroughly rinsed with DI water, oven-dried at 60 ℃ for 30 min, and cured at 180 ℃ in the oven for 5 min. The functionalized fabrics were coded AmCot+CuO.

3.3.3 In-Situ Preparation and Immobilization of ZnO-NPs onto AmCot

A reported procedure (Javed *et al.,* 2021) was adopted to prepare ZnO NPs *in-situ* and immobilize them on the surface of AmCot fabrics. AmCot fabrics were immersed in 250 mL of an aqueous solution of 0.044 M $Zn(NO_3)_2.3H_2O$ and stirred for 30 min. Then, 25 mL of an aqueous alkaline solution prepared from 0.05 M $NaBH_4$ and 0.5 M NaOH was added dropwise to the synthesis bath, and the pH of the synthesis was adjusted to pH 9.5. To form ZnO NPs on the fabric surface, the synthesis bath was heated at 80 ℃ for 1 hour, after which the fabrics were oven-dried at 80 ℃ for 30 min and then cured at 180 ℃ for 5 min. The functionalized fabric was coded AmCot+ZnO.

3.3.4 *In-Situ* Preparation and Immobilization of TiO_2 NPs onto AmCot

For the in-situ preparation and immobilization of TiO_2 NPs onto AmCot, 5.75 mL of 15.9 M HNO_3 was added dropwise to 100 mL of urea solution (10.86 g, 0.083 mol) in cold water with gentle stirring for 30 min to form urea nitrate ($CH_5N_3O_4$, UN) precipitate (El-Naggar *et al*., 2016). After recovery of the UN crystals by vacuum filtration, the crystals were washed in ice-cold and DI water and dried. AmCot fabrics were immersed in a 100 mL ethanolic solution in which 5 mL of $Ti\{OCH(CH_3)2\}_4$ (TIP) was dissolved while shaking at room temperature for 30 min, followed by pad rolling to weight pickup of 100% and dried at 80 ℃ for 5 min. The dried samples were then soaked for 30 min at ambient temperature in 0.01 M UN solution of pH 4, which resulted in the slow release of HNO_3. The treated AmCot fabrics were rinsed with DI water to remove any remaining unreacted chemicals, oven-dried at 80 °C for 15 min, and cured at 180 °C for 5 min for thermo-fixation. The samples were coded AmCot+TiO_2.

3.3.5 *In-Situ* Preparation and Immobilization of Ag-CuO NCPs onto AmCot

In-situ preparation and immobilization of Ag-CuO NCPs onto AmCot fabric was carried out according to the reported procedure (Zhao *et al*., 2020). AmCot fabrics were immersed in 250 mL of an aqueous solution of 0.04 M $AgNO_3$ and 20 mL of an aqueous solution of 0.05 M $CuNO_3.3H_2O$ and stirred for 1 hour at ambient temperature. 20 mL of 25% NH_3 solution was added dropwise to adjust the pH to 9, and stirring continued for another 30 min. The treated fabrics were then immersed in 250 mL of an aqueous solution of 0.5 M NaOH for 5 min and rinsed with DI water. After this, the treated fabrics were reduced in 250 mL alkaline solution of

0.05 M $NaBH_4$ for 15 min with stirring at 30 °C and the fabrics were thoroughly rinsed with DI water and oven-dried at 60 °C for 30 min, then cured at 180 °C for 5 min for thermo-fixation. The samples were coded AmCot+Ag-CuO.

3.3.6 In-Situ Preparation and Immobilization of Ag-ZnO onto NCPs

In-situ, preparation and immobilization of Ag-ZnO was carried out by immersing AmCot fabrics in 125 mL aqueous solution of 0.035 M $Zn(NO_3)_2.3H_2O$ in a reaction bath under stirring for 25 min (Taheri *et al.,* 2021). A 100 mL aqueous solution of 0.025 M $AgNO_3$ was added to the synthesis solution. After 10 min, 25 mL of a prepared alkaline solution of 0.01 M $NaBH_4$ and 0.01 M NaOH solution was added dropwise, and the pH of the solution was adjusted to 9.5. The precursors were reduced after one hour of heating at 80 ℃. The treated fabrics were rinsed with DI water, oven-dried at 60 ℃ for 30 min, and cured at 180 ℃ for 5 min for thermo-fixation. The samples were coded AmCot+Ag-ZnO.

3.3.7 *In-Situ* Preparation and Immobilization of Ag-TiO_2 NCPs onto AmCot

A reported procedure (Görgülüer *et al.,* 2021) was adopted for the *in-situ* preparation and immobilization of Ag-TiO_2 NCPs onto AmCot. To the solution of 265.8 mL DI water and 15 mL 99. 7% v/v of glacial acetic acid (CH_3CO_2H), 4.2 mL of 37% HCl was added and heated to 60 °C. 15 mL of TIP was then added dropwise to the heated mixture under stirring. The reactants were allowed to stir for 2 hours to obtain a 5% TiO_2 colloid suspension. AmCot fabrics were immersed in 60 mL of 5% TiO_2 colloid suspension, to which 8 mL of 0.04 M $AgNO_3$ solution and an alkaline solution of 10 mL of 0.017 M $NaBH_4$ and 10 mL of 0.01 M NaOH were added to prepare Ag-TiO_2 NCPs modified cotton fabrics by adjusting the pH to 9. The fabrics were oven-dried for 4 hours at 75 °C, rinsed with DI water, and then cured for 5 min at 180 °C for thermo-fixation. The samples were coded AmCot+ Ag-TiO_2.

3.3.8 *In-Situ* Preparation and Immobilization of CuO-TiO_2 NCPs onto AmCot

A previously described procedure (Görgülüer *et al*., 2021) was used for the *in-situ* preparation and immobilization of CuO-TiO_2 NCPs on AmCot. To a solution of 265.8 mL of DI water and 15 mL of 99.7 % v/v of CH_3CO_2H, 4.2 mL of 37% HCl was added and heated to 60°C. 15 mL of TIP was then added dropwise to the heated mixture under stirring. The reactants were allowed to stir for 2 hours to obtain a 5% TiO_2 colloid suspension. AmCot fabrics were immersed in 60

mL of 5% TiO_2 colloid suspension and 20 mL of 0.05 M $Cu(NO_3)_2$ added dropwise under stirring. 10 mL of aqueous 25% NH_3 solution was then added dropwise into the mixture to adjust the pH to 9, and stirring continued for 30 min. Then, 10 mL of 0.01 M of NaOH was added to precipitate CuO and TiO_2 colloid. The reaction mass was then left to stand for 10 min. The treated fabric samples were removed, dried for 4 hours at 75 °C, rinsed with DI water, and then cured for 5 min at 180 °C in the oven for thermo-fixation. The samples were coded AmCot+CuO-TiO_2.

3.4 Characterization

3.4.1 Functional Group Analysis

3.4.1.1 Attenuated Total Reflectance Fourier Transform Infrared Spectroscopy (ATR-FTIR)

ATR-FTIR can measure spectra without the need for sample preparation or dilution; it has found applications in the analysis of solid and liquid materials. In ATR-FTIR, light energy is passed through an optical material (i.e., the ATR sensor) that has two major characteristics: optically transparent to the frequency of the energy so that the sensor material absorbs little or none of the radiation and the ATR sensor material has an index of refraction that is higher than that of the surrounding media so the ATR acts as a waveguide, internally reflecting the light energy. By selecting specific optical materials and controlling the fabrication of the sensor, the number of reflections or nodes in an ATR sensor can be precisely adjusted. The effective path length of the sensor is determined by multiplying the number of internal reflections by the depth of penetration of the evanescent wave. At each node, a stationary wave of energy is emitted from the surface, contributing to the overall ATR phenomenon. The ATR mode of spectra acquisition involves passing the IR beam through an internal reflection element IRE), usually an IR-transparent element) with a high refractive index diamond crystal. ATR-FTIR spectra were obtained using an Alpha-T Bruker (Germany) spectrometer in the transmission mode with 50 scans per minute and 2 cm^{-1} resolution, using a diamond crystal ATR accessory at an incident angle of 45^o. A sample size of 6 mm x 6 mm of AmCot and AmCot functionalized by the NPs and NCPs was placed under the ATR accessory, and the optimum force between the sample and ATR crystal accessory was optimized to obtain the transmission spectrum.

3.4.1.2 Micro-Raman Spectroscopy

Micro-Raman spectroscopy is based on an intrinsic material property and measures carbonaceous compounds in Raman active materials. Raman spectroscopy uses inelastic scattered monochromatic light (usually visible wavelength laser light whose frequency is mainly close to the infrared or ultraviolet range) to probe the vibrational energy levels of chemical bonds. It is based on the stress (strain) sensitivity of most Raman vibrational modes in crystalline phases. The difference in energy between the incident photon and the Raman scattered photon equals the energy of the vibration of the scattering molecule. The scattered light is analyzed to get information about specific molecular vibrations that alter because of the stress state of the material. A Raman spectrum is produced by plotting the scattered light intensity against the energy difference. Raman spectroscopy was utilized to study the vibrational properties of AmCot, and AmCot functionalized by the NPs and NCPs using a micro-Raman spectrometer (HORIBA, France) coupled to a charge-coupled device (CCD) detector in the 100–1800 cm^{-1} range. He–Ne laser excitation source was used and operated at λ = 633 nm at 20 mW (power 100%).

3.4.2 X-ray Diffraction (XRD) Pattern

X-ray diffraction is based on constructive interference of monochromatic X-rays and a crystalline sample. These X-rays are generated by a cathode ray tube, filtered to produce monochromatic radiation, collimated to concentrate, and directed toward the sample. The interaction of the incident rays with the sample produces constructive interference (and a diffracted ray) when conditions satisfy Bragg's law ($n\lambda=2d \sin\theta$). An X-ray diffractometer (XRD-7000 X-ray Diffractometer Shimadzu, Japan) using Cu k-alpha radiation (k = 1.54060 Å) was used to analyze the crystalline structure of AmCot functionalized with NPs and NCPs. The instrument was calibrated with a silicon standard by scanning between 10° and 80° with a step size of 0.03º and a dwell time of 0.5 seconds. The fabrics functionalized with NPs and NCPs were folded to fit into the cavities of the aluminum sample holders and pressed with a glass slide to flatten them. Then, the samples were scanned similarly to the standard. The average particle crystalline size of the deposited NPs and NCs on AmCot fabrics was calculated using the Debye-Scherrer equation (Eq. 1):

$$D = \frac{K\lambda}{\beta cos\theta} \quad \text{..... (Eq. 1)}$$

Where λ is the wavelength of the X-ray radiation (Cu Kα= 0.15418 nm), K is the constant, taken as 0.89, β is the line width at half-maximum height, and θ is the diffracting angle.

3.4.3 X-Ray Photoelectron Spectroscopy (XPS)

X-ray photoelectron spectroscopy (XPS) is a surface-sensitive, non-destructive technique used routinely to analyze natural and engineered materials' outermost ~10 nm (~30 atomic layers). XPS is usually used to determine the composition of material surfaces (elemental identification), the relative abundances of these components on surfaces (semi-quantitative analysis), and the chemical state of polyvalent ions by measuring the binding energies of elements, which is related to the nature and strength of their chemical bonds. Element binding energy analysis of AmCot functionalized with NPs and NCPs was performed on an X-ray photoelectron spectrometer (Kratos Axis Ultra DLD, UK) using a monochromated Al Kα (hν=1486.6 eV) X-ray source and scanning area 300 μm x 700 μm. XPS analysis occurs in a vacuum, and Amcot functionalized samples were cut into 1 × 1 cm^2 to fit on the sample holder using desk scissors. The AmCot samples were mounted on the sample holder using tape. The operating pressure of the chamber was maintained at 10^{-10} mbar.

3.4.4 Morphology by Scanning Electron Microscopy (SEM) and Transmission Electron Microscopy (TEM)

SEM is useful for obtaining a three-dimensional image of a sample's surface and viewing large objects. Specimens are imaged with a beam of electrons scanned over a sample's surface to create an image of the surface with exceptional depth of field. This image is achieved by detecting secondary electrons released from the specimen. It is scanned by very high-energy primary electrons (i.e., those emitted from the electron gun in the SEM). A scanning electron microscope (FEI Quanta FEG 250 SEM with EDX, Thermo Fisher) operating at an accelerating 5–12 kV voltage was used to study the morphology of AmCot, and AmCot functionalized with NPs and NCPs. Energy-dispersive X-ray microanalysis (EDX) was carried out for elemental analyses in mapping mode. The samples were mounted on the stubs of the metal sample holder using holey carbon tape and sputter coated with ~60 nm of Palladium and then observed in the

microscope. A Hitachi H-7600 field-emission transmission electron microscope with an operating voltage of 200 kV was used to examine a CuO NP cluster and its size on the selected AmCot+CuO.

3.4.5 Performance Properties

3.4.5.1 Optical Properties

The optical properties of AmCot and AmCot functionalized by NPs and NCPs were recorded on a UV-Vis-DRS spectrophotometer (UV 3600 PLUS, SHIMADZU, Japan) in the 200-800 nm wavelength range and a scan rate of 7 nm/s per using $BaSO_4$ as the reflectance standard. The ultraviolet protection factor (UPF) was evaluated to ascertain the UV shielding ability of AmCot and AmCot functionalized by NPs and NCPs according to AS-NZS 4399:1996. Each evaluation was done in triplicate, and the results were reported as average. The equation (Eq. 2) used to calculate the UPF is as follows.

$$\frac{\sum_{280}^{400} \mathrm{E}\lambda \; \mathrm{x}\mathrm{S}\lambda \; \mathrm{x} \; \Delta\lambda}{\sum_{280}^{400} E\lambda \mathrm{x}\mathrm{T}\lambda \mathrm{x}\mathrm{S}\lambda \mathrm{X}\Delta\lambda} \quad \text{..... (Eq. 2)}$$

Where Sλ is the spectral irradiation of the skin, Eλ is the erythemal spectral effectiveness, Tλ - is the spectral transmittance of the materials, and Δλ is related to increment wavelength in (nm).

3.4.5.2 Antibacterial Activity

3.4.5.2.1 Qualitative Antibacterial Activity Assay

The qualitative assessment of the antibacterial activity of AmCot and AmCot functionalized with NPs and NCPs was conducted using Mueller Hinton Broth (MHB, SRL 49550), according to the AATCC 147 test method (Pinho *et al.*, 2011). Agar media that had been sterilized was placed into Petri dish plates and given time to solidify. Freshly cultivated broth containing Gram-negativee *E. coli* and Gram-positive *S. aureus* bacteria species ($1x10^8$ CFU ml^{-1}, colony-forming units) were streaked (~ 6 cm) on the plates and incubated at 37 ºC for 12 hours. UV sterilized AmCot and AmCot functionalized with NPs and NCPs were applied on the parallel streaks. The Petri dishes were examined for the zone of inhibition after 24 hours of incubation at 37 ºC.

3.4.5.2.2 Antibacterial Wash Durability

The antibacterial activity of AmCot and AmCot functionalized with NPs and NCPs were assessed for wash cycle durability against Gram-negativee *E. coli* and *P. aeruginosa* and Gram-positive *S. aureus and S. pyogenes* bacteria species according to the AATCC 100 2021 test method after every 10 wash cycles up to a total of 50 wash cycles (Xu *et al*., 2016). Each wash cycle was performed in 5 g L^{-1} aqueous liquid detergent solution at 45 ºC for 15 min and 150 rpm. The nutrient agar media was poured into a Petri dish. 100 µL of each bacteria stock with an estimated 1 x 10^8 colony forming units (CFU/ml) were uniformly dispersed on the Petri-dish containing agar media.

Before examining the antibacterial activity, the samples were subjected to UV sterilization. Each functionalized fabric, approximately 6 mm in diameter, was evaluated against a known concentration of bacterial suspension (1x10^8 CFU/ml) plated on Petri dishes and then incubated at 37 ℃ for 24 hours. The zone of inhibition diameter was measured.

3.4.6 Water Absorbency and Water Vapor Permeability

3.4.6.1 Water Absorption

Water absorption of AmCot and AmCot functionalized by NPs and NCPs was determined according to BS 3449: 1990 (Badr and El Nahrawy, 2020). The difference in the weight of the samples before and after soaking in excess DI water for 10 min and hanging them out for another 10 min was recorded. Each sample was evaluated in triplicate, and the average values were reported.

3.4.6.2 Water Vapor Permeability

The open cup test method was used to measure the water vapor permeability according to ASTM E96 (Mustapha *et al*., 2020) of AmCot and AmCot, functionalized by NPs and NCPs. The fabrics were tightly positioned over a shallow dish filled with DI water. Water vapor permeability was estimated using the weight loss of the test assembly over 24 hours, and the vapor transmission rate was reported as g/m^2/day.

CHAPTER 4

Results and Discussion

4.1 Functional Group Analysis by ATR-FTIR

Figure 11(a-c) illustrates the ATR-FTIR spectra of Cot, AmCot, and AmCot functionalized with the NPs and NCPs.

Figure 11a illustrates the spectra of Cot and AmCot. While both spectra show the typical bands of cotton, the spectrum of AmCot exhibits two additional bands at 1730 and 1560 cm-1, attributed to the stretching vibrations of the carbonyl (C=O) and the amine (NH_2) groups, respectively (Xu *et al*., 2018; Xu *et al*., 2019; Xu *et al*., 2021). These bands infer that the esterification reaction occurs between the COOH groups of Am and the OH groups of cellulose of the cotton fabric. Previous research (Xu *et al*., 2019; Hassabo *et al*., 2019) has shown similar bands in the spectra of cotton modified by chitosan, imine, and other amino acids. In both the spectra, the broad band centered at 3331 cm^{-1} is attributed to the stretching vibrations of intra and intermolecular hydroxyl (OH) groups in cellulose and adsorbed water (Hina *et al*., 2018; Tomczak *et al*., 2007). The band at 2897 cm^{-1} is due to the stretching vibration of C-H in cellulose and hemicellulose (Satyanarayana, 2007). The fabrics' hydrophilicity is responsible for water absorption on its surface, and the band at 1623 cm^{-1} is attributed to absorbed water in the fibers (Sizeland *et al*., 2018; Mai *et al*., 2010). The band at 1431 cm^{-1} is associated with the CH_2 symmetric bending of cellulose (Rotaru *et al*., 2018; Rabbi *et al*., 2019; Chung *et al*., 2004). The bands at 1359 and 1318 cm^{-1} are attributed to the bending vibrations of the C-H and C-O groups in cellulose polysaccharides, respectively (Devnani & Sinha, 2019; Tomczak *et al*., 2007; Chung *et al*., 2004). The C-O and O-H stretching vibrations in cellulose are at 1029 cm^{-1}, and the band at 897 cm^{-1} is due to β-glycosidic connections between monosaccharides. Furthermore, a comparison of the spectra of Cot and AmCot indicated that the modification by Am did not cause any chemical structural changes to the cotton fabric (Zhou *et al*., 2019).

The spectra of AmCot functionalized with Ag, CuO, ZnO, and TiO_2 NPs are illustrated in Figure 11b. All the spectra display the typical bands of AmCot, as seen in Figure 11a, with additional bands indicating the presence of the NPs. The spectrum of AmCot+AgO shows an additional band at 1381 cm^{-1}, attributed to Ag-O stretching, confirming the presence of Ag NPs on the

surface of AmCot, in agreement with previous literature on Ag NPs on soft substrates, particularly textiles (Devaraj *et al*., 2013; Elango *et al*., 2018). In the spectra of AmCot+CuO NPs, additional bands at 550 and 546 cm^{-1} are observed, which are due to Cu-O stretching, confirming the deposition of CuO NPs on the cotton fabric (Faisal *et al*., 2013; Elango *et al*., 2018). The additional bands at 661 and 611 cm^{-1} in the spectra of AmCot+ZnO are attributed to Zn-O vibration modes, confirming the deposition of ZnO NPs on the fabric (Busila *et al*., 2015; Boticas *et al*., 2019). Similarly, the spectrum of AmCot+TiO_2 shows an additional band at 594 cm^{-1}, attributed to the vibration mode of the Ti-O-O bond (Rajakumar *et al*., 2012; Hou *et al*., 2005).

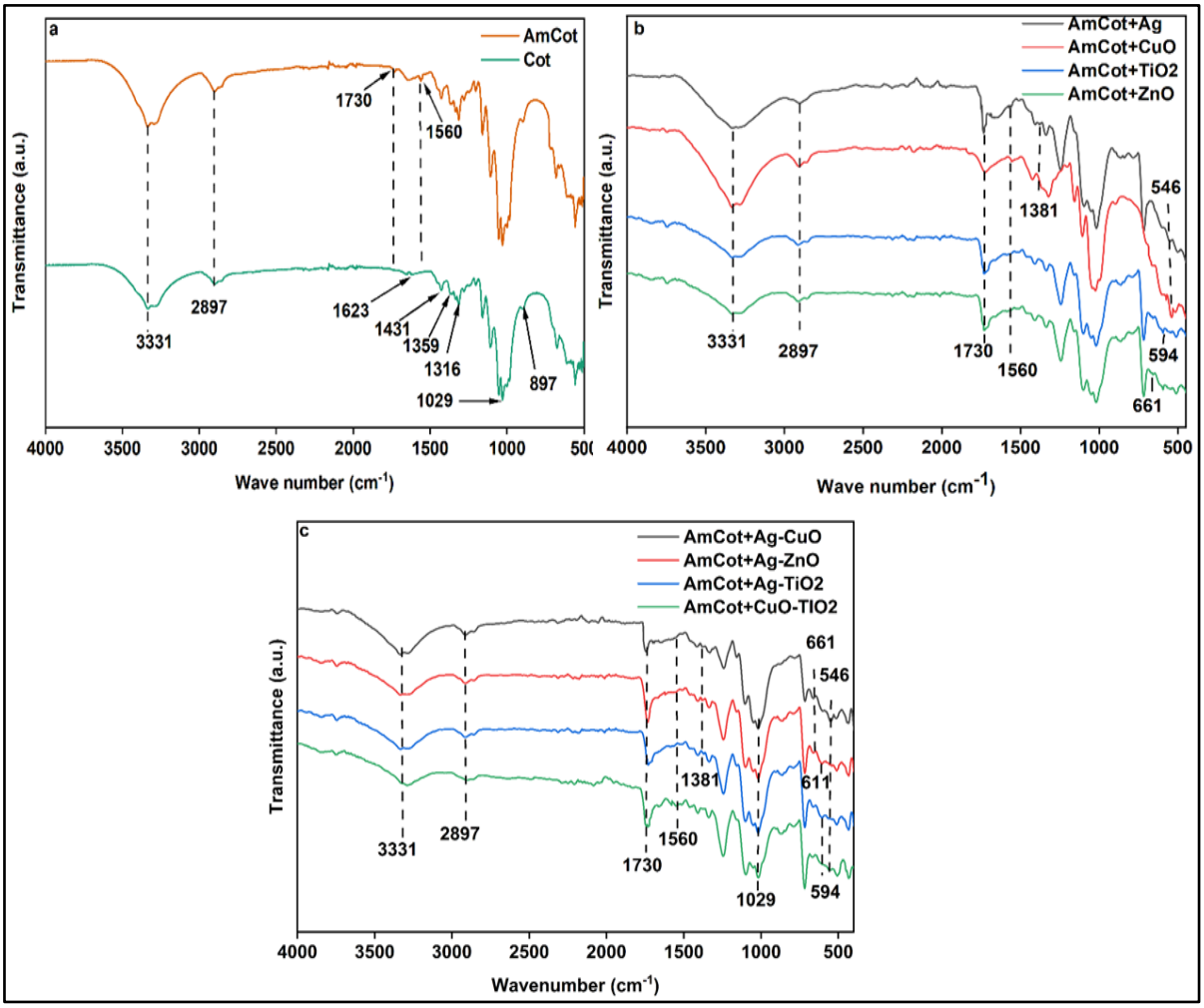

Figure 11. ATR- FTIR spectra of (a) Cot and AmCot, (b) AmCot functionalized by NPs, and (c) AmCot functionalized by NCPs.

Figure 11c illustrates the spectra of AmCot functionalized with Ag-CuO, Ag-ZnO, Ag-TiO_2, and CuO-TiO_2 NCPs. All spectra display the typical bands of AmCot (Figure 11a) and additional bands indicating the deposition of the NCPs. In the spectrum of AmCot+Ag-CuO, the deposition of Ag NPs and CuO NPs on the fabric is evident by additional bands at 1381 and 546 cm^{-1} due to Ag-O and Cu-O bond stretching, respectively (Faisal *et a*l., 2013; Devaraj *et al*., 2013; Elango *et al*., 2018). Additional bands in the spectrum of AmCot+Ag-ZnO, at 1381 cm^{-1} and 661 and 611 cm^{-1}, are due to Ag-O and Zn-O bond stretching, which evidence the deposition of Ag NPs and ZnO NPs on AmCot (Devaraj *et al*., 2013; Elango *et al*., 2018; Busila *et al*., 2015; Boticas *et al*., 2019). In the spectrum of Am+Ag-TiO_2, the additional bands at 1381 and 594 cm-^{1}, ascribed to Ag-O and T-O-O bond stretching, evidence the deposition of Ag NPs and TiO_2 NPs on AmCot (Rajakumar *et al*., 2012; Hou *et al.*, 2005; Elango *et al*., 2018). Additional bands in the spectra of AmCot+CuO-TiO_2 at 546 and 594 cm^{-1}, due to Cu-O and Ti-O-O bond stretching, evidence the deposition of CuO NPs and TiO_2 NPs (Rajakumar *et al.*, 2012; Hou *et al*., 2005; Busila *et al*., 2015; Boticas *et al.*, 2019).

The spectrum of AmCot, functionalized *in situ* with NPs and NCPs, provides further evidence that the chemical structure of the modified cotton fabrics remains intact. This stability is a crucial factor in ensuring the durability of AmCot (Zhu *et al*., 2021; Xu *et al*., 2018; Zhou *et al.*, 2019).

4.2 Micro Raman Spectroscopy Analysis

The Raman spectra of AmCot and AmCot functionalized with Ag, CuO, ZnO, and TiO_2 NPs are illustrated in Figure12 (a-d), while the spectra of AmCot functionalized by the Ag-CuO, Ag-ZnO, Ag-TiO_2, and CuO-TiO_2 NCPs in Figure 13 (a-d)). All spectra exhibited characteristic bands of cotton.

In AmCot (Figure 12a), the bands for asymmetric COC glycosidic ring breathing and skeletal stretching were observed at 1095 cm^{-1} (asymmetric) and 1121 cm^{-1} (symmetric) (Kavkler & Demˇ, 2011; Was-Gubala & Machnowski, 2014). The Raman shift at 643 cm^{-1} is attributed to C-S stretching, confirming the esterification of the COOH amine groups with the OH groups of cellulose (Fateixa *et al*., 2016), and the 328 and 377 cm^{-1} bands are due to CCC ring deformation bending. Additionally, the bands at 438 and 458 cm^{-1} are associated with CCO ring deformation and skeletal bending (Kavkler and Demˇ, 2011; Was-Gubala and Machnowski, 2014).

In the AmCot+Ag spectrum (Figure 12b), the intense bands at 1614 and 1728 cm^{-1} are likely due to a strong electric field around the Ag NPs (Mabrouk *et al.*, 2021; Eskandari *et al.*, 2022). The bands at 1093 cm^{-1} (asymmetric) and 1123 cm^{-1} (symmetric) are attributed to the stretching vibrations of the symmetric and asymmetric COC glycosidic ring respiration and skeletal stretching, respectively (Kavkler and Demˇ, 2011).

In the spectrum of AmCot+CuO (Figure 12c), the bands at 1098 and 1120 cm^{-1} correspond to the COC glucosidic linkage due to skeletal stretching and asymmetric stretching, as well as the band between 1200-1500 cm^{-1} for CH_2 bending, rocking, and scissoring (Was-Gubala and Machnowski, 2014). The Raman shift at 643 cm^{-1} confirms the amine modification of the cotton fabric (Was-Gubala and Machnowski, 2014). No new bands were observed, indicating no chemical structural changes due to the deposition of CuO NPs onto AmCot (Chen *et al*., 2017; Ge *et al*., 2019).

In the AmCot+TiO_2 spectrum (Figure 12c), the bands at 1096 and 1117 cm^{-1} represent a shift in COC glucosidic linkage due to skeletal and asymmetric stretching (Was-Gubala and Machnowski, 2014). Except for a slight change in the intensity of the Raman shifts of AmCot, no significant chemical structural changes in the fabric were observed due to the functionalization of AmCot with TiO_2 NPs, as no new bands were formed.

In the AmCot+ZnO spectrum (Figure 12d), bands at 1094 cm-1 and 1112 cm^{-1} represent the COC unsymmetrical and symmetric stretching and a slight shift from 1121 cm^{-1} to 1112 cm^{-1} attributed to the effect of the morphology of the ZnO NPs deposited onto the surface of AmCot (Mabrouk *et al.*, 2021). Despite slight changes observed, the basic Raman bands of AmCot were not altered upon deposition of ZnO NPs onto the cotton fabric.

Figure 13 (a-d) shows that the Raman spectral bands of AmCot did not change after being functionalized with the NCPs. For instance, the spectrum of AmCot+Ag-CuO (Figure 13a) revealed that Ag-CuO NCPs did not affect the chemical structure of the modified cotton fabric. Similar observations were made in the spectra of AmCot+Ag-ZnO (Figure 13b), AmCot+Ag-TiO_2 (Figure 13c), and AmCot+CuO-TiO_2 (Figure 13d) (da Silva *et al*., 2021). Additionally, the spectra showed that the presence of the NCPs on the surface of AmCot did not change the chemical structure of AmCot in the short range (da Silva *et al*., 2021).

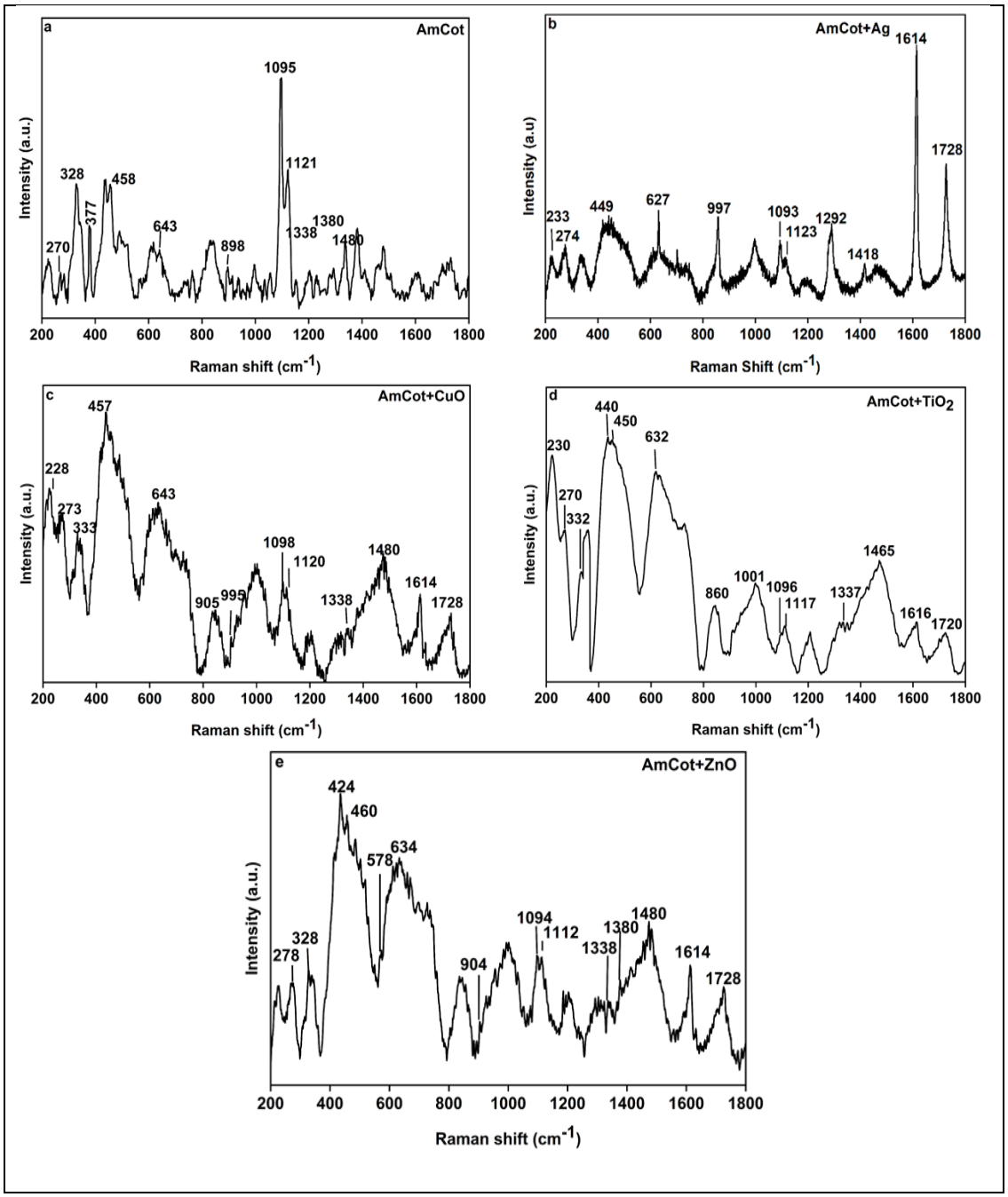

Figure 12. Raman spectra of (a) AmCot, (b) AmCot+Ag, (c) AmCot+CuO, (d) AmCot+TiO_2 and (e) AmCot+ZnO.

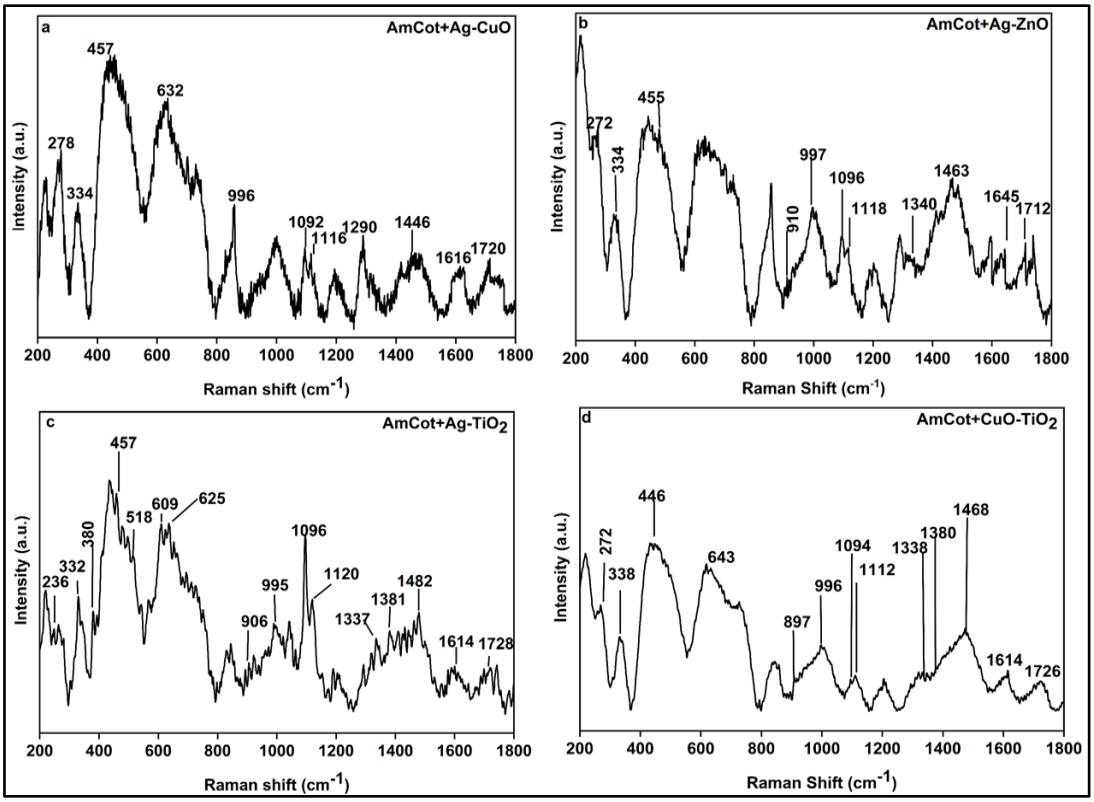

Figure 13. Raman spectra of (a) AmCot+Ag-CuO, (b) AmCot+Ag-ZnO, (c) AmCot+Ag-TiO_2 and (d) AmCot+CuO-TiO_2.

4.3 Structural Analysis

Figures 14 and 15 illustrate the XRD spectra of AmCot functionalized by NPs and NCPs, respectively, and Table 2 shows the average crystallite sizes.

Common to the diffraction patterns in Figures 14 and 15 are the peaks of cotton at diffraction angles (2θ) of 14.9^o, 16.6^o, 22.9^o and 34.4^o which are mapped to the (110), (101), (020), and (040) planes of cellulose I crystalline form, respectively (Klemm *et al*., 2005; Jiang *et al*., 2021) in agreement with ICDD 00–056–1718 (Jiang *et al*., 2021). Additional peaks observed correspond to the respective NPs and NCPs deposited on AmCot, indicating that only pure NPs were deposited on AmCot.

Figure 14a illustrates the XRD diffraction pattern of AmCot+Ag. The four diffraction peaks at 2θ 39.1^o, 44.0^o, 64.2^o, and 77.4^o correspond to the (111), (200), (220), and (311) planes of Ag, respectively, and confirm that the Ag NPs with face-centered cubic (FCC) crystalline planes in

agreement with JCPDS card no. 04-0783 (Hassanien, and Khatoon 2019; Fu *et al*., 2018). The average crystalline size of the deposited Ag NPs, using the Debye-Scherrer equation (Zhang *et al*., 2016), was approximately 30.0 nm (Table 2).

In the XRD pattern of AmCot+CuO (Figure 14b), two peaks were observed at 2θ values of approximately 35.5° and 38.8°, corresponding to the (-111) and (111) monoclinic crystalline planes of CuO in agreement with ICDD card no. 01-089-5899 (El-Nahhal *et al*., 2022; Paz-García*et al*., 2019; Fuku *et al.,* 2020). The absence of additional peaks indicated the purity of the CuO NPs deposited on AmCot. The average crystalline size of the NPs, using the Debye-Scherrer equation, was approximately 18 nm (Table 2).

In Figure 14c, the XRD pattern of AmCot+TiO_2 reveals the presence of five peaks at 2θ values of 36.06°, 41.24°, 56.5°, 63.44°, and 69.1°, which correspond to the (101), (111), (211), (002), and (301) planes of TiO_2, respectively. The TiO_2 NPs exhibit the rutile polymorph, which is the most stable form, and this matches well with JCPDS Card No: 21-1276 (Görgülüer *et al*., 2021). No peaks corresponding to the anatase or brookite polymorphs were observed (Roopan *et al*., 2012). According to the Debye-Scherrer equation, the average crystallite size of the nanoparticles was estimated to be approximately 30 nm (Table 2).

The XRD diffraction pattern of AmCot+ZnO (Figure 14d) shows six peaks at 2θ values of 31.76°, 34.37°, 36.13°, 47.7°, 56.6°, and 62.8°. These correspond to the (100), (002), (101), (102), (110), and (103) planes of the hexagonal wurtzite phase of ZnO, in line with ICCD card no. 01-079-0206 (Hatamie *et al*., 2015; Yogamala *et al*., 2009). According to the Debye-Scherrer equation, the average crystallite size of the NPs deposited onto AmCot was approximately 15.5 nm (Table 2).

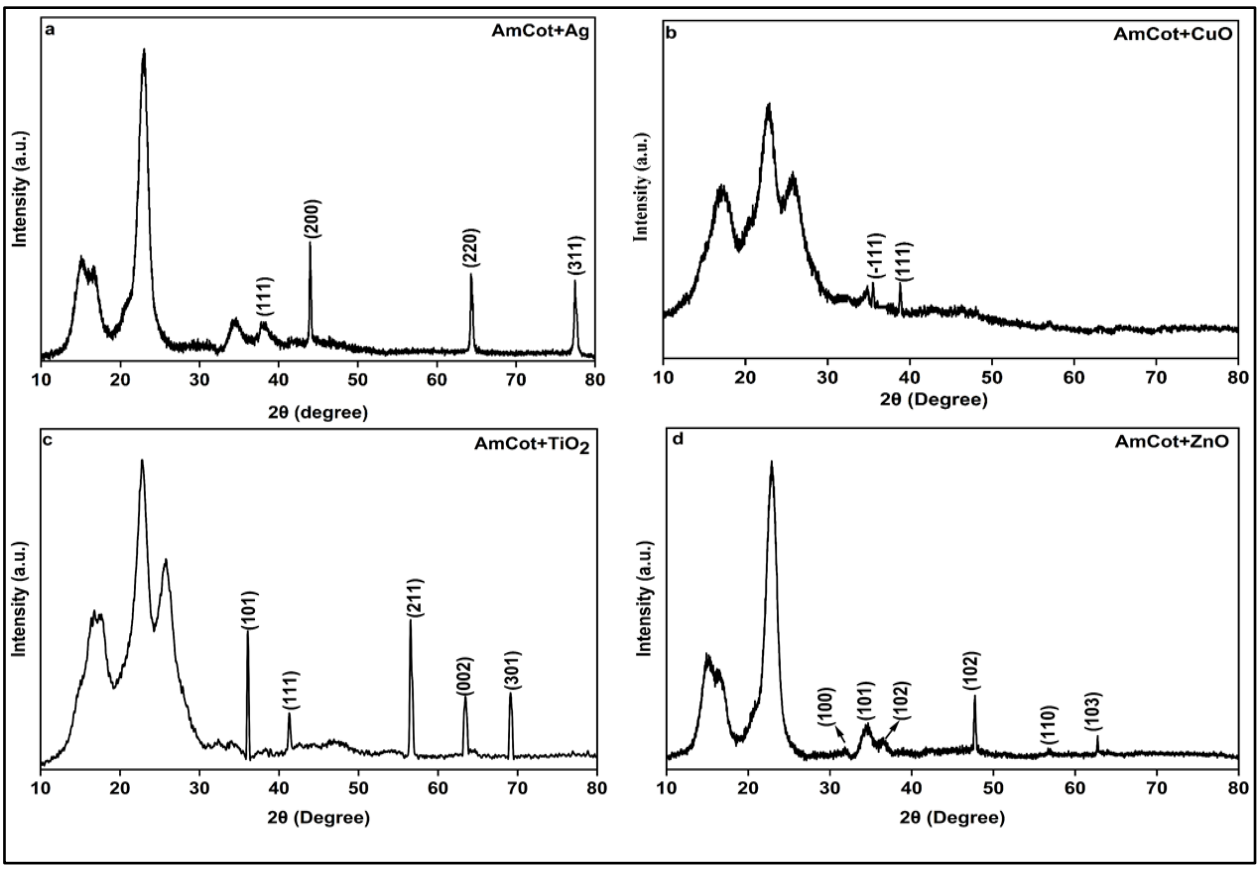

Figure 14. XRD patterns of (a) AmCot+Ag, (b) AmCot+CuO, (c) AmCot+TiO_2, and (d) AmCot+ZnO.

Table 2: Average crystalline size of Ag, CuO, TiO_2, and ZnO NPs on AmCot

Crystal plane	**2θ (º)**	**β (º)**	**D/nm**
Ag NPs on AmCot+Ag			
111	39.1	0.34	27.12
200	44.0	0.27	33.95
220	64.2	0.42	24.92
311	77.4	0.32	34.02
Average crystallite size			**30.1**
Crystal plane	**2θ (º)**	**β (º)**	**D/nm**
CuO NPs on AmCot+CuO			
-111	35.5	0.54	16.28
111	38.8	0.44	19.98
Average crystallite size			**18.13**
Crystal plane	**2θ (º)**	**β (º)**	**D/nm**
TiO_2 NPs on AmCot+TiO2			
101	36.06	0.31	28.16
111	41.24	0.44	20.16
211	56.5	0.24	39.27
002	63.44	0.38	25.68
301	69.1	0.27	37.33
Average crystallite size			**30.12**
Crystal plane	**2θ (º)**	**β (º)**	**D/nm**
ZnO NPs on AmCot+ZnO			
100	31.76	0. 68	12.88
002	34.37	0.57	15.30
101	36.13	0.49	17.82
102	47.7	0.53	17.12
110	56.6	0.69	13.66
103	62.8	0.58	12.47
Average crystallite size			**14.88**

Figure 15a illustrates the XRD pattern of AmCot+ Ag-CuO. The diffractogram shows four peaks at 2θ values of 39.1°, 44.4°, 64.4° and 77.6° corresponding to (111), (200), (220), and (311) planes of face-centered cubic Ag well matched to JCPDS card no. 04-0783 (Hassanien and Khatoon, 2019; Fu et al., 2018) and two not-so-intense peaks at 2θ values of 35.5o and

38.9o corresponding to (-111) and (111) planes of monoclinic crystals of CuO well matched with ICDD 01-089-5899. (El-Nahhal *et al.,* 2022; Paz-García *et al.,* 2019).The average crystalline sizes of the Ag and CuO NPs deposited on Amcot using the Debye-Scherrer equation were approximately 30 and 12 nm, respectively (Table 3).

The XRD pattern of AmCot+Ag-ZnO (Figure 15b) shows four peaks at 2θ values of 39.0°, 44.1°, 64.39°, and 77.54° corresponding to the (111), (200), (220), and (311) planes of face-centered cubic (FCC) crystalline planes of Ag in agreement with JCPDS card no. 04-0783 (Hassanien and Khatoon, 2019; Fu *et al*., 2018) and six peaks at 2θ values of 31.78º, 34.48º, 36.6º, 47.8º, 56.81º and 62.64º corresponding to the (100), (002), (101), (102), (110), and (103) crystal planes, respectively, of the wurtzite structure of ZnO well matched with ICCD card no. 01-079-0206 (Hatamie *et al*., 2015; Yogamalar *et al.,* 2009; Munir *et al.,* 2022). The average crystalline sizes of the Ag and ZnO NPs deposited on AmCot using the Debye-Scherrer equation were approximately 27 and 9 nm, respectively (Table 4).

Figure 15c illustrates the XRD pattern of AmCot+Ag-TiO_2. The diffractogram shows four peaks at 2θ values of 39.1°, 44.4°, 64.4°, and 77.6° corresponding to (111), (200), (220), and (311), respectively, of the FCC crystalline planes of Ag in agreement with JCPDS card no. 04-0783 (Hassanien and Khatoon, 2019; Fu *et al.,* 2018) and five peaks at 2θ values of 36.06°, 41.24°, 56.5°, 63.44° and 69.1° corresponding to the (101), (111), (211), (002) and (301) planes respectively of the rutile polymorph of TiO_2 well-matched to JCPDS card number 21-1276 (Görgülüer *et al*., 2021; Razak *et al.,* 2022; Arya *et al.,* 2021). The average crystalline sizes of the Ag and TiO_2 NPs deposited on AmCot using the Debye-Scherrer equation were approximately 17 and 22 nm, respectively (Table 5).

Figure 15d illustrates the XRD pattern of AmCot+ CuO-TiO_2. The two peaks at 2θ values of 35.5° and 38° correspond to the (-111) and (111) planes, respectively, of CuO's base-centered monoclinic crystal phase in close agreement with ICDD card no 01-089-5899 (El-Nahhal *et al.,* 2022; Paz-García *et al.,* 2019). Additionally, there are five other peaks at 2θ values of 36.06°, 41.24°, 56.5°, 63.44°, and 69.1°, which correspond to (101), (111), (211), (002), and (301) planes, respectively, of the rutile polymorph of TiO_2 (Görgülüer *et al.,* 2021; Razak *et al.,* 2022; Arya *et al.,* 2021).

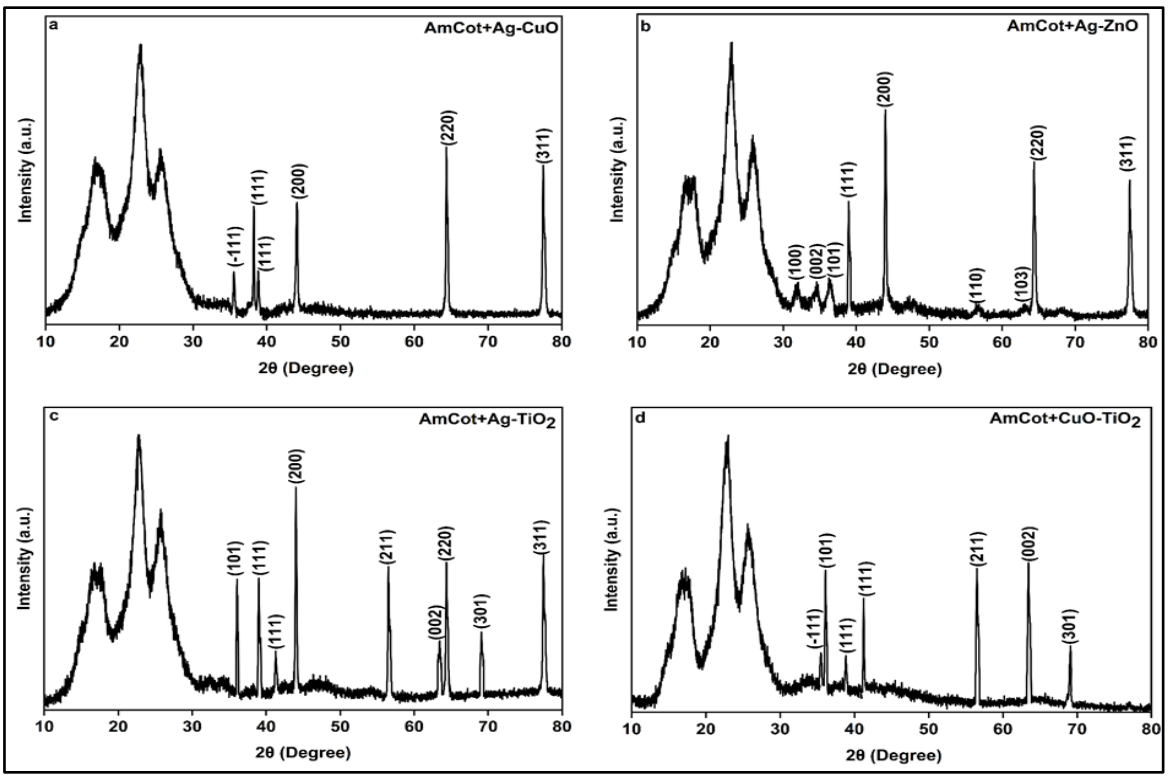

Figure 15. XRD patterns of (a) AmCot+Ag-CuO, (b) AmCot+Ag-ZnO (c) AmCot+Ag-TiO_2 and (d) AmCot+CuO-TiO_2.

Table 3: Average crystalline size of Ag and CuO NPs in AmCot+Ag-CuO

Crystal plane	**2θ (°)**	**β (°)**	**D/nm**
Ag NPs			
111	38.4	0.267	32.90
200	44.7	0.321	27.90
220	64.4	0.307	31.90
311	77.4	0.371	28.69
Average crystallite size			**30.34**
CuO NPs			
-111	35.5	2.63	3.5
111	38.8	0.44	20
Average crystallite size			**11.75**

Table 4: Average crystalline size of Ag and ZnO NPs in AmCot+Ag-ZnO

Crystal plane	**2θ (°)**	**β (°)**	**D/nm**
Ag NPs			
111	38.4	0.403	21.81
200	44.7	0.280	31.93
220	64.4	0.338	28.98
311	77.4	0.406	26.25
Average crystallite size			**27.24**
Crystal plane	**2θ (°)**	**β (°)**	**D/nm**
ZnO NPs			
100	31.76	0.87	9.92
002	34.37	1.64	5.30
101	36.13	0.94	9.29
102	47.7	0.98	9.26
110	56.6	0.78	11.93
103	62.8	1.05	9.26
Average crystallite size			**9.16**

Table 5: Average crystalline size of Ag and TiO_2 NPs in AmCot+Ag-TiO_2

Crystal plane	**2θ (°)**	**β (°)**	**D/nm**
Ag NPs			
111	39.1	0.39	22.59
200	44.4	0.95	9.44
2 2 0	64.4	0.88	11.15
311	77.6	0.44	24.21
Average crystallite size			**16.85**
Crystal plane	2θ (°)	β (°)	D/nm
TiO_2 NPs			
101	36.06	0.59	14.83
111	41.24	0.46	19.28
211	56.5	0.25	37.70
002	63.44	0.52	18.77
301	69.1	0.46	21.91
Average crystallite size			**22.50**

Table 6: Average crystalline size of CuO and TiO_2 NPs in AmCot+CuO-TiO_2

Crystal plane	2θ (°)	β (°)	D/nm
CuO NPs			
-111	35.5	1.05	8.31
111	38.8	0.45	19.56
Average crystallite size			**18.09**
Crystal plane	**2θ (°)**	**β (°)**	**D/nm**
TiO_2 NPs			
101	36.06	0.29	30.10
111	41.24	0.47	18.87
211	56.5	0.20	47.12
002	63.44	0.41	24.40
301	69.1	0.24	42.08
Average crystallite size			**32.51**

4.4 X-ray photoelectron spectroscopy (XPS) Analysis

Figures 16-20 illustrate the XPS spectra of selected functionalized cotton fabrics, AmCot+Ag, AmCot+Ag-CuO, AmCot+Ag-ZnO, AmCot+Ag-TiO_2, and AmCot+CuO-TiO_2.

Figure 16a illustrates the XPS spectrum of AmCot+Ag in wide, displaying the presence of Ag, carbon (C), oxygen (O), sulfur (S), and nitrogen (N). By deconvolution of the C 1s spectrum (Figure 16b), the four peaks with binding energies of 284.47, 286.2, 287.68, and 288.14 eV are attributed to C-C, C-OH, C-S, and C-O-C, respectively (Xu *et al*., 2018; Topalovic *et al*.,2007). The peak at 287.68 eV, corresponding to the C-S bond, indicates ester formation between the COOH groups of Am and OH groups of the cellulose of AmCot. The other peaks originate from the cotton fabric due to the presence of sp^3 carbon. In Figure 16c, the high-resolution spectrum of Ag 3d exhibits two peaks with binding energies of 368.07 and 374.15 eV corresponding to Ag 3d5/2 and Ag 3d3/2, respectively, with a spin-orbit separation of 6.0 eV (Cong *et al*., 2014; Zhou *et al*., 2018; Kwak *et al*., 2015; Zheng *et al*., 2008). The Ag 3d5/2 and Ag 3d3/2 peaks are characteristic of Ag^0 species, indicating that the NPs on AmCot are metallic Ag NPs. The high-resolution spectrum of S 2p (Figure 16d) displays two peaks. The first peak, with a binding

energy of 161.48 eV (S 2p3/2), corresponds to the strongly de-electronated state of the S element, suggesting coordination bonding between S atoms on AmCot and Ag atoms (Secchi *et al*.,2019; Méthivier *et al*., 2015; Battocchio *et al*.,2014). The second S 2p peak with binding energy 165.29 eV (S 2p1/2) corresponds to the S-C bonds formed due to the esterification reaction between the COOH groups of Am and the OH groups of cellulose of Cot (Méthivier *et al.*, 2015). The absence of a peak with a higher binding energy of 168.1 eV verifies the absence of oxidized sulfur species (SOx) (Wang *et al.*, 2021). The binding of Ag atoms with O and N donor atoms also participates in additional coordination binding (Méthivier *et al.*, 2015). According to the literature, the corresponding reference peaks of O 1s and N 1s in Am with binding energies of 401.1 eV (NH_3^+ ions), 532.0 eV (O atom in O=C-O**H bonds), and 532.0 eV (oxygen in O**=C-OH bonds), respectively (Artemenko *et al*., 2021; Zeng *et al*., 2015; Yang *et al*., 2018). Stronger binding of Ag with O and N than with S is indicated by the shift of the O 1s peak towards a lower binding energy from 532.0 to 531.01 eV and the N 1s peak from 401.1 to 399.3 eV [Figure 16 (e, f)], respectively, (Prieto *et al.*, 2012; Méthivier *et al.*, 2015).

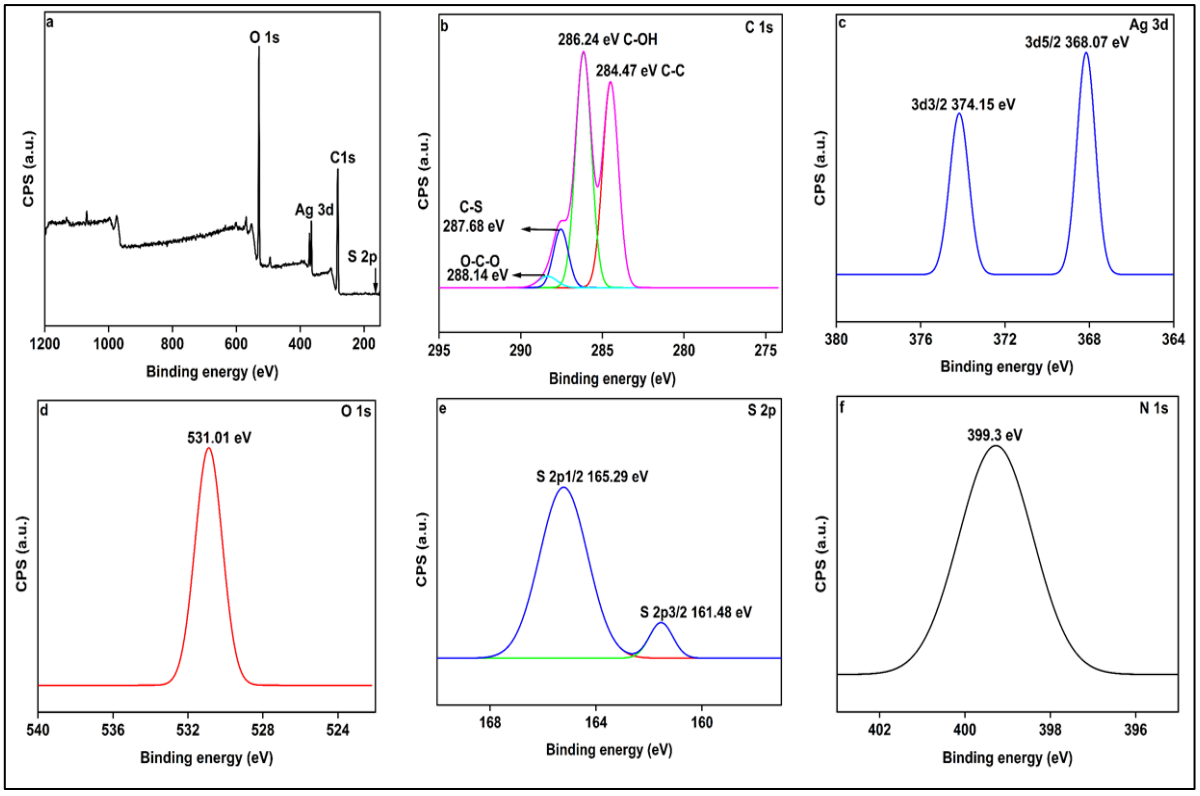

Figure 16. XPS spectra of AmCot+Ag (a) survey, (b) C 1s, (c) Ag 3d, (d) O 1s, (e) S 2p, and (f) N 1s.

Figure 17a illustrates the XPS spectrum of AmCot+Ag-CuO in wide, showing the elements Ag, Cu, C, O, S, and N. The high-resolution spectrum of C 1s in Figure 17b shows four peaks with binding energies of 284.3, 286.1, 287.3, and 288.5 eV corresponding to C-C, C-OH, C-S, and C-O-C bonds which originate from aliphatic carbon (sp^3) in the cellulose of Cot (Xu *et al*., 2017; Xu *et al.,* 2019; Zhou *et al.,* 2018) and C-S bond formed by the esterification reaction between the COOH groups of Am and OH groups of cellulose of Cot (Secchi *et al.,* 2019; Battocchio *et al.,* 2014). The high-resolution Ag 3d spectrum shows two peaks with binding energies of 366.65 eV (3d5/2) and 372.65 eV (3d3/2), with a spin-orbit coupling difference of 6.0 eV, indicating the deposition of pure metallic Ag^0 on the surface of AmCot (Zhou *et al.* 2018; Parvathiraja and Shailajha, 2021; Kwak *et al.,* 2015). In Figure 17d, the high-resolution Cu2p spectrum (Figure 17d), two prominent peaks with binding energies of 934.42 eV for Cu 2p3/2 and 954.85 eV for Cu 2p1/2, with a splitting difference of 20.43 eV between the peaks confirm that a Cu^{2+} state is formed, indicating that CuO NPs were deposited onto AmCot (Shaheen *et al.,* 2021; Siddiqui *et al.,* 2020; Ghodselahi *et al.,* 2008).

CuO NP deposition is further supported by the O 1s peak with a binding energy of 531 eV (El-Nahhal *et al.,* 2018). The formation of coordination bonds between Ag atoms and Cu (110) with Am is evidenced by the first peak with a binding energy of 161.5 eV (S 2p3/2) (Figure 17e), which corresponds to the highly de-electronated state of the S element in the S 2p spectrum and S-C bonds are responsible for the second peak with binding energy of 165.3 eV (Méthivier *et al.,* 2015). Ag binds stronger with O and N than with S (Méthivier *et al.,* 2015), as indicated by the shift of the O 1s peak towards a lower binding energy from 532.0 to 531.4 eV and of the N 1s peak from 401.1 to 399.93 eV [Figure 17(f, g)].

The XPS spectrum of AmCot+Ag-ZnO in wide (Figure18a) shows the peaks for the elements carbon (C 1s), silver (Ag 3d), zinc (2p), and sulfur (S 2p), oxygen (O1s) and nitrogen (N 1s). In the spectrum of C1s (Figure 18b), there are four peaks with binding energies of 284.7, 286.4, 287.8, and 288.1 eV corresponding to C-C, C-C-OH, C-S, and C-O-C bonds, respectively (Xu *et al.,* 2017; Xu *et al*., 2019; Zhou *et al.,* 2018). Figure 18c shows two peaks with binding energies of 1021.97 and 1044.85 eV corresponding to Zn 2p3/2 and Zn 2p1/2, respectively, indicating that Zn deposited onto AmCot was in the Zn^{2+} ionic form confirming the deposition of ZnO NPs onto AmCot.

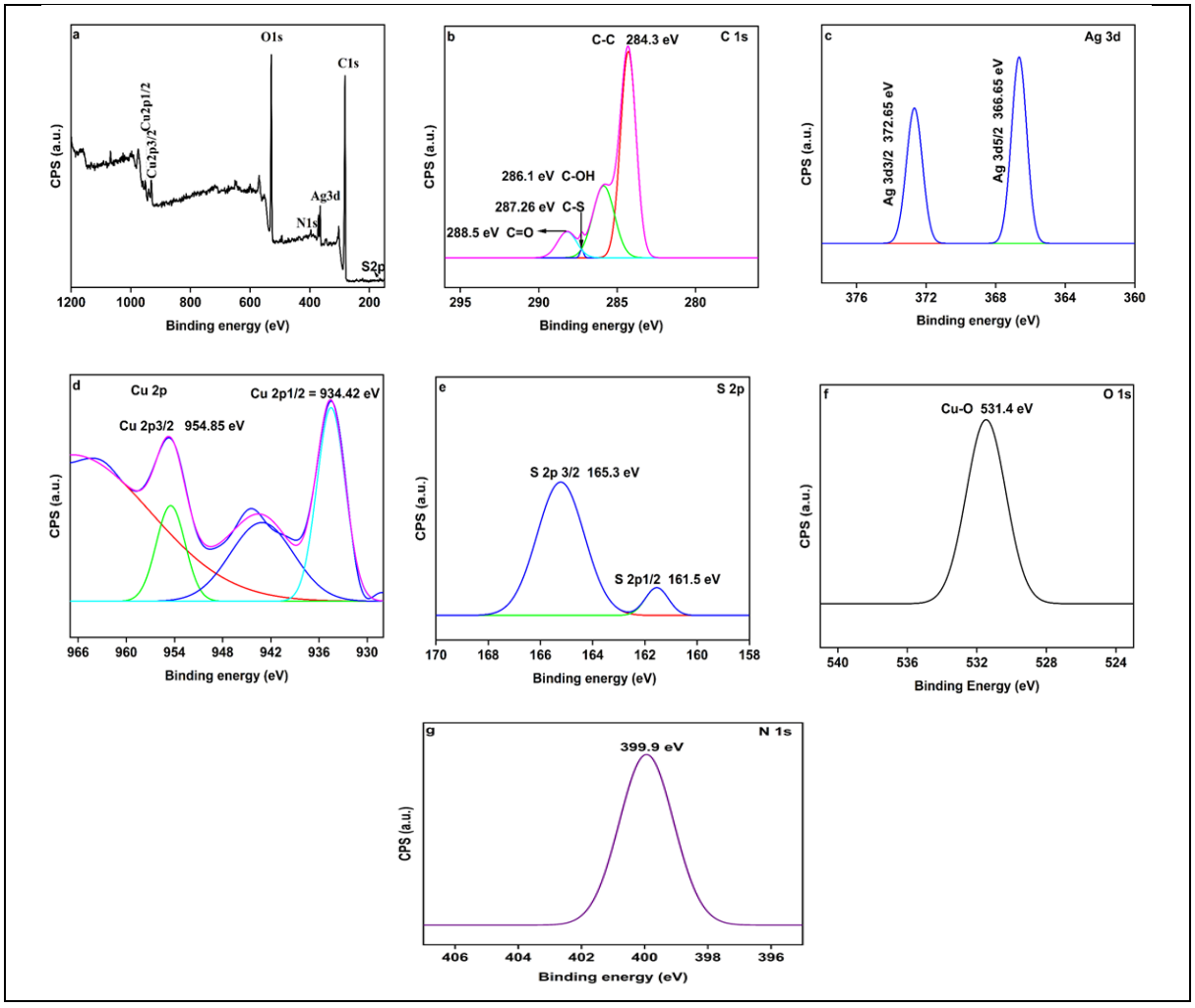

Figure 17. XPS spectra of AmCot+Ag-CuO (a) in wide, (b) C 1s, (c) Ag 3d, (d) Cu2p, (e) S 2p, (f) O 1s, and (g) N 1s.

The spin-orbit splitting of 22.88 eV between these two peaks was for the photoelectrons produced from Zn^{+2} ions in the ZnO crystal lattice (Gan *et al.*, 2015; Liang *et al.*, 2015). Figure 18d shows the Ag spectrum with two peaks with binding energies of 365.1 eV (3d5/2) and 371.1eV(3d3/2), with a 6.0 eV spin-orbit slitting difference between the peaks indicating the presence of metallic Ag^0 on the surface of AnCot (Parvathirajaand and Shailajha, 2021; Xu *et al.*, 2018). The minor shifts in binding energies compared to bulk Ag (368.3 eV for 3d3/2 and 374.3 eV for 3d1/2) are due to electron transfer from Ag^0 NPs to ZnO NPs (Zheng *et al.*, 2008; Das *et al.*, 2010). In the Zn-O bonding of the wurtzite structure of the ZnO NPs, the O^{2-} ions are responsible for the O 1s peak (Figure 18e), which has a binding energy of 530.4 eV (Das *et al.*, 2010).

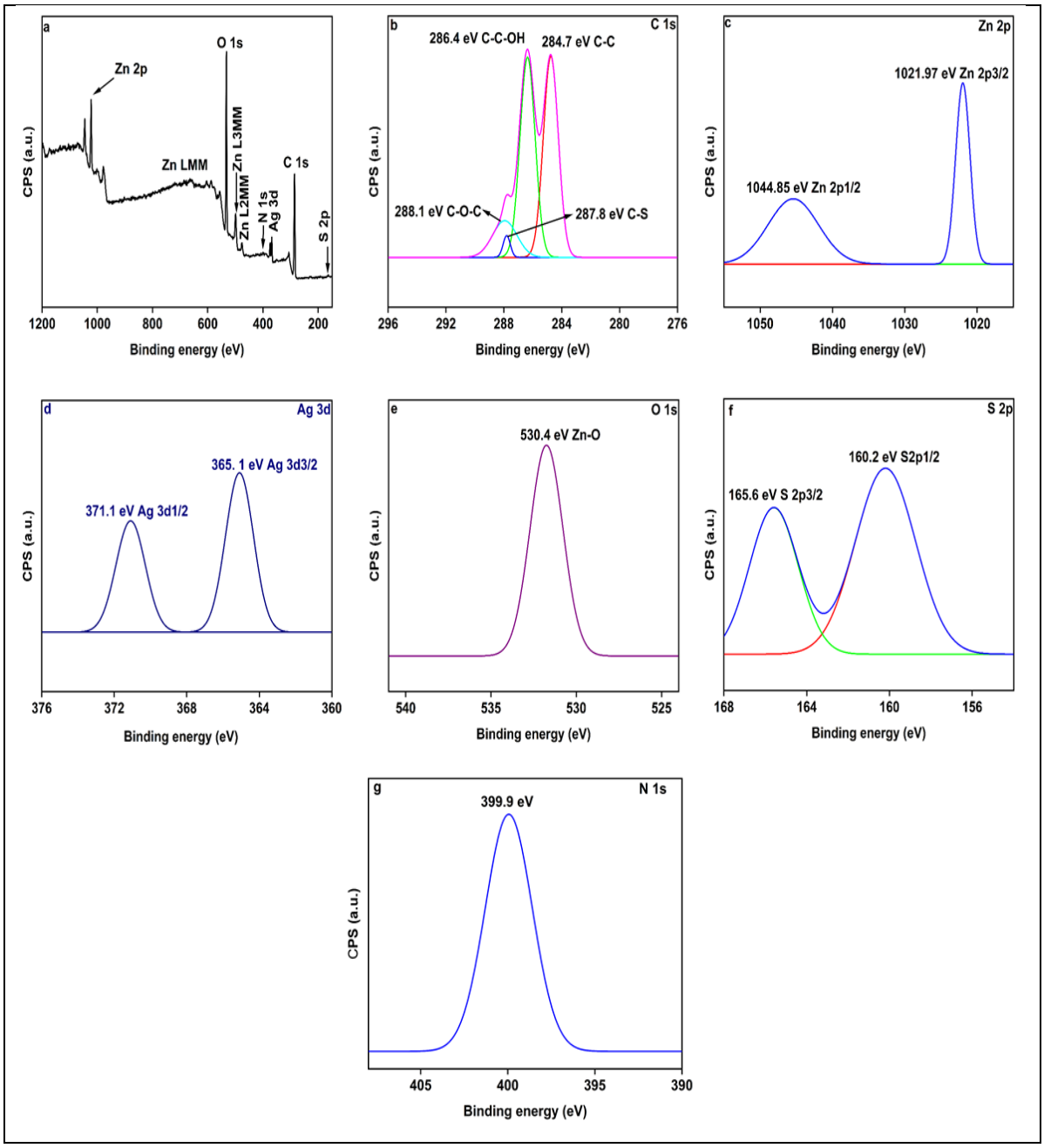

Figure 18. XPS spectra of AmCot+Ag-ZnO (a) in wide, (b) C 1s, (c) Zn 2pd, (d)Ag 3d, (e) S 2p, (f) O 1s and (g) N 1s.

The high-resolution spectrum of S 2p at high resolution (Figure 18f) indicates that coordination bonds are formed between Ag atoms in Ag NPs and Zn^{2+} ions in ZnO NPs with S, as seen from the S 2p3/2 peak with a binding energy of 160.2 eV, corresponding to the strongly de-electronated state of S (Secchi *et al.*, 2019; Méthivier *et al.*, 2015; Battocchio *et al.*, 2014). The

second peak with a binding energy of 165.6 eV (S 2p1/2) results from the S-C bonds (Méthivier *et al.*, 2015). Figures 18(f,g) show that the O 1s peak shifts towards lower binding energy from 532.0 to 531.01 eV, inferring stronger binding between Zn^{+2} ions and O (Morozov *et al.*, 2015) and that the N 1s peak shifts from 401.1 to 399.9 eV, again indicating stronger binding of Zn^{+2} ions with N rather than S atoms (Elbadawy *et al.*, 2022).

Figure 19a illustrates the XPS spectrum of AmCot+Ag-TiO_2 in wide, showing peaks corresponding to carbon (C 1s), silver (Ag 3d), titanium (Ti 2p), sulfur (S 2p), oxygen (O1s), and nitrogen (N 1s). In the deconvoluted high-resolution spectrum of C 1s (Figure 19b), there are three peaks with binding energies of 284.28, 286.1, and 288.01 eV, corresponding to C-C, C-OH, and O-C-O bonds, respectively, formed by the C bonding in the cellulose of AmCot. The deconvoluted high-resolution spectrum of Ag 3d (Figure 19c) shows two peaks with binding energies of 366 and 372 eV, corresponding to Ag 3d5/2 and Ag 3d3/2, respectively (Cong *et al*., 2014; Zhou *et al.*, 2018; Kwak *et al*., 2015; Zheng *et al.*, 2008). The spin-orbit coupling difference in the 3d doublet of 6.0 eV confirms that the produced Ag NPs were metallic Ag^0, and no peaks corresponding to Ag_2O (367.8 eV) or AgO (367.4 eV) are evidenced (Mai *et al.*, 2010).

The core levels of Ti 2p1/2 and Ti 2p3/2 at high-resolution (Figure 19d) with binding energies of 464.1 and 458.6 correspond to Ti^{4+} ions in the rutile phase of TiO_2 NPs (Yu *et al*., 2011). The 2p doublet slitting difference of 5.7 eV in the spin-orbit coupling agrees with the literature for the deposition of TiO_2 NPs (Li *et al*., 2017; Li *et al.*, 2015). In the deconvoluted spectrum of S 2p (Figure 19e), the peak with binding energy 160.5 eV (S 2p3/2) corresponds to the strongly de-electronated state of the S element, inferring the formation of coordination bonds between Ti and Ag atoms with the S of Am (Secchi *et al.*, 2019; Méthivier *et al.*, 2015; Battocchio *et al*., 2014). The second peak of binding energy, 165.5 eV (S 2p1/2), corresponds to the S-C bonds formed by the esterification reaction between the COOH groups of Am and the OH groups of cellulose in AmCot (Méthivier *et al.*, 2015). The deconvoluted spectrum of O 1s (Figure 19f) shows two peaks with binding energies of 531.1 and 533 eV. The first peak with a binding energy of 531.1 eV corresponds to Ti-O, and the second peak with a binding energy of 533 eV corresponds to O-Ti-O (Parvathiraja and Shailajha, 2021). The shift of the O 1s peak to lower binding energy from 532.0 to 531.4 eV and of the N 1s peak (Figure 19g) from the binding

energy of 401.1 to 399.3 eV indicates that Ag atoms and Ti^{+4} bind to O and N more strongly than to S (Prieto *et al.*,2012; Méthivier *et al.*, 2015).

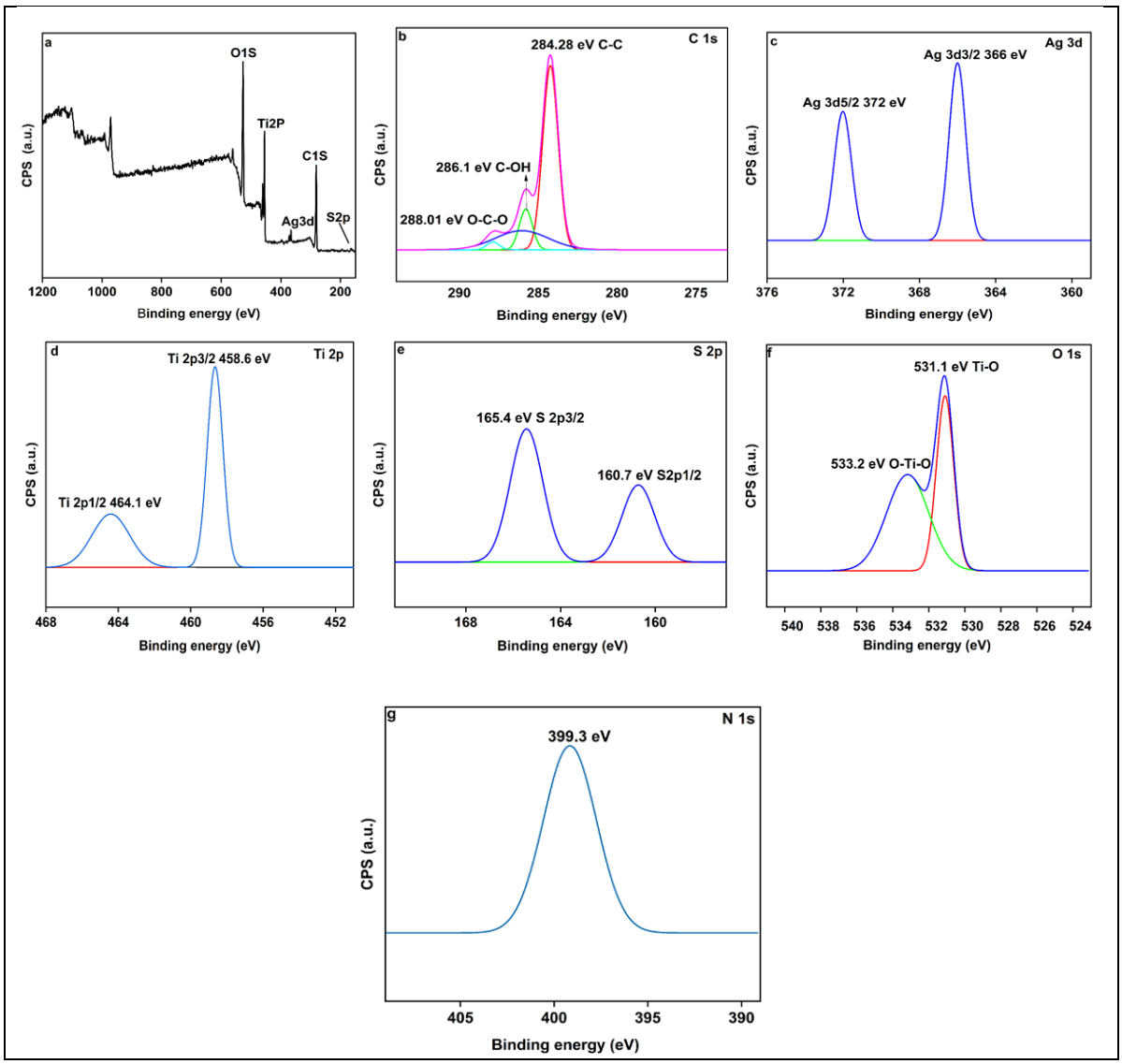

Figure 19. XPS spectra of AmCot+Ag-TiO_2 in (a) in survey, (b) C 1s, (c) Ag 3d, (d) Ti 2p, (e) S 2p, and (f) O 1s and (g) N 1s.

Figure 20a illustrates the XPS spectrum of AmCot+CuO-TiO_2 in wide, showing the elements carbon (C 1s), copper (Cu 2p), titanium (Ti 2p), nitrogen (N 1s), oxygen (O 1s), and sulfur (S 2p). The deconvoluted C 1s spectrum in (Figure 20b) shows three peaks with binding energies of 284.5, 286.15, and 287.22 eV, corresponding to C-C, C-OH, and C-S bonds and representing aliphatic (sp^3) carbon bonding in the cellulose of AmCot. In the high-resolution spectrum of Cu

2p (Figure 20c), two prominent peaks with binding energies of 934.5 eV (Cu 2p3/2) and 954.3 eV (Cu 2p1/2) and with a 20 eV difference in spin-orbit coupling due to doublet slitting between the peaks confirm that a Cu^{2+} state is formed, indicating that CuO NPs were deposited onto AmCot (Shaheen *et al*., 2021; Siddiqui *et al.*, 2020; Ghodselahi *et al.*, 2008). The deconvoluted high-resolution spectrum of Ti (Figure 20d) shows two peaks with binding energies of 458.6 and 464.1 eV, corresponding to Ti 2p1/2 and Ti 2p3/2, respectively. The presence of Ti^{4+} ions is evidenced by the energy splitting difference in the spin-orbit coupling of approximately 5.5 eV between Ti 2p1/2 and Ti 2p3/2, which is consistent with the previous findings for rutile phase TiO2 (Li *et al.*, 2017; Li *et al.*, 2015). In the deconvoluted spectrum of S 2p (Figure 20e), the first peak with a binding energy of 160.5 eV (S 2p3/2) corresponds to the highly de-electronated state of the S element, inferring that coordination bonds between Ti atoms and Cu^{+2} ions with NH_2 groups were formed. The second peak in the spectrum, with a binding energy of 165.5 eV (S 2p1/2), corresponds to the S-C bonds, further confirming ester formation (Méthivier *et al.*, 2015). In the high-resolution spectrum of O 1s (Figure 20f), the two peaks with binding energies of 531.4 and 533.4eV indicate Cu-O and Ti-O bonds, respectively (Parvathiraja and Shailajha, 2021). Cu+2 ions bind to O and N more strongly than to S, as evidenced by a shift of the O 1s peak toward a lower binding energy from 532.0 to 531.4 eV and the N 1s peak from 401.1 to 399.8 eV (Figure 20g).

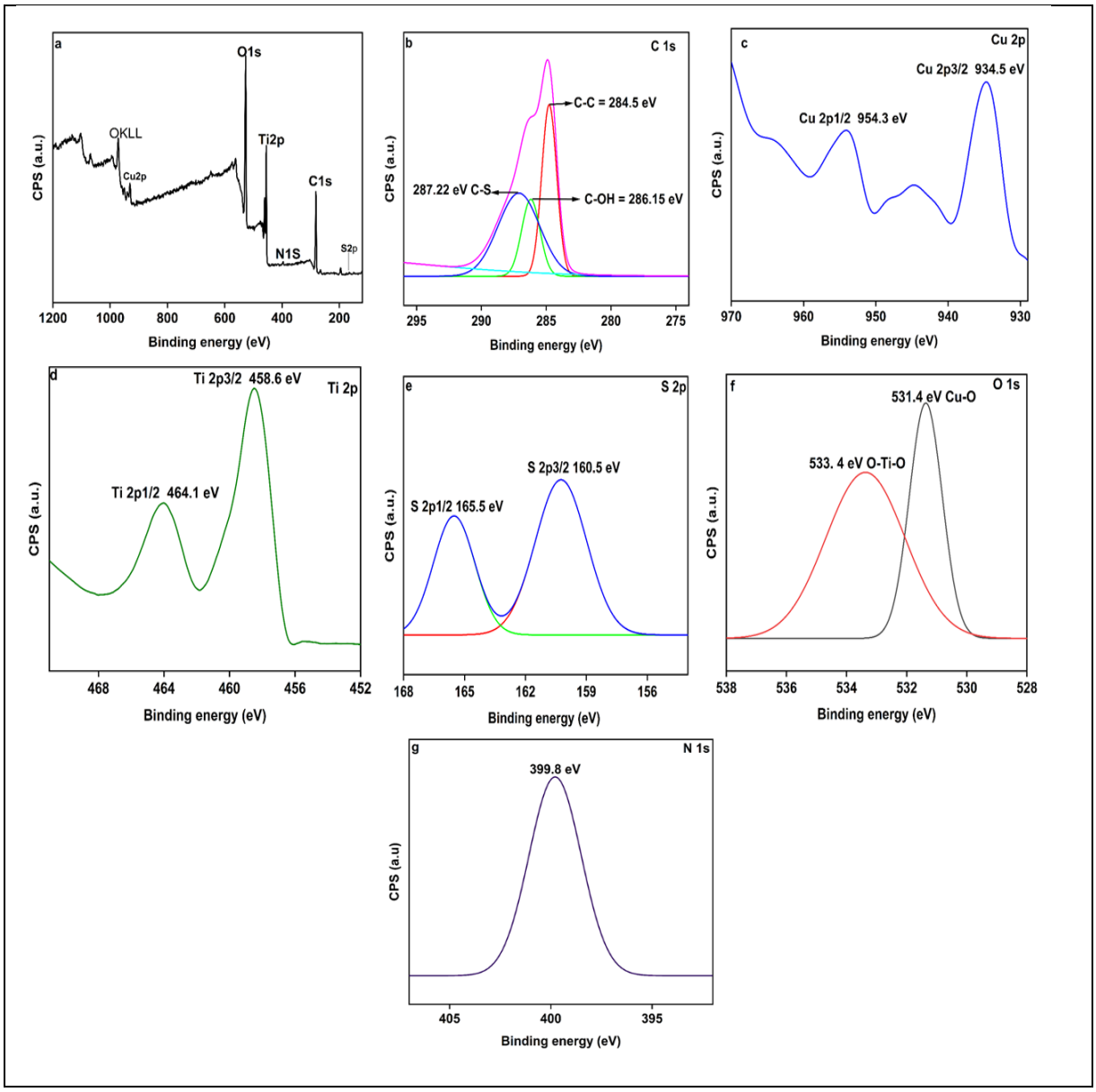

Figure 20. XPS spectrum of AmCot+CuO-TiO_2 (a) in survey, (b) C 1s, (c) Cu 2p, (d) Ti 2p, (e) S 2p, (f) O 1s, and (g) N 1s.

4.5 Surface Morphology and Elemental Mapping

Figures 21-24 illustrate the SEM micrographs of AmCot, AmCot+Ag, AmCot+CuO, AmCot+ZnO, AmCot+TiO_2, and AmCot functionalized with Ag-CuO, Ag-ZnO, Ag-TiO_2 and CuO-TiO_2 NCPs at magnifications of 100, 1000, and 5000X.

Micrographs a-c in Figure 21 show the surface morphology of AmCot. At the low magnification of 100 X (micrograph a), the gaps between the cotton fiber weaves are seen, indicating that

fabric esterification by Am occurs essentially on the surface of the fibers (El-Nahhal *et al.*, 2022). The fibers show a smooth texture at higher magnification (micrographs b and c). They are free of surface deposits with numerous embedded folds and fibrils, inferring that the scouring and bleaching process removed significant impurities from the surface of the fibers prior to the in situ deposition of the metal and metal oxide NPs and NCPs (El-Nahhal *et al.*, 2021). After the in situ deposition of Ag NPs, the surface of AmCot+Ag (micrographs d-f) shows that the fibers appear rough due to the dispersed and agglomerated NPs, in agreement with the literature, which suggests that the natural qualities of cotton fabric allow Ag NPs to be spontaneously collected and settled onto the fabric (Yang *et al.*, 2012; El-Naggar *et al.*, 2022).

The morphology of the surface of AmCot+CuO NP (Figure 21 and micrographs g-i) shows that the fibers are densely coated with homogeneously dispersed particles and aggregates of the NPs. These observations agree with a previous study that reported a homogeneous distribution of biogenically synthesized CuO NPs on cotton fabrics, as compared with the smooth surface of the control fabric (Shaheen *et al.*, 2021). The formation of aggregates of CuO NPs on AmCot+CuO is in agreement with the literature that large agglomerates of nanofibers or flakes of CuO-NPs are formed and well adhered onto the surface of cotton fabrics treated with starch and curcumin (El-Nahhal *et al.*, 2021) and tiny sized CuO-NPs' bind with fabrics, penetrate the cotton microfibrils deeply and thus adhere more tightly.

Figure 22(a-f) illustrates the morphology of AmCot, AmCot+TiO_2, and AmCot+ZnO. Micrographs of AmCot in Figure 22 (a-c) are solely for reference. In AmCot+TiO_2 (micrographs d-f), large agglomerates of TiO_2 NPs are deposited on the fibers contrary to those reported in the literature when using TIP as the precursor (Radetić, 2013; Solovitch *et al.*, 2010). This contradictory morphology is attributed to the variation in synthesis parameters of TiO_2 NPs and requires further investigation.

Micrographs g-i (Figure 22) show that in AmCot+ZnO, the fibers are densely coated with ZnO NPs as semi-spherical particles and small aggregates. This supports the contention that the wet chemical process essentially leads to forming small ZnO NPs and particles (Yousuf *et al.*, 2019; Taheri *et al.*, 2021; Salat *et al.*, 2018).

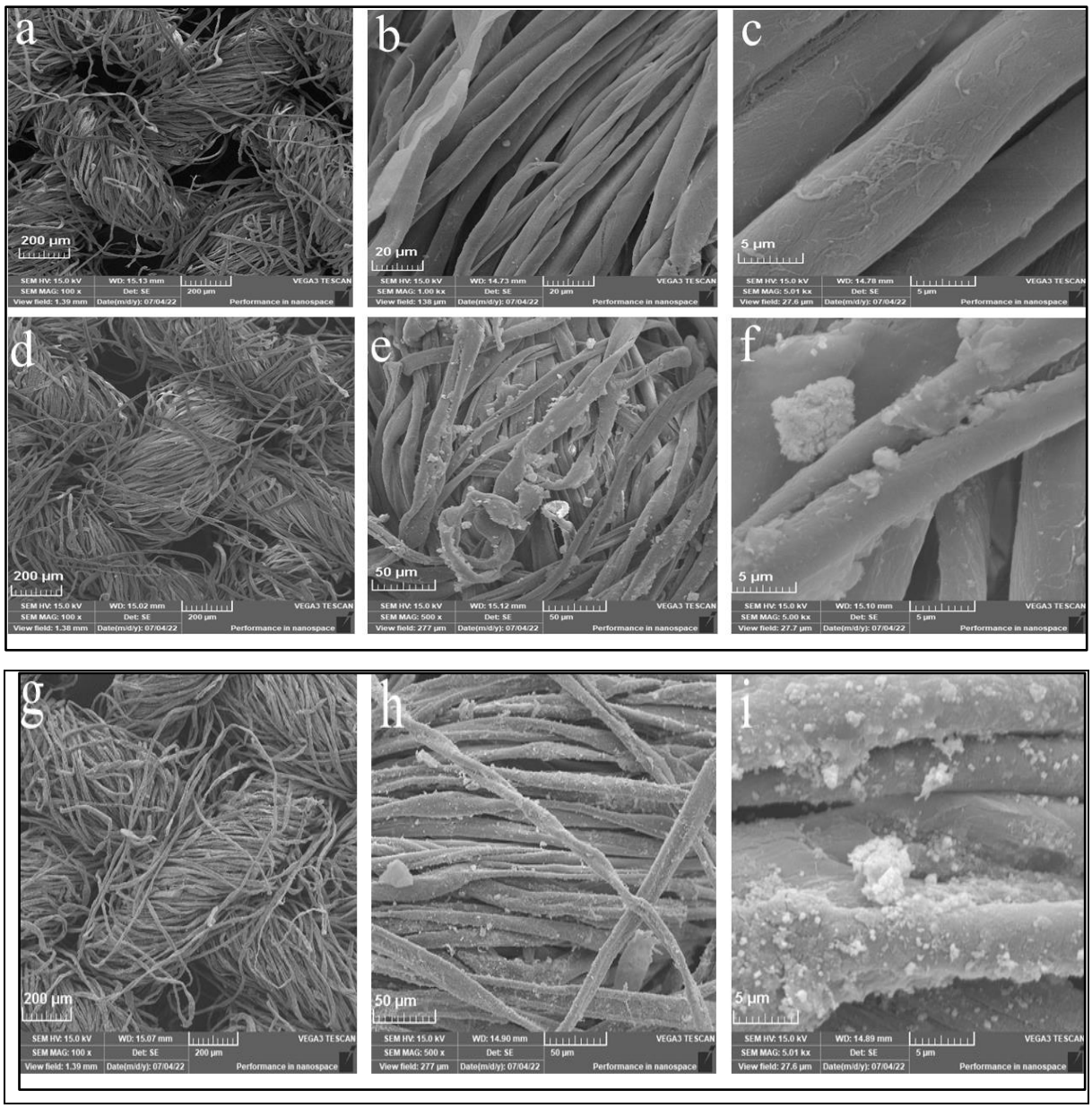

Figure 21. SEM micrographs at 100, 1000, and 5000X magnification of (a-c) AmCot, (d-f) AmCot+Ag, and (g-i) AmCot+CuO.

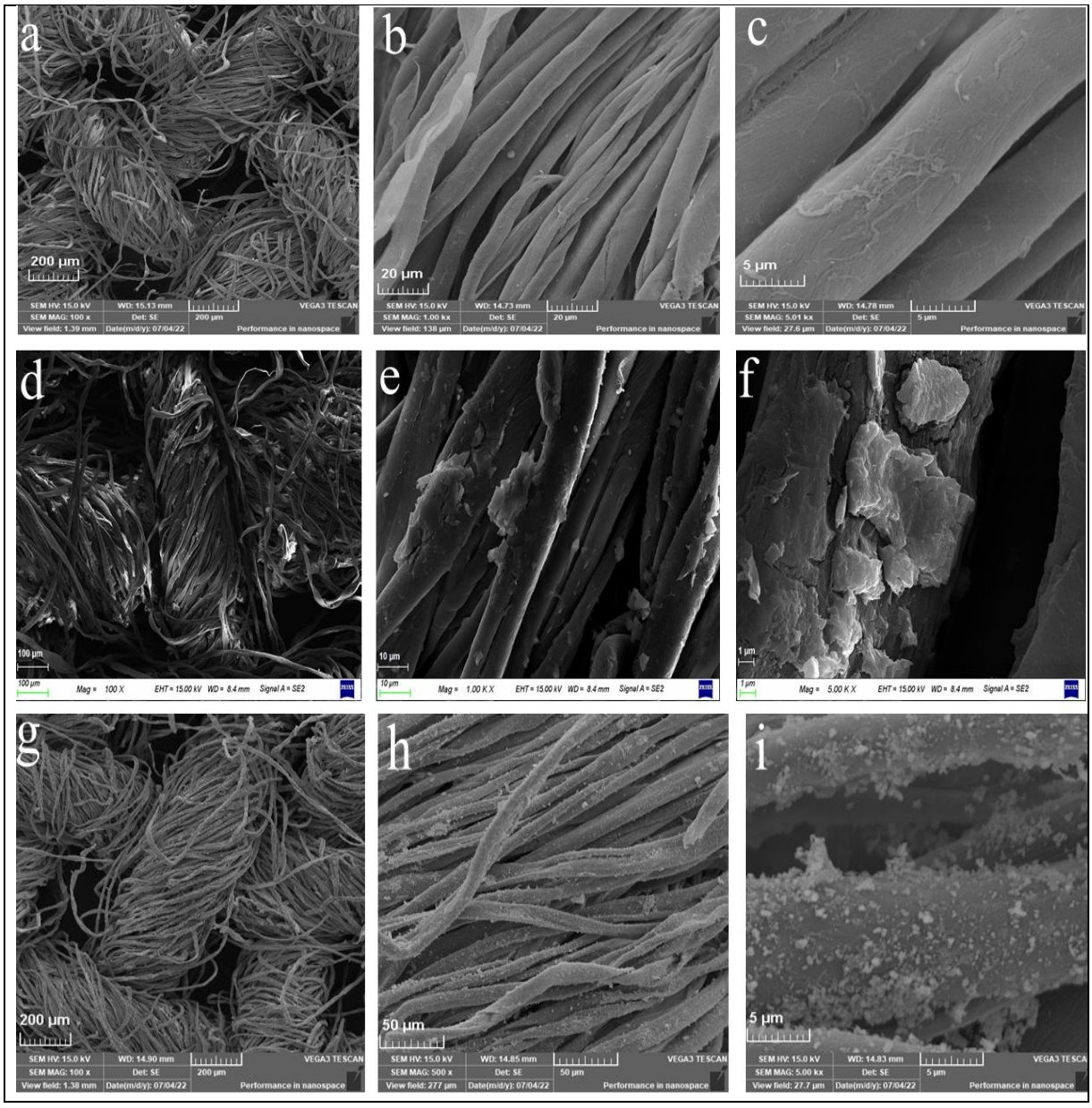

Figure 22. SEM micrographs at 100, 1000, and 5000X magnification of (a-c) AmCot, (d-f) AmCot+TiO_2, and (g-i) AmCot+ZnO.

Figure 23(a-i) illustrates the micrographs of AmCot, AmCot+Ag-CuO and AmCot+Ag-ZnO. Micrographs of AmCot in Figure 23(a-c) are for reference. The fiber surfaces of AmCot+Ag-CuO (micrographs (d-f) and AmCot+Ag-ZnO (g-i) are rough due to the deposition of the individual and aggregated particles of the NCPs. Modification of Cot by Am helps in the distribution of the NCP particles evenly and in the coordination bonding of Ag0, Cu^{2+}, and

Zn2+ions to N, S, and O donor atoms of AmCot (El-Nahhal *et al*., 2022; El-Nahhal *et al*., 2020; Elango *et al*., 2018; Bușilă *et al.*, 2015).

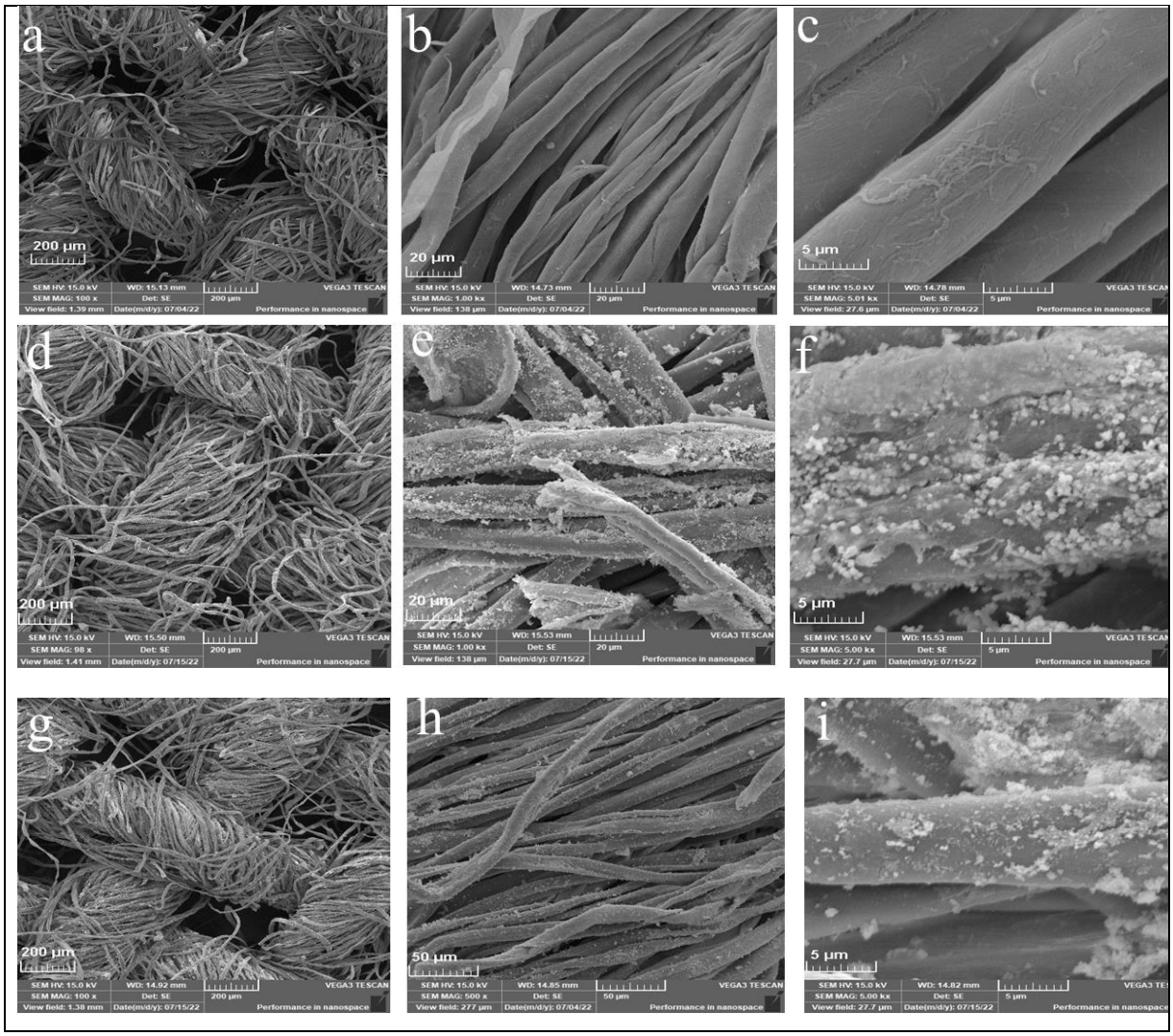

Figure 23. SEM micrographs at 100, 1000, and 5000X magnification of (a-c) AmCot, (d-f) AmCot+Ag-CuO, and (g- i) AmCot+Ag-ZnO.

Figure 24 illustrates the SEM micrographs of AmCot, AmCot+Ag-TiO_2, and AmCot+CuO-TiO_2. Micrographs of AmCot in Figure 24(a-c) are for reference. The fiber surfaces of AmCot+Ag-TiO_2 (micrographs (d-f) and AmCot+CuO-TiO_2 (g-i) are not as rough as the AmCot functionalized with Ag-CuO and Ag-ZnO NCPs due to inadequate concentration and deposition of larger sized aggregated particles of the NCPs. However, the fiber surfaces of AmCot+CuO-TiO_2 fibers are rougher than AmCot+Ag-TiO_2 because of the smaller size of the

aggregated CuO NPs compared to those of Ag NP aggregates. The observations agree with the literature (Ibrahim *et al.*, 2019).

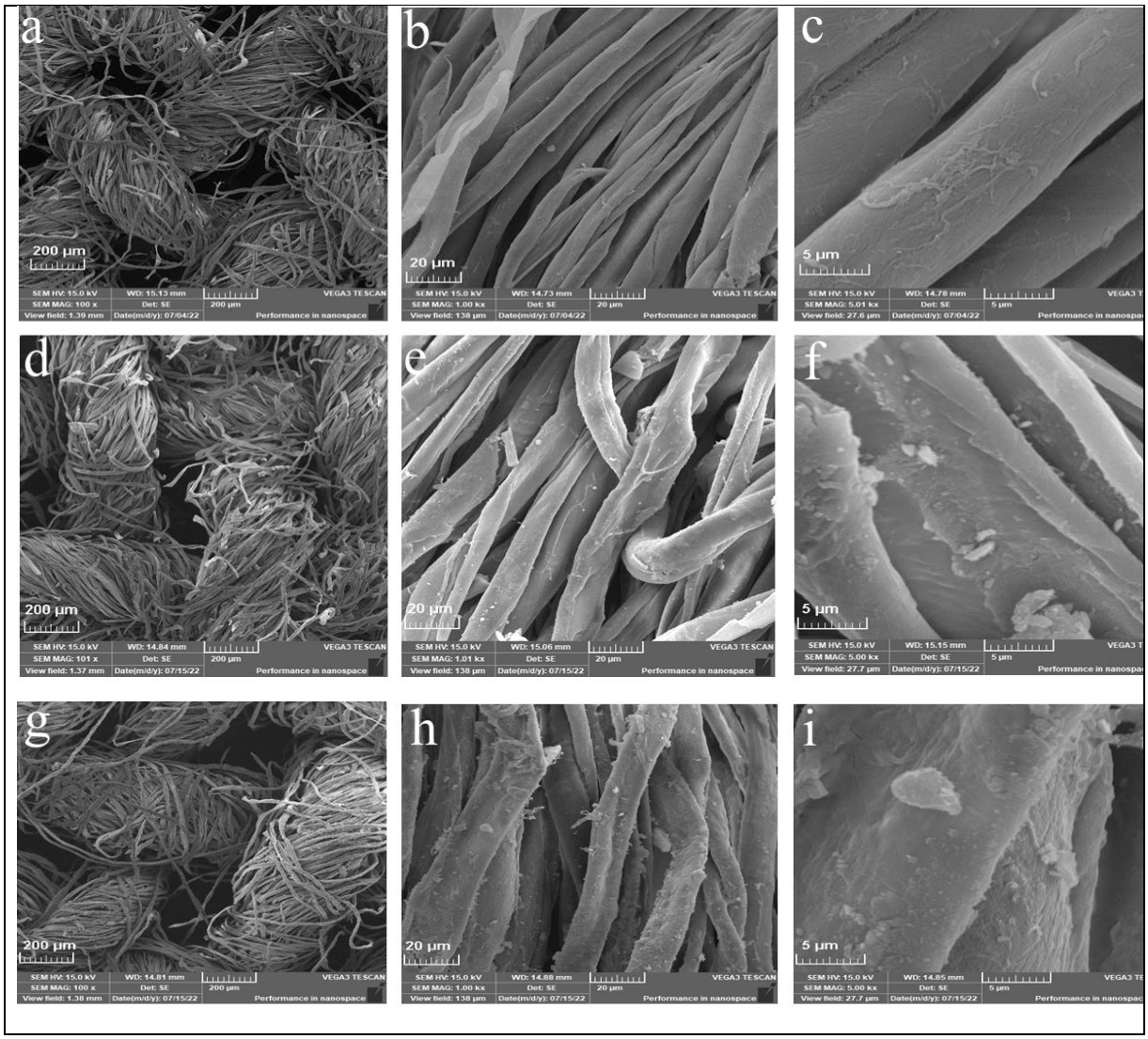

Figure 24. SEM micrographs at 100, 1000, and 5000X magnification of (a-c) AmCot, (d-f) AmCot+Ag-TiO_2, and (g-i) AmCot+CuO-TiO_2.

The elemental mapping of the fibers of AmCot, AmCot+Ag, and AmCot+CuO is depicted in Figure 25(a-c). The elemental mapping for AmCot (reference), AmCot+TiO_2, and AmCot+ZnO is in Figure 26(a-c). Figure 27(a-c) illustrates the elemental mapping for AmCot, AmCot+Ag-CuO, and AmCot+Ag-ZnO. Lastly, the elemental mapping for AmCot (reference), AmCot+Ag-TiO_2, and AmCot+CuO-TiO_2 is presented in Figure 28(a-c).

The distribution of elements C, O, S, and N is consistent on the surfaces of the fibers of all Am-modified, NP, and NCP functionalized fabrics. The C and O elements come from the cellulose of Cot and Am, while S and N come from Am.

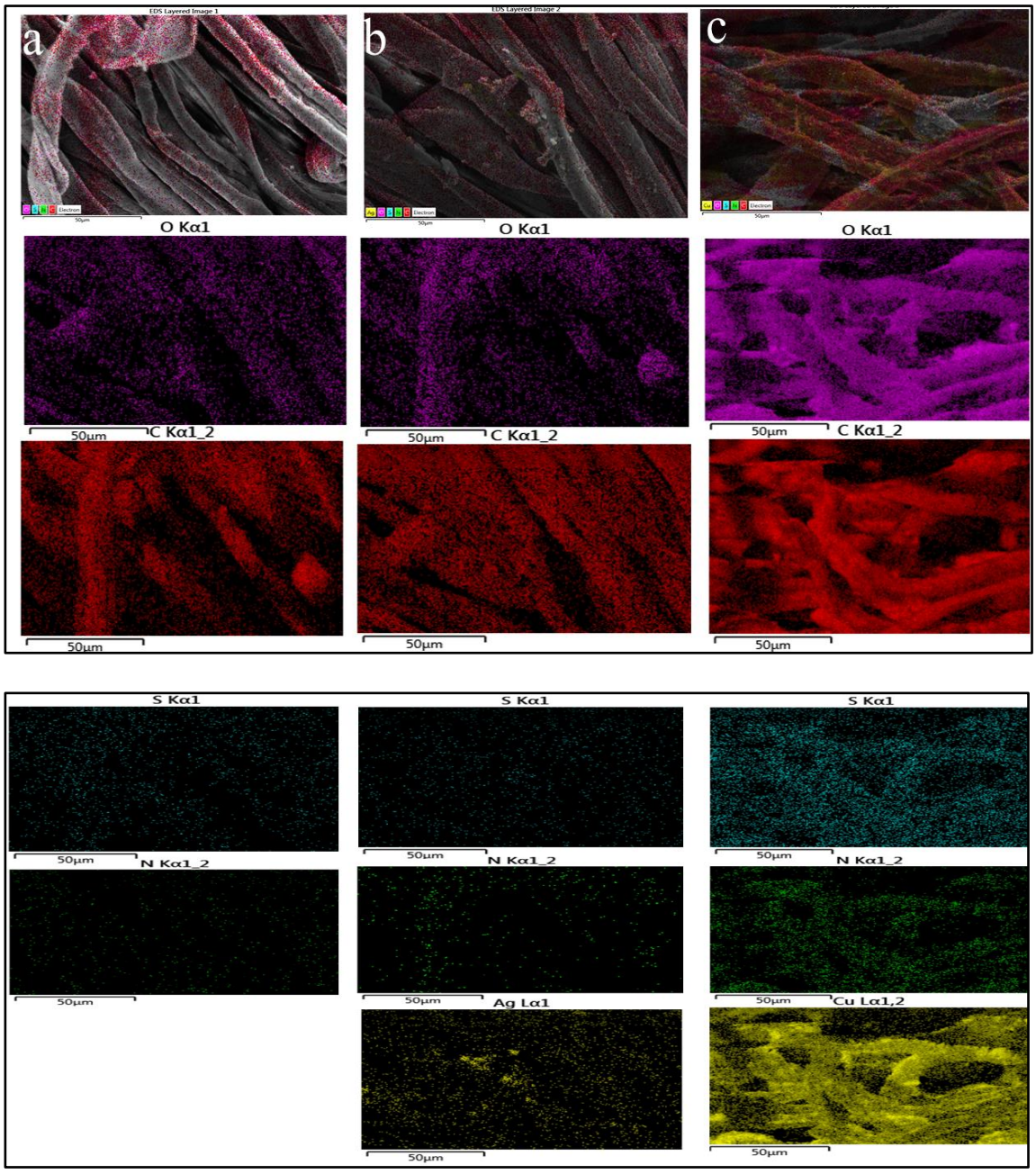

Figure 25. Elemental mapping of (a) C, O, S, and N in AmCot, (b) C, O, S, N, and Ag in AmCot+Ag, (c) C, O, S, N, and Cu in AmCot+CuO.

The distribution of these elements, especially S and N, across the surfaces of all fabrics is due to the esterification reaction between Am and Cot, supporting the FTIR and XPS analyses. This finding aligns with a previous study that mapped the elements after modifying cotton fabric with carboxymethyl chitosan and amino acid (Xu *et al*., 2018; Xu *et al*., 2019; Hassabo *et al*., 2019).

In AmCot+Ag and AmCot+CuO [Figure 25 (b, c)], in addition to the elements C, O, S, and N, the well-distributed elements Ag and Cu, respectively, on the fibers infer Ag and CuO NP deposition (Shahidi *et al*., 2018; Zhu *et al.,* 2021),. Similarly, in AmCot+TiO_2 and AmCot+ZnO [Figure 26(b, c)], the well-distributed elements Ti and Cu, respectively, on the fibers infer TiO_2 and CuO NP deposition, supporting the XRD and XPS analyses of the respective AmCot functionalized with Ag, CuO, TiO_2, and ZnO NPs. The observations agree with the literature demonstrating the uniform distribution of ZnO NPs on the surface of cotton fabrics and cotton modified by starch (Salat *et al.,* 2018; El-Nahhal *et al.*, 2020)

The elemental analysis of AmCot functionalized with NCPs (Ag-CuO, Ag-ZnO, Ag-TiO_2, and CuO-TiO_2), in addition to the elements C, O, S, and N, showed the presence of well-distributed elements Ag, Zn, Ti, and Cu on the fibers. This infers Ag, ZnO, TiO_2, and CuO NP deposition, supporting the XRD and XPS analyses of the respective AmCot functionalized with NCPs. These observations align with previous literature regarding the distribution of Ag and Ti elements on cotton fabric modified by carboxymethyl chitosan (Xu *et al.,* 2021) and another report demonstrating the distribution of Ti and Cu on amine-modified cotton fabric confirming the deposition of TiO_2 and CuO NPs onto the surface of AmCot (Thampi *et al.,* 2015).

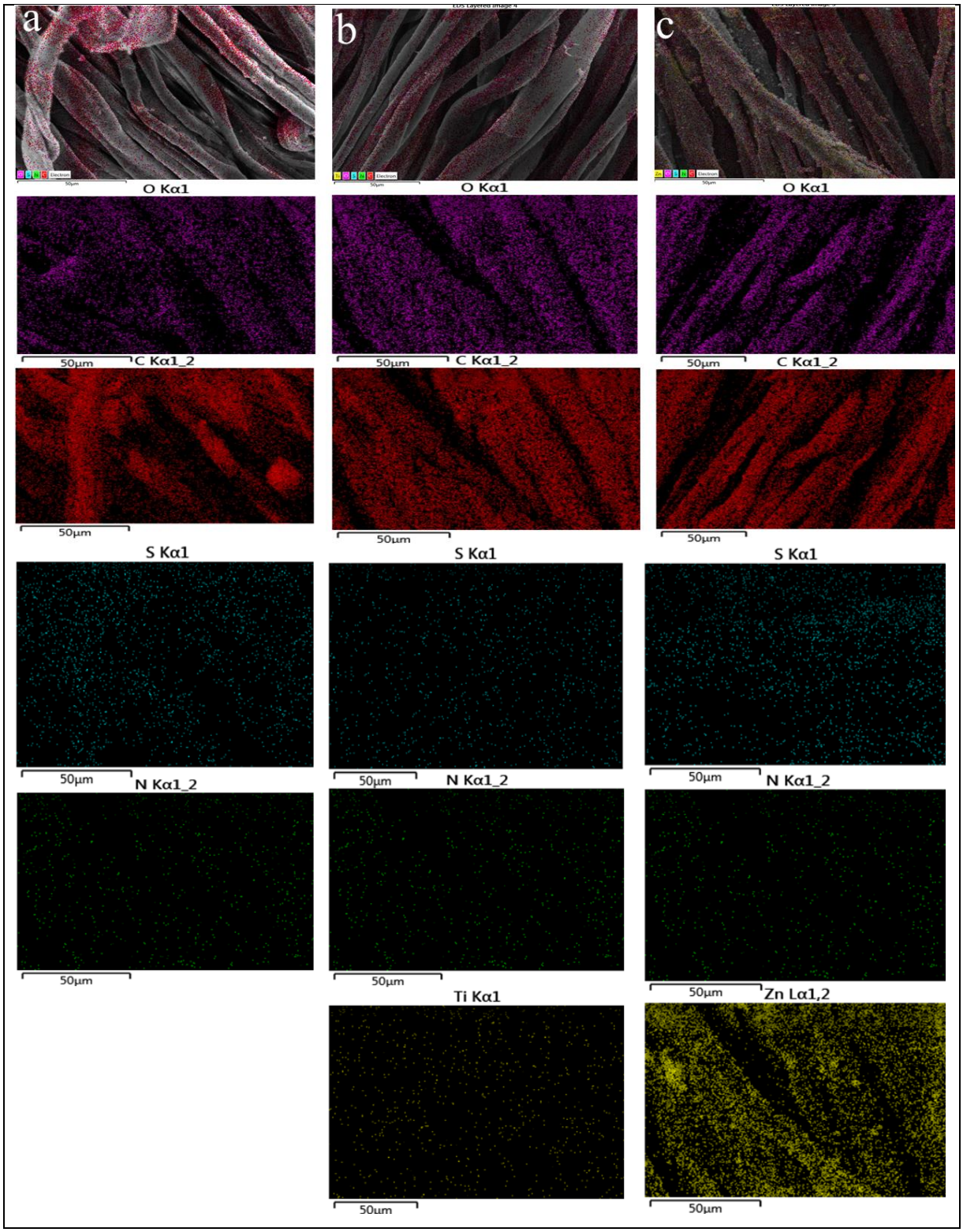

Figure 26. Elemental mapping of (a) C, O, S, and N in AmCot, (b) C, O, S, N, and Ti in AmCot+TiO_2, (c) C, O, S, N, and Zn in AmCot+ZnO.

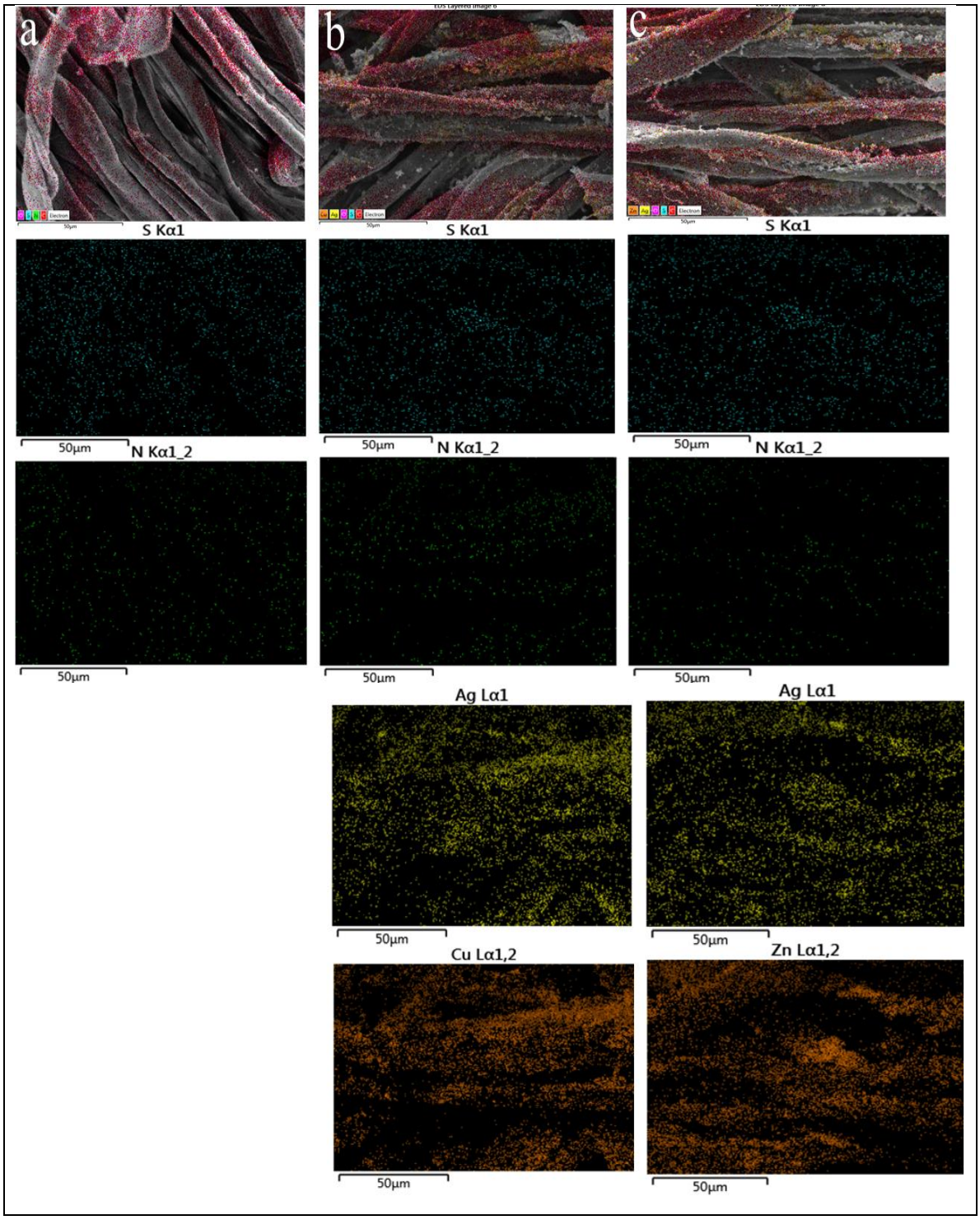

Figure 27. Elemental mapping of (a) S and N in AmCot, (b) S, N, Ag, and Cu in AmCot+Ag-CuO, and (c) S, N, Ag, and Zn in AmCot+Ag-ZnO.

.

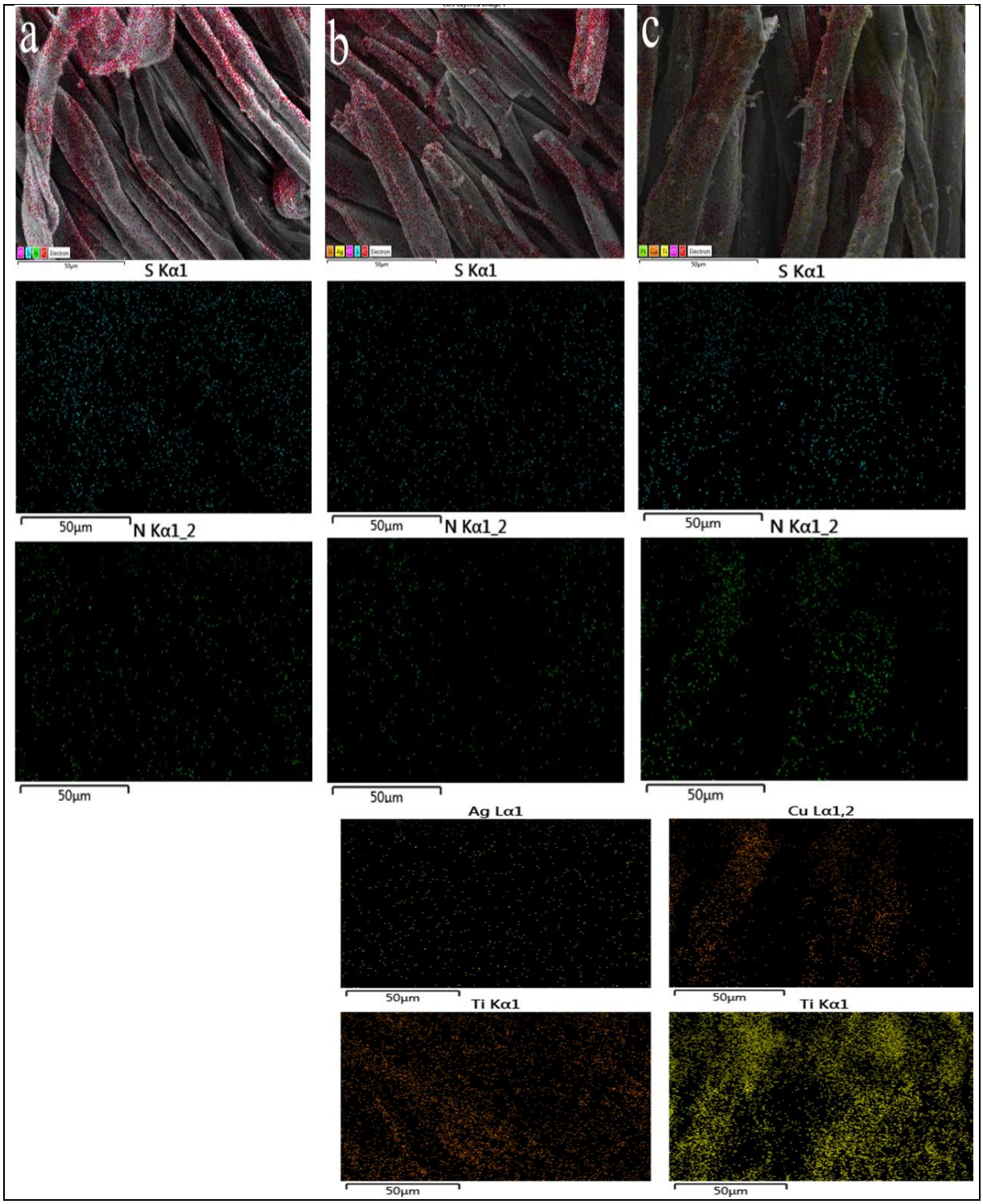

Figure 28. Elemental mapping of (a) S and N in AmCot, (b) S, N, Ag, and Ti in AmCot+Ag-TiO_2, (c) S, N, Cu, and Ti in AmCot+CuO-TiO_2.

4.6 TEM Analysis of a Selected Functionalized AmCot

The TEM analysis of the selected AmCot+CuO was performed to determine the morphology and particle distribution of the CuO NPs. Figure 29 (a, b) illustrates that the CuO NPs are present as aggregates. The particle size distribution of the primary particles within the aggregates ranges from 6 to 24 nm with a mean size of 13.3 nm [Figure 29(c, d)]. The mean size closely matches the average crystalline size of approximately 18.0 nm calculated by XRD.

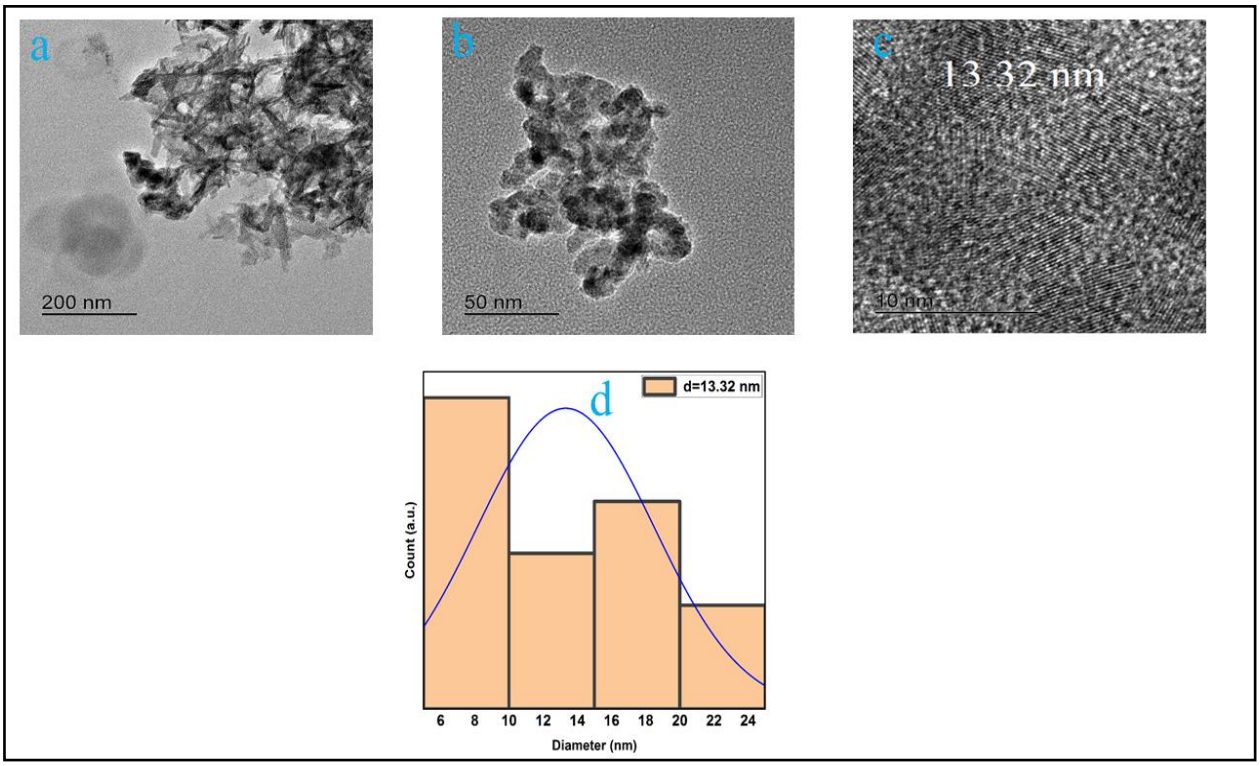

Figure 29. TEM micrograph (a, b) CuO NP aggregate, (c) CuO NPs, and (d) histogram of particle size distribution**.**

4.7 UV-radiation Blocking Properties

Exposure to solar ultraviolet (UV) radiation in the ranges of 280-315 nm (UVB) and 315-400 nm (UVA) can cause the skin to darken after exposure. Prolonged exposure to sensitive skin can result in photoallergic reactions, a slight reduction in skin smoothness, and loss of elasticity. The effectiveness of UV protection in fabrics is measured using the UV-protection factor (UPF). This factor is influenced by various factors such as fabric type, color, weight, thickness, and laundering. According to the Australian Radiation Protection and Nuclear Safety Agency (2019), Table 7 illustrates UPF ratings and protection categories. Fabric UPF can be affected

by porousness, chemical composition, particle size, fabric structure, and color. The UPF values have a direct relationship with color intensity and an inverse relationship with the L* value in the CIE L*a*b* color space system. The CIE L*a*b* color space, established by the Commission Intern0ationale de L'Eclairage (CIE) in 1978, is a 3D color space that accurately measures and compares perceivable colors. In this system, L* represents lightness, a* indicates the red/purple-green/blue axis, and b* indicates the blue/purple-yellow axis. Darker-colored or coated fabrics offer better UV protection than lighter or uncoated fabrics, as they absorb more UV radiation.

Table 7: UPF ratings and protection categories (Australian Radiation Protection and Nuclear Safety Agency, 2019).

UPF rating	**Protection**	**% UVR blocked**
15-24	Good	93.5-95.9
25-39	Very good	96-97.4
40-50, 50+	Excellent	>97.5

AmCot and AmCot functionalized with NPs and NCPs were evaluated for UV protection factor (UPF). Figures 30 (a-d) and 31(a-d) illustrate the UV-visible absorbance and transmittance spectra of AmCot and AmCot functionalized with NPs and NCPs, respectively.

AmCot [Figure 30(c, d)] transmits approximately 42% of UVA and UVB radiation, indicating poor UVA and UVB blocking capabilities. Its UPF rating is 7.54, suggesting ineffective protection against UV radiation (Table 8). This is due to its off-white cream color resulting from bleaching, scouring, and esterification with Am, which agrees with findings from various studies indicating that light-colored uncoated or modified cotton fabric offers low UV radiation protection (Porrawatkul *et al.,* 2022; Fouda *et al.,* 2018).

The absorption of UVA radiation increased significantly after the functionalization of AmCot with NPs and NCPs. The varying color developed as a function of surface plasmon, the effect

on porosity as a function of fabric weave, the concentration of NPs and NCPs, their size, and distribution on AmCot are responsible for different UPF values, as depicted in Table 8.

Ag NPs in AmCot+Ag have an average particle size of approximately 30 nm. The fabric's color is brown and shows a prominent absorbance peak at 320 - 430 nm, which means it absorbs UVA radiation (Figure 30a). AmCot+Ag has a UPF value of 27 and is categorized as having "very good" UV-blocking properties. This agrees with the literature that applying Ag NPs colloid onto cotton fabric enhanced UV-radiation protection (Rajaboopathi and Thambidurai, 2018).

Approximately 11% of UVA and UVB radiation is transmitted by AmCot+CuO (Figure 30c). AmCot+CuO has "excellent" UV blocking characteristics with a UPF rating of approximately 58.5 (Table 8) achieved by depositing small-sized CuO NPs that are densely populated and evenly distributed on AmCot. Additionally, AmCot+CuO has a small value of L*) due to the presence of the CuO NPs. Various studies have shown that cotton fabrics treated with CuO NPs and other copper-based NPs like Cu and Cu_2O NPs have exhibited excellent UPF (Ibrahim *et al.,* 2019; Rezaie *et al.,* 2017).

AmCot+TiO_2 displays very good UVA and UVB radiation protection characteristics with a UPF value of 26.5 and transmits approximately 25 % UVA and UVB radiation [Figure 30(c, d)]. The optical properties of TiO_2 NPs usually make them superior in UV protection (Ibrahim *et al.,* 2019; Radetić, 2013). However, the deposition of TiO_2 NPs as large agglomerates and no uniform distribution on the fabric resulted in AmCot+TiO_2 displaying the "very good" UPF category instead of "excellent".

AmCot+ZnO has a UPF value of approximately 17.7 (Table 8), which categorizes it as "good" and allows for 35% transmission of UVA and UVB radiation [Figure 30(c, d)]. Similar results have been obtained in the literature (Shaheen *et al*., 2016; Fouda *et al*., 2018).

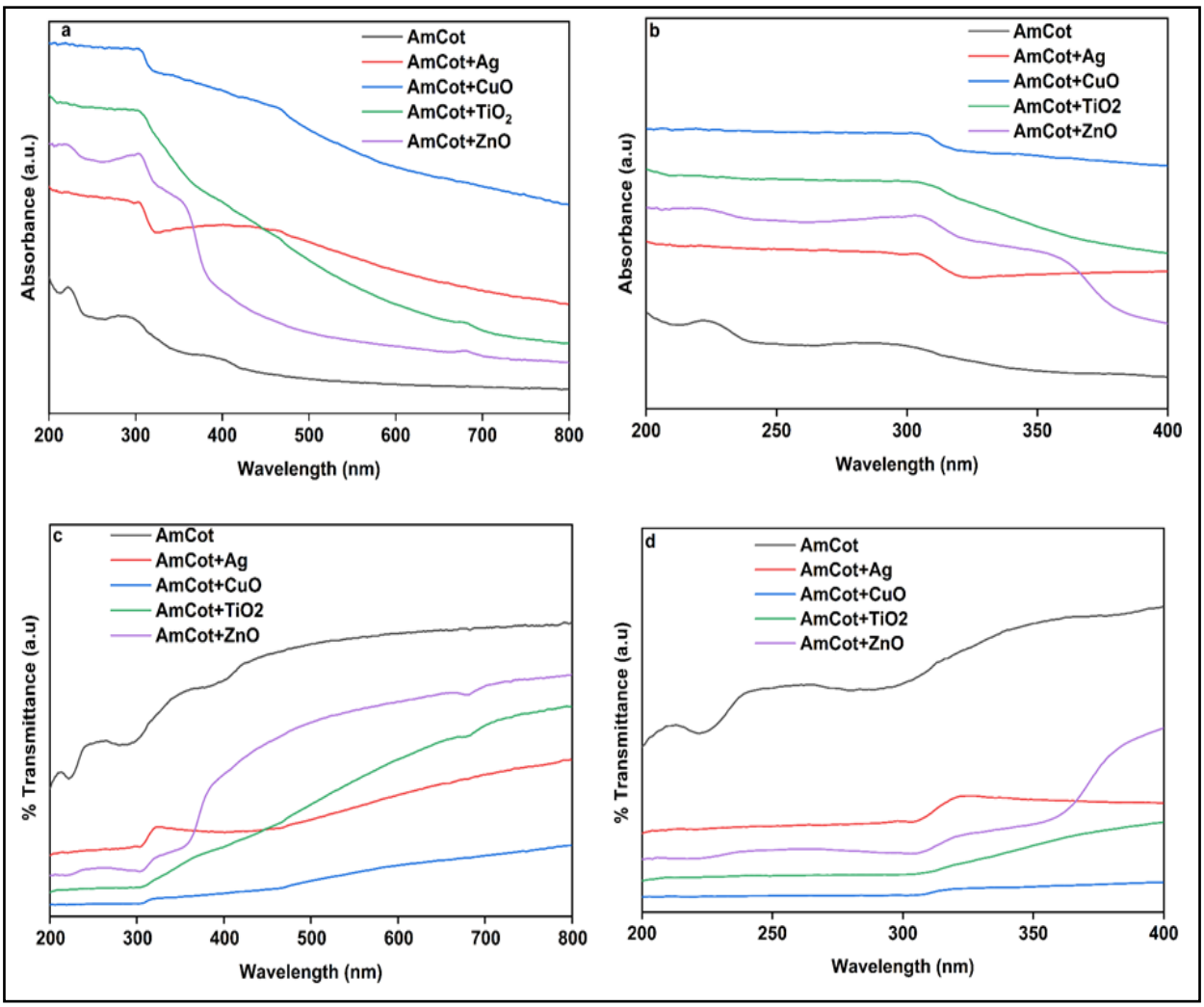

Figure 30. UV-DRS (a, b) absorbance spectra and (c, d) transmittance spectra of AmCot, AmCot+Ag, AmCot+CuO, AmCot+TiO_2, and AmCot+ZnO.

AmCot+Ag-CuO and AmCot+Ag-ZnO have high UVA and UVB-blocking ability by transmitting approximately 20 and 10% UVA and UVB radiation corresponding to UPFs of 36 and 48, giving "very good" and "excellent" UV protection, respectively [Figure 31(c.d) and Table 8]. Following the functionalization of AmCot by Ag-CuO and Ag-ZnO NCPs, the original light color of AmCot is substantially darkened, resulting in a higher UPF value. The synergetic effect is usually expected when NCPs are applied to cotton fabric (Li *et al.*, 2017). However,

due to various factors such as the coating effect, fiber type, and particle size of the NPs, the value of UPF for NCPs varies.

AmCot+Ag-TiO_2 and AmCot+CuO-TiO_2 [Figure 31(c.d) have lower UVA and UVB-blocking ability than AmCot+Ag-CuO and AmCot+Ag-ZnO, transmitting approximately 28% and 30% UVA and UVB radiation corresponding to UPFs of 36 and 48, giving "very good" UV protection (Table 8). The synergetic effect usually expected when applying NCPs to cotton fabric (Li *et al.*, 2017) is not attained due to the large-sized agglomerates of the TiO_2 NPs.

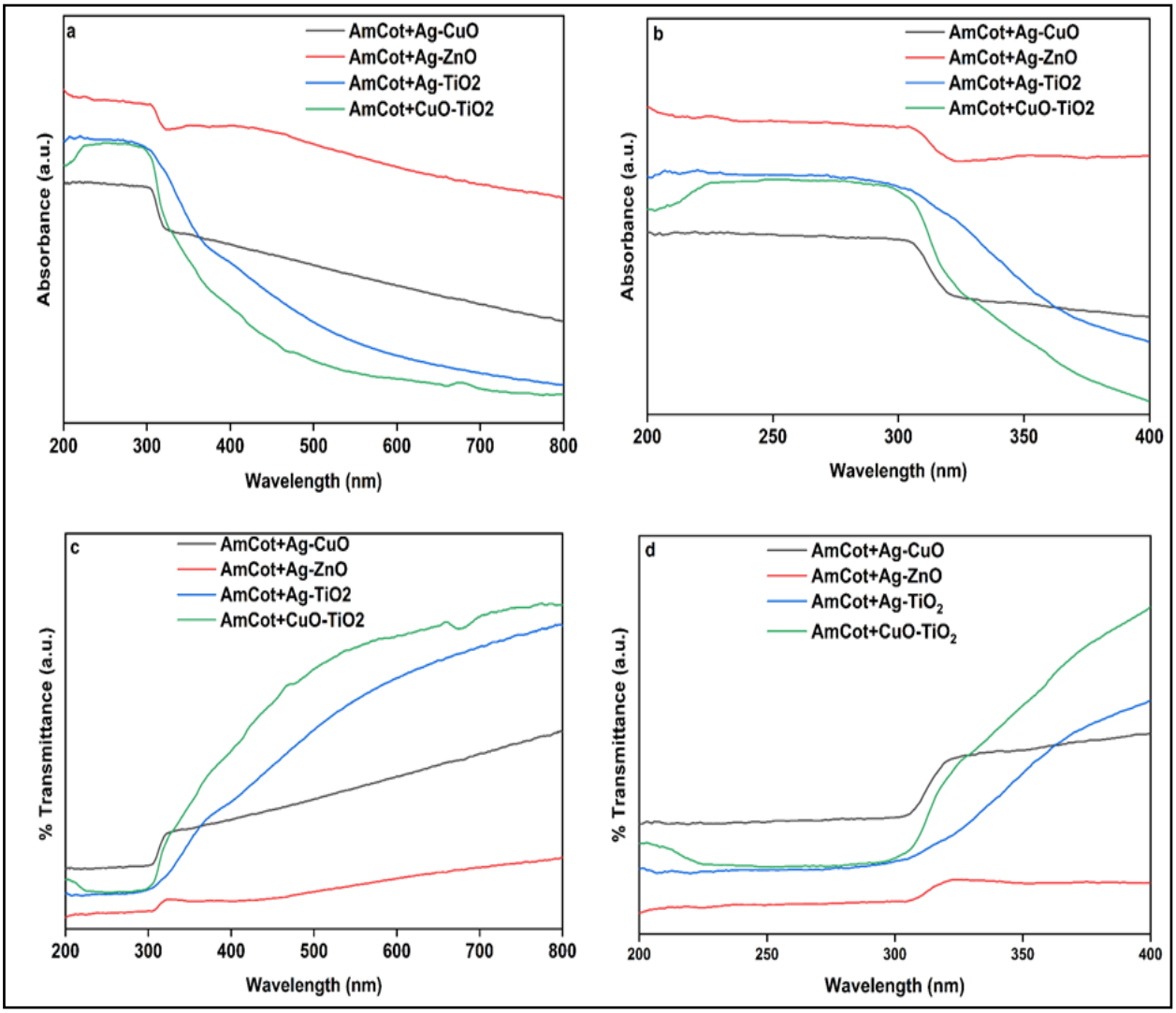

Figure 31. UV–Vis DRS (a, b) absorbance spectra and (c, d) transmittance spectra of AmCot+Ag-CuO, AmCot+Ag-ZnO, AmCot+Ag- TiO_2 and AmCot+CuO-TiO_2

Table 8: UPF values and UV protection category of AmCot and AmCot functionalized with NPs and NCPs.

Sample code	UPF values	UV protection category
AmCot	7.54±0.12	Poor
AmCot+Ag	27.76±0.34	Very good
AmCot+CuO	58.5 ± 0.62	Excellent
AmCot+TiO_2	26.5±0.80	Very good
AmCot+ZnO	16.97±0.24	Good
AmCot+Ag-CuO	36.21 ± 0.42	Very Good
AmCot+Ag-ZnO	48.2±0.56	Excellent
AmCot+Ag-TiO_2	28.5 ± 0.62	Very good
AmCot+CuO-TiO_2	26.5 ± 0.32	Very good

4.8 Antibacterial Activity

The antibacterial activity of AmCot and AmCot functionalized with NPs and NCPs against Gram-negative *E. coli* and Gram-positive *S. aureus* bacterial strains were tested using the AATCC 147 test method. The representative optical images of the tests are illustrated in Figures 32 and 33. The AATCC 147 method, also known as the Parallel Streak method, is used to qualitatively assess the antibacterial activity of diffusible antimicrobial agents on treated textiles. In simple terms, it measures the treated fabric's ability to inhibit the growth of microbes, known as being bacteriostatic (Güner and Aşkun, 2023). This method offers a convenient and quick alternative to the more tedious AATCC 100, making it an excellent screening tool.

The growth of both bacterial species is observed under AmCot, which served as the control sample after 24 hours of incubation, illustrated in Figure 32 (b) against Gram-positive *E. coli* and Figure 32(l) against Gram-negative *S. aureus*). No bacterial growth, however, occurs under AmCot functionalized with Ag, CuO, and ZnO NPs against *E.coli* [Figure 32(d, f, t)] and *S. aureus* [Figure 32(n,p, t)] and the parallel streaks of the bacteria cultures over which the functionalized fabrics are placed are almost obliterated due to the high antibacterial activity of the NPs. AmCot+TiO_2 shows low antibacterial activity against *E. coli* [Figure 32 (h] and even lower activity against *S. aureus* [Figure 32(r)]. This is attributed to the fact that TiO_2 NPs are not active without exposure to visible or UV radiation (Zhang *et al.*, 2019) and also because of the large size of agglomerated particles of the NPs.

Under AmCot functionalized, with Ag-CuO, Ag-ZnO, and Ag-TiO_2, the absence of *E. coli* [Figure 33(b, d, f) and *S. aureus* [Figure 33(j, i, n) growth is consistent across the NCPs inferring high antibacterial activity NCPs (Naebe *et al.,* 2022). However, AmCot+CuO-TiO_2 displays low antibacterial activity against *E. coli* [Figure 33(h)] and even lower activity against *S. aureus* [Figure 33(p)], which is very similar to AmCot+TiO_2 [Figure 32(h, r)]. This reduced activity is attributed to the inactivity of TiO_2 NPs without exposure to visible or UV radiation (Zhang *et al*., 2019), as well as the large size of agglomerated particles of the NPs.

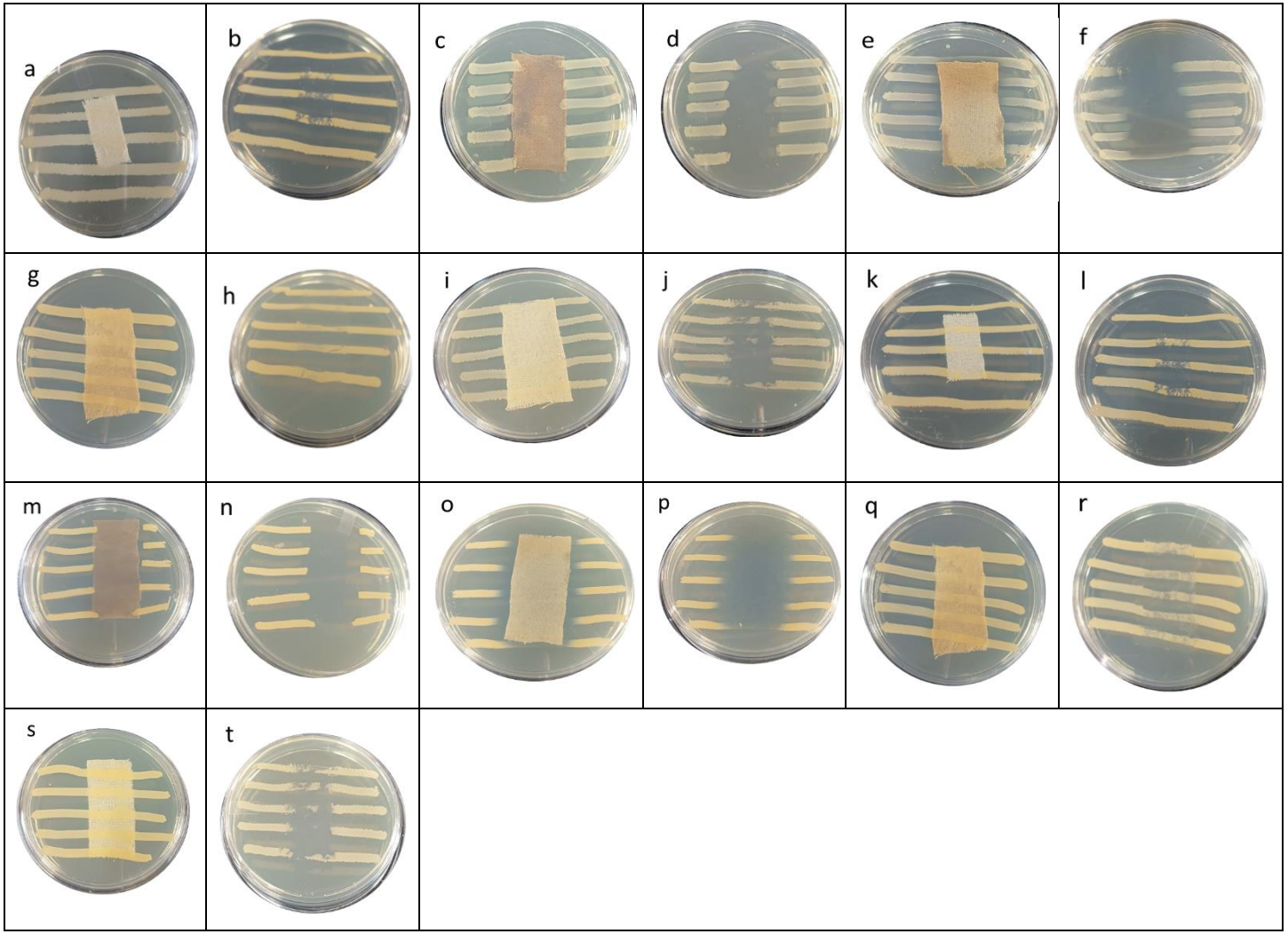

Figure 32. Optical images of the antibacterial activity according to the AATCC 147 test method of (a,b) AmCot, (c,d) AmCot+Ag (e,f) AmCot+CuO, (g,h) AmCot+TiO_2 and (i,j) AmCot+ZnO against *E. coli*, and (k,l) AmCot, (m,n,) AmCot+Ag, (o,p) AmCot+CuO, (q, r) AmCot+TiO_2, and (s,t) AmCot+ZnO against *S. aureus.*

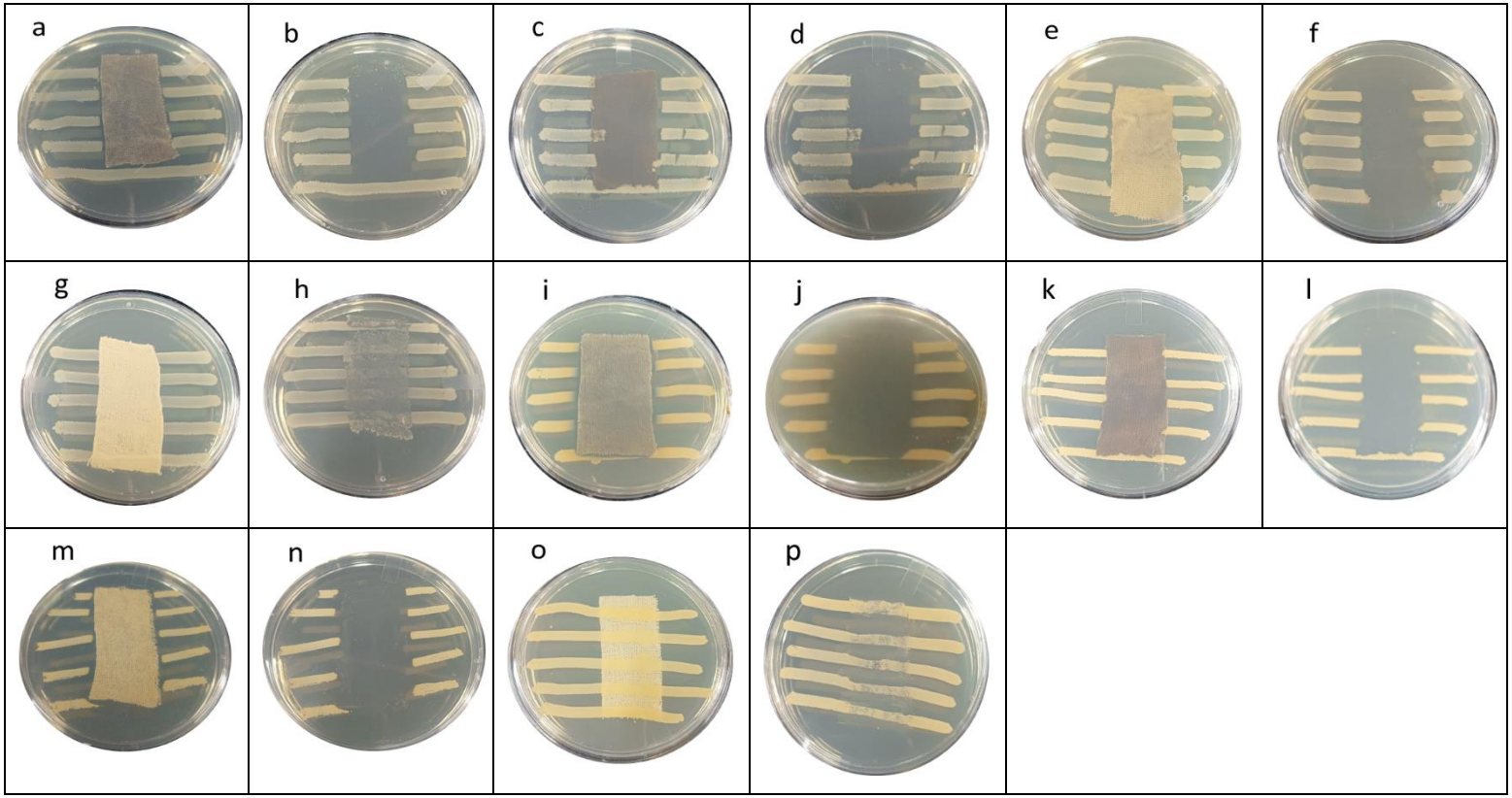

Figure 33. Optical images of the antibacterial activity according to the AATCC 147 test method of (a,b) AmCot+Ag-CuO, (c,d) AmCot+Ag-ZnO (e,f) AmCot+Ag-TiO_2, (g,h) AmCot+CuO-TiO_2 against *E. coli*, and (i,j) AmCot+Ag-CuO, (k,l) AmCot+Ag-ZnO (m,n) AmCot+Ag-TiO_2, and (o, p) AmCot+CuO-TiO_2 against *S. aureus.*

4.8.1 Antibacterial Wash Durability of the Functionalized Cotton Fabrics

Laundering robustness is an important criteria for antibacterial cotton materials for imparting bacterial infection (Gao *et al*., 2021). It was evaluated qualitatively by measuring the diameter of the inhibition zones of washed cotton fabrics functionalized with Ag, CuO, TiO_2 and ZnO NPs and Ag-CuO, Ag-ZnO, Ag-TiO_2 and CuO-TiO_2 NCPs after each ten laundering cycles for up to 50 washing cycles. The optical image of the zones of inhibition (ZOI) of AmCot, AmCot+Ag, AmCot+CuO, AmCot+ZnO and AmCot+TiO_2 against gram negative bacteria E. *coli* and *P. aeruginosa*, and gram-positive bacteria *S. aureus* and *S. pyogenes* were depicted in Figure 34 and the diameter of ZOI of AmCot, AmCot+Ag, AmCot+CuO and AmCot+ZnO were displayed in Tables (9, 10 and 11), respectively. The control sample (AmCot), has no antibacterial activity, whereas AmCot+Ag, AmCot+CuO, AmCot+ZnO have excellent antibacterial activity, as seen by their ZOIs.

At 0 wash cycle, the ZOIs of AmCot+Ag, AmCot+CuO and AmCot+ZnO against *S. aureus* is ca. 10%, 7.9% and 3.5% lower, respectively, than against *E. coli*. This impact is related to *S. aureus* having a thicker peptidoglycan layer than *E. coli* (Slavin *et al*., 2017). AmCot+TiO_2 is not active without exposure to visible or UV radiation (Zhang et al., 2019). Besides this, the size of AmCot+TiO_2 formed as large aggregates and agglomerates, as depicted in the SEM image (Figure 22), affects the killing ability of the functionalized cotton fabric. AmCot+Ag, AmCot+CuO and AmCot+ZnO demonstrated outstanding antibacterial activity persistence after 50 laundry cycles. The percentage decrease of the ZOIs of AmCot+Ag after 50 wash cycles against gram-negative bacterial strains, *E. coli*, was approximately 4% and the percentage decline in the ZOI of AmCot+Ag after 50 wash cycles against gram-negative bacterial strains *P. aeruginosa* was approximately 9.5% (Table 9). While the percentage decrease of the ZOIs of AmCot+Ag after 50 wash cycles against gram-positive bacteria strains of *S. aureus and S. pyogenes* were approximately 12.5 and 9.8%, respectively (Table 9). Even after several washing cycles, Ag NPs immobilized onto textile substrates in the presence of fixing agents such as chitosan, carboxymetyl compound, and amino acids demonstrated outstanding antibacterial activities against gram-negative *E.coli* and gram-positive *S. aureus* bacterial species (Zhou *et al*., 2019; Xu *et al*., 2017; Xu *et al*., 2016).

The percentage decrease of the ZOIs of AmCot+CuO after 50 wash cycles against gram-negative bacteria strains *E. coli* and *P. aeruginosa* were approximately 7.5% and 9.1%, respectively (Table 10), and against gram-positive bacteria strains *S. aureus* and *S. pyogenes* were approximately 6% and 8.4%, respectively, (Table 10). CuO NPs applied to the surface of a soft substrate have been examined for anti-bacterial and anti-fungal activity (Alagarasan *et al*., 2021; Rezaie, 2017; Shahidi et al., 2018). It has been demonstrated that the produced CuO NPs are highly effective against both *S. aureus* and *E. coli*. In addition, the antibacterial efficacy was verified after 15 washes. The findings demonstrate that the antibacterial characteristics were significant, with no colonies spreading over the agar plate after 15 cycles of washing (Alagarasan *et al*., 2021).

AmCot+TiO_2 were didn't show antibacterial activity against gram-negative *E.coli* and *P. aeruginosa* and gram-positive *S. aureus* and *S. pyogenic* (Figure 34). The ZOI of inhibition determined before washing was approximately 6 mm, which corresponds to the diameter of the AmCot+TiO_2 sampled for the antibacterial wash durability test (Table 11), demonstrating that AmCot+TiO_2 is inactive without exposure to visible or UV rays (Zhang *et al.*, 2019).

The percentage decrease of ZOI of AmCot+ZnO after 50 wash cycles against gram-negative *E. coli* and *P. aeruginosa* were approximately 8 and 11%, respectively, (Table 12). Similarly, the percentage decrease of ZOI of AmCot+ZnO after 50 wash cycles against gram-positive *S. aureus* and *S. pyogenes* were approximately 11% and 10%, respectively, (Table 12). ZnO NPs coated on cotton fabrics have strong antibacterial properties against microorganisms up to 10 washing cycles in the presence of surfactants (El-Nahhal *et al.*, 2017).

Bacteria Strains	**AmCot+Ag**	**AmCot+CuO**	**AmCot+ZnO**	**AmCot+TiO_2**
E. coli	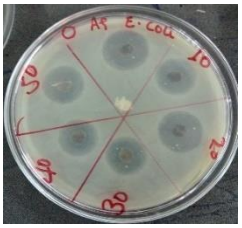		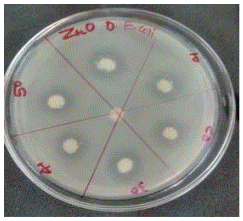	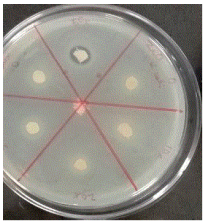
P. aeruginosa	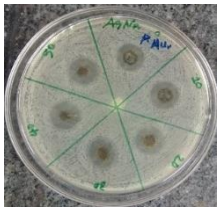	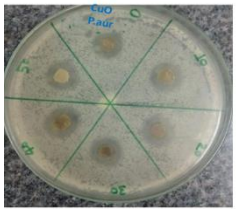	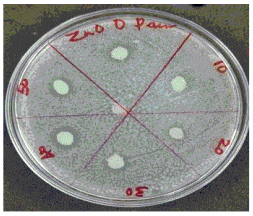	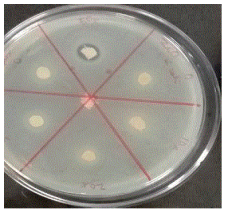
S. aureus		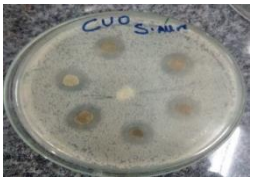	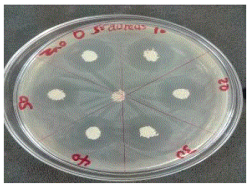	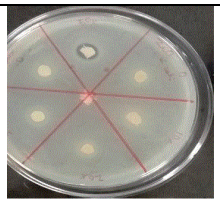
S. pyogenes	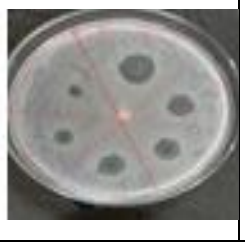		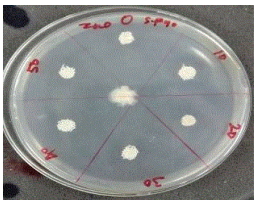	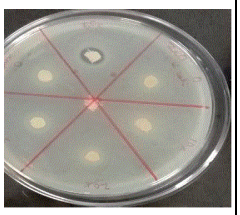

Figure 34. Optical images of AmCot+Ag, AmCot+CuO, AmCot+ ZnO and AmCot+TiO_2 antibacterial washing durability up to washing 50 wash cycle.

Table 9: Zone of inhibition diameter of AmCot+Ag against *E. coli*, *P.aeruginosa*, *S. aureus*, and *S. pyogenes*

Bacterial strain	**Zone of inhibition diameter (mm)**						
	Laundering cycles						
	Control (AmCot)	**0**	**10**	**20**	**30**	**40**	**50**
E. coli	ND	20.2± 0.2	20.18± 0.2	20.1± 0.3	19.8± 0.4	19.6± 0.9	19.5± 0.5
P. aeruginosa	ND	18.07±0.7	17.90±0.5	17.89±0.3	16.98±0.6	16.6±0.4	16.3± 0.3
S. aureus	ND	18.4± 0.35	18.1± 0.8	17.5± 0.4	16.6± 0.2	16.1± 0.3	16.1± 0.4
S. pyogenes	ND	16.49± 0.1	16.09±0.1	15.78±0.2	15.64±0.3	15.2±0.5	14.88±0.2

Table 10: Zone of inhibition diameter of AmCot+CuO against *E. coli*, *S. aureus*, *P. aeruginosa* and *S. pyogenes*

		Inhibition zone diameter (mm)					
Bacterial species		Washing Cycle					
	Control	unwashed	10	20	30	40	50
E. coli	ND	18.4±0.3	18.2±0.1	17.8±0.4	17.6±0.2	17.29±0.2	17.01±0.2
P. aeruginosa	ND	16.4±0.2	16.1±0.1	15.7±0.3	15.2±0.1	15.0±0.15	14.87±0.23
S. aureus	ND	16.9±0.4	16.8±0.1	16.5±0.2	16.2±0.1	16.0±0.15	15.9±0.23
S. pyogenes	ND	13.4± 0.1	13.2±0.1	12.78±0.2	12.64±0.3	12.5±0.5	12.28±0.2

Table 11: Zone of inhibition diameter of AmCot+TiO_2 against *E. coli*, *P.aeruginosa, S. aureus*, and *S. pyogenes.*

		Inhibition zone diameter (mm)					
Bacterial species		Washing Cycle					
	Control	unwashed	10	20	30	40	50
E. coli	ND	6.15±0.01	6.01±0.1	6.0±0.01	6.0±0.2	6.0±0.01	6.0±0.02
P. aeruginosa	ND	6.14±0.02	6.0±0.01	6.0±0.02	6.0±0.01	6.0±0.10	6.0±0.03
S. aureus	ND	6.1±0.04	6.0±0.01	6.0±0.02	6.0±0.01	6.0±0.12	6.0±0.11
S. pyogenes	ND	6.12± 0.1	6.01±0.1	6.0±0.2	6.0±0.3	6.0±0.05	6.0±0.02

Table 12: Zone of inhibition diameter of AmCot+ZnO against *E. coli, S. aureus, P. aeruginosa* and *S. pyogenes.*

	Inhibition zone diameter (mm)						
Bacterial species	Washing Cycle						
	Control	unwashed	10	20	30	40	50
E. coli	ND	19.5± 0.08	19.2± 0.07	19.1 ± 0.1	18.4± 0.1	18.1 ± 0.2	17.94 ±0.1
P. aeruginosa	ND	17.5± 0.1	17.1± 0.1	16.9 ± 0.1	16.6 ±0.18	16.1 ±0.1	15.74 ± 0.26
S. aureus	ND	18.0 ± 0.01	17.6 ± 0.3	17.2 ± 0.1	16.8 ±0.01	16.1 ± 0.05	16.05 ± 0.06
S. pyogenes	ND	11.3 ± 0.2	11.1 ±0.03	11.1 ± 0.02	10.7 ±0.21	10.4 ± 0.05	10.03 ± 0.1

Figure 35 illustrates the representative optical images of the ZOIs of AmCot+Ag-CuO, AmCot+Ag-ZnO, AmCot+Ag-TiO_2, and AmCot+CuO-TiO_2 up to 50 wash cycles and the respective measured ZOIs after every 10 wash cycles up to 50 wash cycles are depicted in Tables 13-16. The ZOIs of AmCot+Ag-CuO (Table 13) and AmCot+Ag-ZnO (Table 14) are larger compared to those of AmCot+Ag-TiO_2 (Table 15) and AmCot+CuO-TiO_2 (Table

16) inferring excellent antibacterial activity after 50 wash cycles. The percentage decrease of the ZOIs of AmCot+Ag-CuO after 50 wash cycles against Gram-negative bacteria *E. coli* and *P. aeruginosa* is ca. 9.5 and 6.3%, respectively, and after 50 wash cycles against Gram-positive bacteria *S. aureus* and S. pyogenes is ca. 7 and 6.6%, respectively (Table 13). AmCot+Ag-CuO exhibits larger ZOIs against the tested bacteria strains than AmCot+Ag and AmCot+CuO, evidencing synergism created due to the Ag-Cu NCP (Fu *et al*., 2018; Khatami *et al*.,2018; Hassabo *et al.*, 2019).

The ZOI of AmCot+Ag-ZnO against Gram-positive S. aureus is approximately 4% lower after 0 wash cycles compared to its ZOI against Gram-negative *E. coli*. This difference is attributed to *S. aureus* having a thicker peptidoglycan layer than E. coli (Slavin *et al.*, 2017). After 50 wash cycles, the ZOI of AmCot+Ag-ZnO against Gram-negative *E. coli* and *P. aeruginosa* decreases by approximately 7.2% and 14%, respectively (Table 14). In addition, after 50 wash cycles, there is a decrease of approximately 15% in the ZOI of AmCot+Ag-ZnO against Gram-positive *S. aureus* and approximately 10% against *S. pyogenes* (Table 14). According to Table 13 and optical images in Figure 35, AmCot+Ag-ZnO demonstrates larger ZOIs against the tested bacteria strains compared to AmCot+Ag and AmCot+ZnO, indicating the synergistic effect of the Ag-Zn NCP. These results agree with existing literature, which illustrates the synergistic effect of Ag-ZnO NCPs in killing microorganisms (Liang *et al.,* 2015; Porrawatkul *et al.*, 2022).

The ZOIs of AmCot+Ag-TiO_2 against Gram-negative *E. coli* and *P. aeruginosa* decreased by approximately 9.6% and 18.13% after 50 wash cycles (Table 15). Similarly, the ZOIs of AmCot+Ag-TiO_2 against Gram-positive *S. aureus* and *S. pyogenes* decreased by approximately 19.5% and 15% after 50 wash cycles (Table 15). These results demonstrate the durability of the NCPs with very effective antibacterial properties post-wash.

The ZOIs of AmCot+CuO-TiO_2 decreases by approximately 9.3% and 18% after 50 wash cycles against Gram-negative *E. coli* and *P. aeruginosa*, respectively (Table 16). Additionally, after 50 wash cycles, the ZOI decrease in AmCot+CuO-TiO_2 against Gram-positive *S. aureus* and S. *pyogenes* is approximately 18% and 16%, respectively, indicating very good antibacterial wash durability (Yamada *et al.,* 2016; Benabbo *et al.,* 2007).

Bacterial strain	**AmCot+Ag-CuO**	**AmCot+Ag-ZnO**	**AmCot+Ag-TiO_2**	**AmCot+CuO-TiO_2**
E. coli		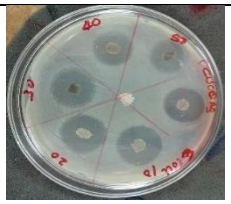		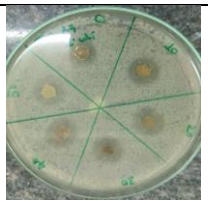
P. aeruginosa	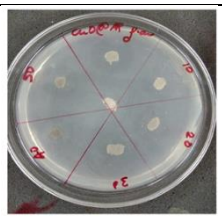	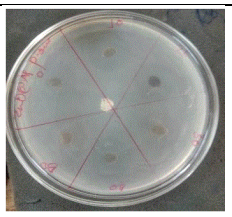	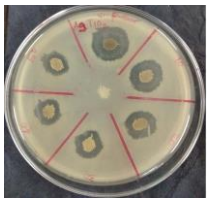	
S. aureus	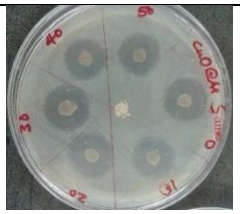	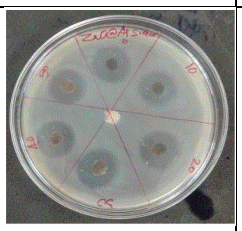	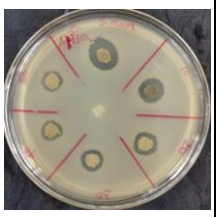	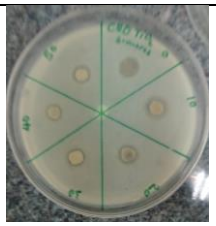
S. pyogenes	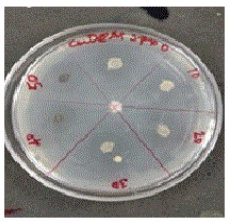		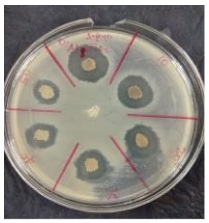	

Figure 35. Optical images of antibacterial durability of AmCot+Ag-CuO, AmCot+Ag-ZnO, AmCot+Ag-TiO_2, and AmCot+CuO-TiO_2 after 50 wash cycles.

Antimicrobial resistance mechanisms can spread across multiple bacterial genera. The organism can acquire genes, and enzymes like lactamases prevent antibacterial agents from taking effect. Bacteria may develop efflux pumps, preventing antibacterial agents from reaching their target location. They may also acquire genes for a metabolic pathway, resulting in altered cell walls without antimicrobial agent binding sites, or acquire mutations that limit access of antimicrobial agents to the intracellular target site via downregulation of porin genes (Tenover, 2006). Drug resistance in *E. coli* is induced by the interaction of several resistance mechanisms arising from acquiring exogenous resistance determinants or spontaneous mutations. Extended-spectrum beta-lactamases (ESBLs), carbapenemases, aminoglycoside-modifying enzymes (AMEs), and quinolone resistance determinants are

usually found on mobile genetic elements. In contrast, porin-efflux mechanisms are activated by spontaneous changes to inherited structures (Poirel *et al.,* 2018).

P. aeruginosa's mechanisms of drug resistance could be classified broadly into three groups: intrinsic, acquired, and adaptive. The low outer membrane permeability of P. aeruginosa, which is 12–100 times lower than *E. coli's*, as well as the presence of β-lactamases like OXA-50 and AmpC and antibiotic efflux pumps, are some indicators of its intrinsic resistance mechanisms (Langendonk et al., 2021). Acquired resistance mechanisms from horizontal gene transfer in *P. aeruginosa* make it a very drug-resistant opportunistic gram-negative bacteria strain.

Gram-positive bacteria such as *S. aureus* possess a thicker peptidoglycan layer than Gram-negative bacteria, spanning over 80 nm with covalently attached teichoic and teichuronic acids. The cell wall destruction from the physical interaction between antibiotic agents and the cell wall is more detrimental for gram-negative bacteria as they lack the thick peptidoglycan layer found in Gram-positive bacteria, which could act as a protective layer (Slavin *et al.*, 2017).

NPs designed for antibacterial application have bactericidal effects due to their increased reactivity from having high surface-to-volume ratios. The exact mechanism of the antibacterial effects of metallic and metal oxide NPs and their NCPs against Gram-positive and Gram-negative bacteria is still an active research topic. Many sulfur-containing proteins are found in bacterial cell membranes, which have been proposed as preferred locations for Ag NP interactions with the bacterium (Roque-ruiz *et al.*, 2018). It has been demonstrated that the Ag NPs had a higher propensity to react with phosphorus and sulfur compounds after attaching to the cell membrane and penetrating inside the bacteria (Yucelen *et al.*, 2015). Moreover, it has been suggested that the antibacterial mechanism of Ag NPs is caused by oxidation, which produces extracellular reactive oxygen species (ROS) (Yucelen *et al.*, 2015).

CuO-NPs' antibacterial activity has been linked to several variables, including their tiny size, which allows interaction with bacteria cell walls and membranes (Usman *et al.,* 2022). Additionally, it has been proposed that the inactivation of cytoplasmic membrane-associated proteins, which affects the transport system and inhibits the selective permeability function, contributes to the nanoparticles' inhibitory action (Espı *et al.,* 2008). Regarding the killing

mechanism of ZnO NPs, the characteristic mechanisms reported in the literature are direct contact of ZnO NPs with cell walls, destroying bacterial cell integrity (Brayner *et al.*, 2006), liberation of antimicrobial ions, mainly Zn2+ ions (Kasemets *et al.*, 2009), and ROS formation (Taheri *et al*., 2021)

Table 13: Zone of inhibition diameter of AmCot+Ag-CuO against *E. coli, S. aureus, P. aeruginosa* and *S. pyogenes*

Bacterial strain	**Zone of inhibition diameter (mm)**						
	Laundering cycles						
	Control (AmCot)	**0**	**10**	**20**	**30**	**40**	**50**
E. coli	ND	22.4± 0.8	22.2± 0.2	21.9± 0.6	21.3± 0.3	20.8± 0.6	20.3± 0.4
p. aeruginosa	ND	19.3 ±0.2	19.1±0.1	19.0±0.03	18.8±02	18.5±0.3	18.1 ±0.1
S. aureus	ND	19.6± 0.8	19.5± 0.2	19.3± 0.2	19.0± 0.2	18.9± 0.2	18.8± 0.7
S. pyogenes	ND	15.5± 0.2	15.3±0.01	15.1±0.07	14.8±0.3	14.2±0.27	14.0±0.1

Table 14: Zone of inhibition diameter of AmCot+Ag-ZnO against *E. coli, S. aureus, P. aeruginosa* and *S. pyogenes.*

	Inhibition zone diameter (mm)						
Bacterial species	Washing Cycle						
	Control	unwashed	10	20	30	40	50
E. coli	ND	22.6±0.06	22.6 ± 0.04	22.4± 0.05	21.8 ± 0.08	21.6± 0. 04	21.1 ±0.2
P. aeruginosa	ND	21.0±0.04	20.9 ± 0.2	20.2 ± 0.1	19.8 ± 0.15	19.5 ±0.18	18.2 ±0.2
S. aureus	ND	21.7± 0.1	21.4 ±0.1	20.91±0.0 4	20.2 ± 0.2	19.7 ± 0.1	18.5 ± 0.2
S. pyogenes	ND	17.3± 0.1	16.8 ±0.1	16.4 ± 0.10	16.0 ±0.01	15.9 ± 0.04	15.7± 0.1

Table 15: Zone of inhibition diameter of AmCot+Ag-TiO_2 against *E. coli*, *S. aureus*, *P. aeruginosa* and *S. pyogenes.*

		Inhibition zone diameter (mm)					
Bacterial species		Washing Cycle					
	Control	unwashed	10	20	30	40	50
E. coli	ND	18.7± 0.1	18.4± 0.1	18.01±0.09	`17.92±0.08	17.42±0.34	16.9±0.17
P. aeruginosa	ND	22.0± 0.1	20.4±0.05	19.37±0.17	18.91±0.21	18.31±0.20	18.01±0.18
S. aureus	ND	14.3±0.1	12.9±0.05	12.75±0.13	12.51±0.06	11.81±0.03	11.51±0.01
S. pyogenes	ND	20.9±0.1	19.5±0.12	18.19±0.17	17.91±0.13	17.27±0.28	17.0±0.2

Table 16: Zone of inhibition diameter of AmCot+CuO-TiO_2 against *E. coli*, *S. aureus*, *P. aeruginosa* and *S. pyogenes.*

		Inhibition zone diameter (mm)					
Bacterial species		Washing Cycle					
	Control	unwashed	10	20	30	40	50
E. coli	ND	12.18 ±0.1	12.1±0.2	11.88±0.1	11.86±0.6	11.71±0.2	11.04±0.5
P. aeruginosa	ND	8.5±0.24	8.0±0.2	7.7±0.4	7.3±0.3	7.1±0.4	6.89± 0.5
S. aureus	ND	9±0.2	8.3±0.21	8.0±0.2	7.88±0.06	7.6±0.2	7.3±0.26
S. pyogenes	ND	8.1±0.31	7.8±0.2	7.3±0.12	7.03±0.27	6.91±0.1	6.8±0.3

4.9 Water Absorbency and Vapor Permeability

For cotton to feel comfortable against human skin, it needs to have the ability to allow water vapor to pass through and absorb moisture. Figure 36(a, b) shows the water absorption and

vapor transmission rate characteristics of Cot, AmCot, AmCot+Ag, AmCot+CuO, AmCot+TiO_2, and AmCot+ZnO, while Figure 37(a,b) presents the water absorption and vapor permeability properties of AmCot+Ag-CuO, AmCot+Ag-ZnO, AmCot+Ag-TiO_2, and AmCot+CuO-TiO_2. The figures illustrate that modifying the fiber surface with Am and then functionalizing it with NPs and NCs only slightly changes the water absorbency (about 10%) and vapor permeability (about 14.5%). The reduced water permeability and absorbency are attributed to the formation of ester between the -COOH groups of Am and the hydrophilic -OH groups of cellulose chains in cotton (Noman *et al*., 2020).

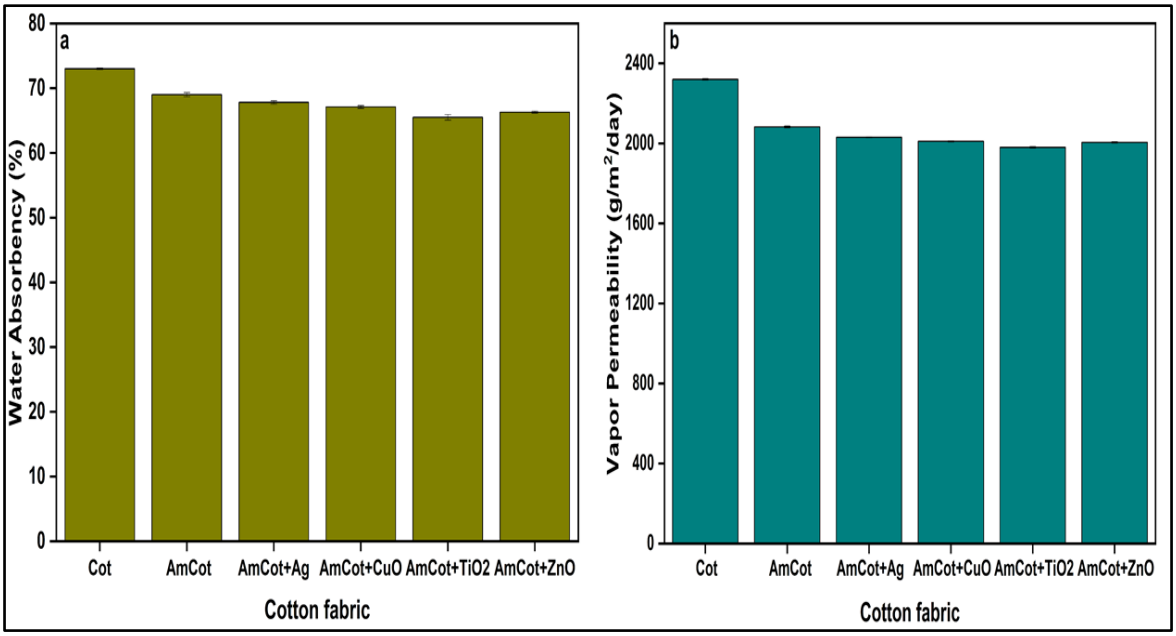

Figure 36. Physical nature of Cot, AmCot, AmtCot+Ag, AmCot+CuO, AmCot+ZnO and AmCot+TiO_2 (a**)** water absorbency and (b**)** vapor permeability.

Due to the bonding of dispersed Ag, CuO, TiO_2, and ZnO NPs and Ag-CuO, Ag-ZnO, Ag-TiO_2, and CuO-TiO_2 NCPs on the surface and between the fibers of cellulose of AmCot, the concentration of -OH groups that can absorb water are reduced. The formation of coordination bonds between the donor atoms in Am, Ag^{+}, Cu^{2+}, Ti^{4+}, and Zn^{2+} ions causes a steric hindrance effect. Consequently, the spaces (pores) between individual fibers are narrowed, leading to a longer path for water molecules to pass through the fabric (Rai *et al.*, 2012). The study shows that the surface modification and functionalization methods did not compromise the desirable physical properties of cotton fabrics, and critical properties were maintained. The vapor permeability of cotton fabric functionalized with TiO_2 nanoparticles

is lower than that of other test fabric samples, as shown in Figure 36b. TiO_2 nanoparticles on the cotton fabric surface improve hydrophobicity (Das *et al.*, 2009).

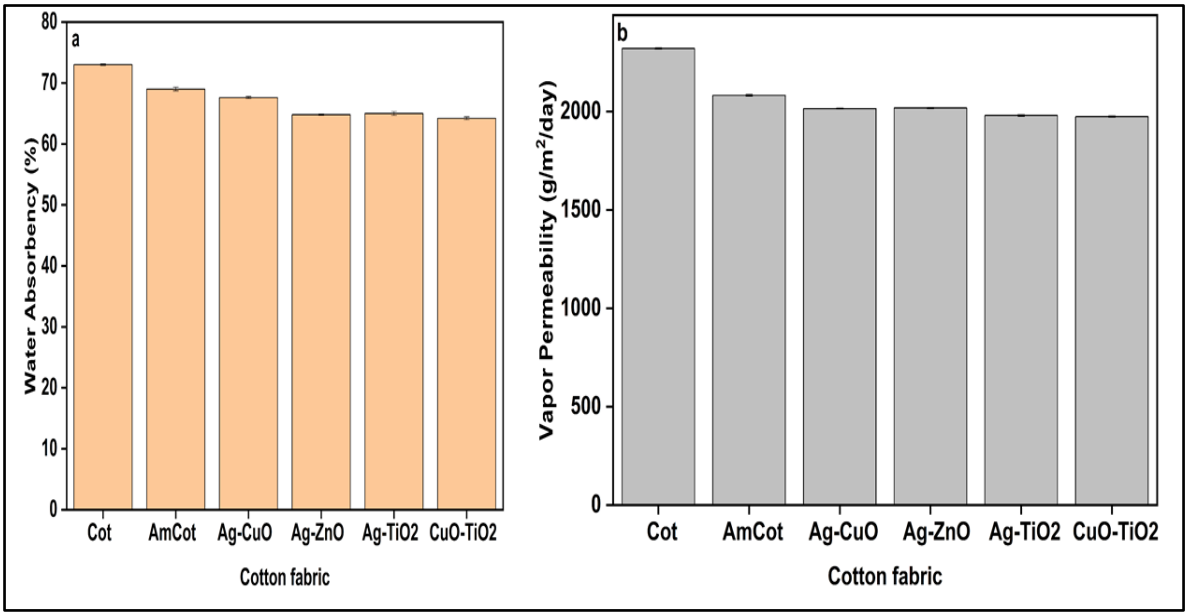

Figure 37. Physical nature of Cot, AmCot, AmtCot+Ag-CuO, AmCot+Ag-ZnO, AmCot+Ag-TiO_2,and AmCot+CuO-TiO_2 (a**)** water absorbency and (b**)** vapor permeability.

5. Conclusions and Recommendations

5.1 Conclusions

This research explored the feasibility of preparing antibacterial cotton fabrics with superior wash durability. Scoured and bleached cotton fabrics (Cot) were first modified by esterification with L-methionine (AmCot) and then in situ functionalized with Ag, CuO, ZnO, and TiO2 NPs, and Ag-CuO, Ag-ZnO, Ag-TiO_2, and CuO-TiO2 NCPs by the wet chemical method. FTIR bands at 1730 cm^{-1} and 1560 cm^{-1}, ascribed to the asymmetric stretching of COOR and NH_2 groups, respectively, evidenced that Am entered into esterification with cotton OH groups. FTIR and micro-Raman spectroscopy showed that functionalization did not alter the cotton fabric's chemical structure. XRD analysis showed high purity of the NPs and NCPs deposited on the fabrics. They matched well with the cubic face center for Ag NPs, monoclinic lattice structure for CuO NPs, wurtzite structure for ZnO NPs, and rutile polymorph for TiO_2. The particle size varied depending on the precursor type and NP or NCP preparation conditions, with the average crystallite size ranging from 10-34 nm. The variation in particle size of the NPs and NCPs deposited on AmCot was seen in the SEM micrographs. In addition, the NPs were well dispersed and populated as a combination of discrete to agglomerated particles on the fiber surfaces. Their good dispersion was also revealed by EDS element mapping of the elements Ag, Cu, Ti, and Zn from select regions of the functionalized fibers, supported by the XRD and XPS analyses. Additionally, good dispersion of the donor atoms, S, N, and O of Am, was observed, inferring that esterification occurred across the fiber surfaces and supporting the FTIR analysis. XPS analyses of AmCot functionalized with NCPs revealed the chemical states of the NPs in the NCPs and that they were coordinately bound with Am's three donor atoms.

While AmCot functionalized with TiO_2 NPs did not show any significant antibacterial activity, when tested qualitatively, AmCot functionalized with other NPs demonstrated high antibacterial activity against gram-negative *E. coli* and *P. aeruginosa,* as well as gram-positive *S. aureus* and *S. pyogenes* bacteria species even after 50 wash cycles. The ZOI data indicated that AmCot functionalized with Ag-CuO and Ag-ZnO NCPs were the most effective, indicating synergistic properties of the NCPs.

The functionalized AmCot displayed UPF category ratings ranging from good to excellent, with AmCot+CuO and AmCot+Ag-ZnO NCPs being the most efficient. The functionalized

fabrics' desirable vapor permeability and water absorbability properties were maintained within 10 and 14.5%, inferring that the surface modification and functionalization processes did not deteriorate the desired physical nature and were within the range acceptable by the industry.

5.2 Recommendations

Studying the minimum inhibition concentration and cytotoxicity is the next step in studying durable antibacterial fabrics with inorganic nanoparticles. It is also recommended that naturally occurring biocompatible compounds in Ethiopia be explored for not only cotton but also synthetic and semisynthetic fabric surface modification and as binders, particle size control, and surface immobilization of inorganic NPs with possible self-cleaning and UV-blocking properties. Extensive work should be done with key stakeholders, taking advantage of Ethiopia's tremendous opportunities in cotton production and the textile industry to produce smart and functionalized textiles alongside conventional textiles. It is strongly advised that such technologies be expanded to produce fire-retardant, smart military, and domestic, antibacterial UV-protective clothing. This encourages further intensive research for commercialization and mass production for public use. Future studies should also explore fabric functionalization with organic NPs for microbial mitigation.

References

Abidi, N., Cabrales, L., & Hequet, E. (2009). Functionalization of a cotton fabric surface with titania nanosols: applications for self-cleaning and UV-protection properties. *ACS applied materials and interfaces*, *1*(10), 2141-2146.

Abou Elmaaty, T. M., Elsisi, H., Elsayad, G., Elhadad, H., & Plutino, M. R. (2022). Recent advances in functionalization of cotton fabrics with Nanotechnology. *Polymers*, *14*(20), 4273.

Abramov, O. V., Gedanken, A., Koltypin, Y., Perkas, N., Perelshtein, I., Joyce, E., & Mason, T. J. (2009). Pilot scale sonochemical coating of nanoparticles onto textiles to produce biocidal fabrics. *Surface and coatings technology*, *204*(5), 718-722.

Abramova, A., Gedanken, A., Popov, V., Ooi, E. H., Mason, T. J., Joyce, E. M., & Bayazitov, V. (2013). A sonochemical technology for coating of textiles with antibacterial nanoparticles and equipment for its implementation. *Materials letters*, *96*, 121-124.

Adugna, B., Sharew, B., & Jemal, M. (2021). Bacterial profile, antimicrobial susceptibility pattern, and associated factors of community-and hospital-acquired urinary tract infection at Dessie Referral Hospital, Dessie, Northeast Ethiopia. *International journal of microbiology*, 1, 1-14.

Aguilera, J., de Gálvez, M. V., Sánchez-Roldán, C., & Herrera-Ceballos, E. (2014). New advances in protection against solar ultraviolet radiation in textiles for summer clothing. *Photochemistry and photobiology*, *90*(5), 1199-1206.

Alagarasan, D., Harikrishnan, A., Surendiran, M., Indira, K., Khalifa, A. S., & Elesawy, B. H. (2021). Synthesis and characterization of CuO nanoparticles and evaluation of their bactericidal and fungicidal activities in cotton fabrics. *Applied nanoscience*, 11, 1-10.

Ali, S., Birhane, M., Bekele, S., Kibru, G., Teshager, L., Yilma, Y., & Gudina, E. K. (2018). Healthcare associated infection and its risk factors among patients admitted to a tertiary hospital in Ethiopia: longitudinal study. *Antimicrobial resistance and infection control*, *7*(1), 1-9.

Anandgaonker, P., Kulkarni, G., Gaikwad, S., & Rajbhoj, A. (2019). Synthesis of TiO_2 nanoparticles by electrochemical method and their antibacterial application. *Arabian journal of chemistry*, *12*(8), 1815-1822.

Arendsen, L. P., Thakar, R., & Sultan, A. H. (2019). The use of copper as an antimicrobial agent in health care, including obstetrics and gynecology. *Clinical microbiology reviews*, *32*(4), 10-1128.

AS-NZS. (1996). Australian/New Zealand Standard. Sun Protective Clothing–Evaluation and Classification. https://www.arpansa.gov.au accessed on March 20, 2024

Attia, N. F., Osama, R., Elashery, S. E., Kalam, A., Al-Sehemi, A. G., & Algarni, H. (2022). Recent advances of sustainable textile fabric coatings for UV protection properties. *Coatings*, *12*(10), 1597.

Australian Radiation Protection and Nuclear Safety Agency, 2019 https://www.arpansa.gov.au accessed on March 23, 2024

Badry, R., El-Nahass, M. M., Nada, N., Elhaes, H., & Ibrahim, M. A. (2023). Structural and UV-blocking properties of carboxymethyl cellulose sodium/CuO nanocomposite films. *Scientific reports*, 13(1), 1123.

Basch, A., & Lewin, M. (1973). The influence of fine structure on the pyrolysis of cellulose. II. Pyrolysis in air. *Journal of polymer science: Polymer chemistry edition*, 11(12), 3095-3101.

Bogdanović, U., Lazić, V., Vodnik, V., Budimir, M., Marković, Z., & Dimitrijević, S. (2014). Copper nanoparticles with high antimicrobial activity. *Materials letters*, 128, 75-78.

Brayner, R., Ferrari-Iliou, R., Brivois, N., Djediat, S., Benedetti, M. F., & Fiévet, F. (2006). Toxicological impact studies based on Escherichia coli bacteria in ultrafine ZnO nanoparticles colloidal medium. *Nano letters*, *6*(4), 866-870.

Butola, B. S. (2019). Recent advances in chitosan polysaccharide and its derivatives in antimicrobial modification of textile materials. *International journal of biological macromolecules*, 121, 905-912.

Calizo, I., Alim, K. A., Fonoberov, V. A., Krishnakumar, S., Shamsa, M., Balandin, A. A., & Kurtz, R. (2007, February). Micro-Raman spectroscopic characterization ZnO quantum dots, nanocrystals, and nanowires. In *Quantum dots, particles, and nanoclusters IV*, 6481, 96-103.

Cao, H., & Liu, X. (2010). Silver nanoparticles-modified films versus biomedical device-associated infections. *Wiley Interdisciplinary Reviews: Nanomedicine and nanobiotechnology*, *2*(6), 670-684.

Cuscó, R., Alarcón-Lladó, E., Ibáñez, J., Artús, L., Jiménez, J., Wang, B., & Callahan, M. J. (2007). Temperature dependence of Raman scattering in ZnO. *Physical review B*, 75(16), 165202.

Da Silva Jr, J. B., Espinal, M., & Ramón-Pardo, P. (2020). Antimicrobial resistance: time for action. *Revista panamericana de salud pública*, 14(2), *44*.

Daeschlein, G. (2013). Antimicrobial and antiseptic strategies in wound management. *International wound journal*, *10*(s1), 9-14.

Das, B., Das, A., Kothari, V., Fanguiero, R., & Araujo, M. D. (2009). Moisture flow through blended fabrics–Effect of hydrophilicity. *Journal of engineered fibers and fabrics*, 4(4), 155892500900400405.

Das, J., Pradhan, S. K., Sahu, D. R., Mishra, D. K., Sarangi, S. N., Nayak, B. B., & Roul, B. K. (2010). Micro-Raman and XPS studies of pure ZnO ceramics. *Physica B: condensed matter*, 405(10), 2492-2497.

Debbichi, L., Marco de Lucas, M. C., Pierson, J. F., & Kruger, P. (2012). Vibrational properties of CuO and Cu4O3 from first-principles calculations, and Raman and infrared spectroscopy. *The Journal of physical chemistry C*, 116(18), 10232-10237.

Deng, Y., Handoko, A. D., Du, Y., Xi, S., & Yeo, B. S. (2016). In situ Raman spectroscopy of copper and copper oxide surfaces during electrochemical oxygen evolution reaction: identification of CuIII oxides as catalytically active species. *ACS catalysis*, 6(4), 2473-2481.

De Rosa, I. M., Kenny, J. M., Puglia, D., Santulli, C., & Sarasini, F. (2010). Morphological, thermal and mechanical characterization of okra (Abelmoschus esculentus) fibres as potential reinforcement in polymer composites. *Composites science and technology*, 70(1), 116-122.

Deshmukh, S. P., Patil, S. M., Mullani, S. B., & Delekar, S. D. (2019). Silver nanoparticles as an effective disinfectant: A review. *Materials science and engineering: C*, 97, 954-965.

Devnani, G. L., & Sinha, S. (2019). Extraction, characterization and thermal degradation kinetics with activation energy of untreated and alkali treated Saccharum spontaneum (Kans grass) fiber. *Composites part B: engineering*, 166, 436-445.

El-Naggar, M. E., Shaarawy, S., & Hebeish, A. A. (2018). Multifunctional properties of cotton fabrics coated with in situ synthesis of zinc oxide nanoparticles capped with date seed extract. *Carbohydrate polymers*, 181, 307-316.

El-Naggar, M. E., Shaheen, T. I., Zaghloul, S., El-Rafie, M. H., & Hebeish, A. (2016). Antibacterial activities and UV protection of the in situ synthesized titanium oxide nanoparticles on cotton fabrics. *Industrial and engineering chemistry research*, 55(10), 2661-2668.

El-Nahhal, I. M., Elmanama, A. A., El Ashgar, N. M., Amara, N., Selmane, M., & Chehimi, M. M. (2017). Stabilization of nano-structured ZnO particles onto the surface of cotton fibers using different surfactants and their antimicrobial activity. *Ultrasonics sonochemistry*, 38, 478-487.

El-Nahhal, I. M., Salem, J., Anbar, R., Kodeh, F. S., & Elmanama, A. (2020). Preparation and antimicrobial activity of ZnO-NPs coated cotton/starch and their functionalized ZnO-Ag/cotton and Zn (II) curcumin/cotton materials. *Scientific reports*, 10(1), 5410.

El-Nahhal, I., Salem, J., Kodeh, F., Anbar, R., & Elmanama, A. (2021). Preparation of CuO-NPs coated cotton, starched cotton and its CuO-Ag nanocomposite, Cu (II) curcumin complex coated cotton and their Antimicrobial Activities. *Journal of nanomedicine and nanotechnol*ogy 12, 566.

El-Nahhal, I. M., Salem, J., Kodeh, F. S., Elmanama, A., & Anbar, R. (2022). CuO–NPs, CuO–Ag nanocomposite and Cu (II)-curcumin complex coated cotton/starched cotton antimicrobial materials. *Materials chemistry and physics*, 285, 126099.

Eskandari, V., Sahbafar, H., Zeinalizad, L., Mahmoudi, R., Karimpour, F., Hadi, A., & Bardania, H. (2022). Coating of silver nanoparticles (AgNPs) on glass fibers by a chemical method as plasmonic surface-enhanced Raman spectroscopy (SERS) sensors to detect molecular vibrations of Doxorubicin (DOX) drug in blood plasma. *Arabian journal of chemistry*, 15(8), 104005.

Espitia, P. J. P., Soares, N. D. F. F., Coimbra, J. S. D. R., de Andrade, N. J., Cruz, R. S., & Medeiros, E. A. A. (2012). Zinc oxide nanoparticles: synthesis, antimicrobial activity and food packaging applications. *Food and bioprocess technology*, 5, 1447-1464.

Fateixa, S., Wilhelm, M., Nogueira, H. I., & Trindade, T. (2016). SERS and Raman imaging as a new tool to monitor dyeing on textile fibres. *Journal of Raman spectroscopy*, 47(10), 1239-1246.

Fijan, S., & Šostar Turk, S. (2012). Hospital textiles, are they a possible vehicle for healthcare-associated infections. *International journal of environmental research and public health*, 9(9), 3330-3343.

Fouda, A., Saad, E. L., Salem, S. S., & Shaheen, T. I. (2018). In-Vitro cytotoxicity, antibacterial, and UV protection properties of the biosynthesized Zinc oxide nanoparticles for medical textile applications. *Microbial pathogenesis*, 125, 252-261.

Fuku, X., Modibedi, M., & Mathe, M. (2020). Green synthesis of Cu/Cu 2 O/CuO nanostructures and the analysis of their electrochemical properties. *SN applied sciences*, 2, 1-15.

Fu, F., Gu, J., Zhang, R., Xu, X., Yu, X., Liu, L., & Yao, J. (2018). Three-dimensional cellulose based silver-functionalized ZnO nanocomposite with controlled geometry: synthesis, characterization and properties. *Journal of colloid and interface science*, 530, 433-443.

Galkina, O. L., Sycheva, A., Blagodatskiy, A., Kaptay, G., Katanaev, V. L., Seisenbaeva, G. A., & Agafonov, A. V. (2014). The sol–gel synthesis of cotton/TiO_2 composites and their antibacterial properties. *Surface and coatings technology*, 253, 171-179.

Gao, S., Su, J., Wang, W., Fu, J., & Wang, H. (2021). Highly efficient and durable antibacterial cotton fabrics finished with zwitterionic polysulfobetaine by one-step eco-friendly strategy. *Cellulose*, 28, 1139-1152.

Gatou, M. A., Lagopati, N., Vagena, I. A., Gazouli, M., & Pavlatou, E. A. (2022). ZnO nanoparticles from different precursors and their photocatalytic potential for biomedical use. *Nanomaterials*, 13(1), 122.

Gedanken, A. (2004). Using sonochemistry for the fabrication of nanomaterials. *Ultrasonics sonochemistry*, 11(2), 47-55.

Ghayempour, S., & Montazer, M. (2017). Ultrasound irradiation based in-situ synthesis of star-like Tragacanth gum/zinc oxide nanoparticles on cotton fabric. *Ultrasonics sonochemistry*, 34, 458-465.

Ghodselahi, T., Vesaghi, M. A., Shafiekhani, A., Baghizadeh, A., & Lameii, M. (2008). XPS study of the Cu@ Cu2O core-shell nanoparticles. *Applied surface science*, 255(5), 2730-2734.

Görgülüer, H., Çakıroğlu, B., & Özacar, M. (2021). Ag NPs deposited TiO_2 coating material for superhydrophobic, antimicrobial and self-cleaning surface fabrication on fabric. *Journal of coatings technology and research*, 18, 569-579.

Gutema, G., Håkonsen, H., Engidawork, E., & Toverud, E. L. (2018). Multiple challenges of antibiotic use in a large hospital in Ethiopia–a ward-specific study showing high rates of hospital-acquired infections and ineffective prophylaxis. *BMC health services research*, 18, 1-7.

Haque, M., Sartelli, M., McKimm, J., & Bakar, M. A. (2018). Health care-associated infections–an overview. *Infection and drug resistance*, 11, 2321-2333.

Hasan, R. (2018). Production of antimicrobial textiles by using copper oxide nanoparticles. *International journal of contemporary research and review*, 9, 20195-20202.

Hassan, B. S., Islam, G. M. N., & Haque, A. N. M. A. (2019). Applications of nanotechnology in textiles: A review. *Advanced research in textile engineering*, 4(2), 1038-1048.

Hassabo, A. G., El-Naggar, M. E., Mohamed, A. L., & Hebeish, A. A. (2019). Development of multifunctional modified cotton fabric with tri-component nanoparticles of silver, copper and zinc oxide. *Carbohydrate polymers*, 210, 144-156.

Hatamie, A., Khan, A., Golabi, M., Turner, A. P., Beni, V., Mak, W. C., & Willander, M. (2015). Zinc oxide nanostructure-modified textile and its application to biosensing, photocatalysis, and as antibacterial material. *Langmuir*, 31(39), 10913-10921.

Hina, K., Zou, H., Qian, W., Zuo, D., & Yi, C. (2018). Preparation and performance comparison of cellulose-based activated carbon fibres. *Cellulose*, 25, 607-617.

https://thecounter.org/fda-approves-genetically-modified-cotton-human-consumption accessed on August 12, 2023.

Ibrahim, M. M., Mezni, A., El-Sheshtawy, H. S., Zaid, A. A. A., Alsawat, M., El-Shafi, N., & Altalhi, T. (2019). Direct Z-scheme of Cu_2O/TiO_2 enhanced self-cleaning,

antibacterial activity, and UV protection of cotton fiber under sunlight. *Applied surface science*, 479, 953-962.

Ibrahim, N. A., Nada, A. A., Eid, B. M., Al-Moghazy, M., Hassabo, A. G., & Abou-Zeid, N. Y. (2018). Nano-structured metal oxides: synthesis, characterization and application for multifunctional cotton fabric. *Advances in natural sciences: nanoscience and nanotechnology*, 9(3), 035014.

Islam, M. S., Akter, N., Rahman, M. M., Shi, C., Islam, M. T., Zeng, H., & Azam, M. S. (2018). Mussel-inspired immobilization of silver nanoparticles toward antimicrobial cellulose paper. *ACS Sustainable chemistry and engineering*, 6(7), 9178-9188.

Jagadeeshan, S., & Parsanathan, R. (2019). Nano-metal oxides for antibacterial activity. *Advanced nanostructured materials for environmental remediation*, 25, 59-90.

Javed, A., Wiener, J., Tamulevičienė, A., Tamulevičius, T., Lazauskas, A., Saskova, J., & Račkauskas, S. (2021). One step in-situ synthesis of zinc oxide nanoparticles for multifunctional cotton fabrics. *Materials*, 14(14), 3956.

Jeevanandam, J., Barhoum, A., Chan, Y. S., Dufresne, A., & Danquah, M. K. (2018). Review on nanoparticles and nanostructured materials: history, sources, toxicity and regulations. *Beilstein journal of nanotechnology*, 9(1), 1050-1074.

Jiang, H. Y., Ouyang, Z. Y., Hu, R., Wan, J., & Zhu, J. J. (2021). Self-cleaning Finishing of Cotton Fabric with TiO_2/Ag_2 S/rGO Composite. *Fibers and polymers*, 23, 1-9.

Joshi, M., Khanna, R., Shekhar, R., & Jha, K. (2011). Chitosan nanocoating on cotton textile substrate using layer-by-layer self-assembly technique. *Journal of applied polymer science*, 119(5), 2793-2799

Kalayu, A. A., Diriba, K., Girma, C., & Abdella, E. (2019). Incidence and bacterial etiologies of surgical site infections in a Public Hospital, Addis Ababa, Ethiopia. *The 0pen microbiology journal*, 13(1), 20-29.

Kampf, G. (2020). How long can nosocomial pathogens survive on textiles? A systematic review. *GMS Hygiene and infection control*, 15, PMC7273332.

Kasemets, K., Ivask, A., Dubourguier, H. C., & Kahru, A. (2009). Toxicity of nanoparticles of ZnO, CuO and TiO_2 to yeast Saccharomyces cerevisiae. *Toxicology in vitro*, 23(6), 1116-1122.

Kasumov, A. M., Strelchuk, V. V., Kolomys, O. F., Bykov, O. I., Yukhymchuk, V. O., Zahornyi, M. M., ... & Ievtushenko, A. I. (2021). Properties of nanosized ZnO: Ho films deposited using explosive evaporation. *Semiconductor physics, quantum electronics and optoelectronics*, 24(2), 139-147.

Kavkler, K., & Demšar, A. (2011). Examination of cellulose textile fibres in historical objects by micro-Raman spectroscopy. *Spectrochimica Acta Part A: Molecular and biomolecular spectroscopy*, 78(2), 740-746.

Khatami, M., Varma, R. S., Zafarnia, N., Yaghoobi, H., Sarani, M., & Kumar, V. G. (2018). Applications of green synthesized Ag, ZnO and Ag/ZnO nanoparticles for making clinical antimicrobial wound-healing bandages. *Sustainable Chemistry and pharmacy*, 10, 9-15.

King, D. G., & Pierlot, A. P. (2009). Absorption of nanoparticles by wool. *Coloration technology*, 125(2), 111-116.

Klemm, D., Heublein, B., Fink, H. P., & Bohn, A. (2005). Cellulose: fascinating biopolymer and sustainable raw material. *Angewandte chemie international edition*, *44*(22), 3358-3393.

Kucuk, M., & Ovecoglu, M. L. (2020). Fabrication of SiO2-ZnO NP/ZnO NR hybrid coated cotton fabrics: the effect of ZnO NR growth time on structural and UV protection characteristics. *Cellulose*, 27(3), 1773-1793.

Kumar, A., Sharma, M., & Vaish, R. (2023). $BaTiO_3$ nanoparticles embedded antibacterial cotton fabric with UV protection characteristics. *Journal of natural bibers*, 20(1), 2139325.

Kurtz, E. J., Yelverton, C. B., Camacho, F. T., & Fleischer, Jr, A. B. (2008). Use of a silklike bedding fabric in patients with atopic dermatitis. *Pediatric dermatology*, 25(4), 439-443.

Kwak, W. G., Oh, M. H., & Gong, M. S. (2015). Preparation of silver-coated cotton fabrics using silver carbamate via thermal reduction and their properties. *Carbohydrate polymers*, 115, 317-324.

Labi, A. K., Obeng-Nkrumah, N., Owusu, E., Bjerrum, S., Bediako-Bowan, A., Sunkwa-Mills, G., & Newman, M. J. (2019). Multi-centre point-prevalence survey of hospital-

acquired infections in Ghana. *Journal of hospital infection*, 101(1), 60-68.

Leyland, N. S., Podporska-Carroll, J., Browne, J., Hinder, S. J., Quilty, B., & Pillai, S. C. (2016). Highly Efficient F, Cu doped TiO_2 anti-bacterial visible light active photocatalytic coatings to combat hospital-acquired infections. *Scientific reports*, 6(1), 24770.

Liang, Y., Guo, N., Li, L., Li, R., Ji, G., & Gan, S. (2015). Fabrication of porous 3D flower-like Ag/ZnO heterostructure composites with enhanced photocatalytic performance. *Applied surface science*, 332, 32-39.

Li, R., Che, J., Zhang, H., He, J., Bahi, A., & Ko, F. (2014). Study on synthesis of ZnO nanorods and its UV-blocking properties on cotton fabrics coated with the ZnO quantum dot. *Journal of nanoparticle research*, 16, 1-12.

Li, S., Zhu, T., Huang, J., Guo, Q., Chen, G., & Lai, Y. (2017). Durable antibacterial and UV-protective Ag/TiO_2@ fabrics for sustainable biomedical application. *International journal of nanomedicine*, 12, 2593-2606.

Li, S., Huang, J., Ge, M., Cao, C., Deng, S., Zhang, S., & Lai, Y. (2015). Robust flower-like TiO2@ cotton fabrics with special wettability for effective self-cleaning and versatile oil/water separation. *Advanced materials interfaces*, 2(14), 1500220.

Li, Z., Meng, J., Wang, W., Wang, Z., Li, M., Chen, T., & Liu, C. J. (2017). The room temperature electron reduction for the preparation of silver nanoparticles on cotton with high antimicrobial activity. *Carbohydrate polymers*, 161, 270-276.

Linic, S., Aslam, U., Boerigter, C., & Morabito, M. (2015). Photochemical transformations on plasmonic metal nanoparticles. *Nature materials*, 14(6), 567-576.

Lin, B., Qiu, B., Qiu, L., Si, Z., Chu, F., Chen, X., & Yan, F. (2013). Imidazolium-Functionalized SiO2 Nanoparticle Doped Proton Conducting Membranes for Anhydrous Proton Exchange Membrane Applications. *Fuel cells*, 13(1), 72-78.

Liou, J. W., & Chang, H. H. (2012). Bactericidal effects and mechanisms of visible light-responsive titanium dioxide photocatalysts on pathogenic bacteria. *Archivum immunologiae et therapiae experimentalis*, 60, 267-275.

Liu, M. S., Lin, M. C. C., Tsai, C. Y., & Wang, C. C. (2006). Enhancement of thermal conductivity with Cu for nanofluids using chemical reduction method. *International*

journal of heat and mass transfer, 49(17-18), 3028-3033.

Mabrouk, M. M., Mansour, A. T., Abdelhamid, A. F., Abualnaja, K. M., Mamoon, A., Gado, W. S., & Ayoub, H. F. (2021). Impact of aqueous exposure to silver nanoparticles on growth performance, redox status, non-specific immunity, and histopathological changes of Nile Tilapia, Oreochromis niloticus, challenged with Aeromonas hydrophila. *Aquaculture reports*, *21*, 100816.

Mai, L., Wang, D., Zhang, S., Xie, Y., Huang, C., & Zhang, Z. (2010). Synthesis and bactericidal ability of Ag/TiO2 composite films deposited on titanium plate. *Applied surface science*, 257(3), 974-978.

Marković, D., Tseng, H. H., Nunney, T., Radoičić, M., Ilic-Tomic, T., & Radetić, M. (2020). Novel antimicrobial nanocomposite based on polypropylene non-woven fabric, biopolymer alginate and copper oxides nanoparticles. *Applied surface science*, 527, 146829.

Martinez-Gutierrez, F., Olive, P. L., Banuelos, A., Orrantia, E., Nino, N., Sanchez, E. M., & Av-Gay, Y. (2010). Synthesis, characterization, and evaluation of antimicrobial and cytotoxic effect of silver and titanium nanoparticles. *Nanomedicine: nanotechnology, biology and medicine*, 6(5), 681-688.

Medici, S., Peana, M., Nurchi, V. M., & Zoroddu, M. A. (2019). Medical uses of silver: history, myths, and scientific evidence. *Journal of medicinal chemistry*, 62(13), 5923-5943.

Mengesha, R. E., Kasa, B. G. S., Saravanan, M., Berhe, D. F., & Wasihun, A. G. (2014). Aerobic bacteria in post-surgical wound infections and pattern of their antimicrobial susceptibility in Ayder Teaching and Referral Hospital, Mekelle, Ethiopia. *BMC research notes*, 7(1), 1-6.

Méthivier, C., Humblot, V., & Pradier, C. M. (2015). L-Methionine adsorption on Cu (110), binding and geometry of the amino acid as a function of coverage. *Surface science*, 632, 88-92.

Mohammad, N. F., Ahmad, R. N., Rosli, N. M., Manan, M. A., Marzuki, M., & Wahi, A. (2021). Sol gel deposited hydroxyapatite-based coating technique on porous titanium niobium for biomedical applications: A mini review. *Materials today: proceedings*, *41*, 127-135.

Mohammed, A., Seid, M. E., Gebrecherkos, T., Tiruneh, M., & Moges, F. (2017). Bacterial isolates and their antimicrobial susceptibility patterns of wound infections among inpatients and outpatients attending the University of Gondar Referral Hospital, Northwest Ethiopia. *International journal of microbiology*, 2017(1), 8953829.

Montaser, A. S., Wassel, A. R., & Al-Shaye'a, O. N. (2019). Synthesis, characterization and antimicrobial activity of Schiff bases from chitosan and salicylaldehyde/TiO_2 nanocomposite membrane. *International journal of biological macromolecules*, 124, 802-809.

Montazer, M., Alimohammadi, F., Shamei, A., & Rahimi, M. K. (2012). Durable antibacterial and cross-linking cotton with colloidal silver nanoparticles and butane tetracarboxylic acid without yellowing. *Colloids and surfaces B: biointerfaces*, 89, 196-202.

Morris, H., & Murray, R. (2020). Medical textiles. *Textile progress*, 52(1-2), 1-127.

Munir, M. U., Ashraf, M., Abid, H. A., Javid, A., Riaz, S., Khanzada, H., & Iqbal, K. (2022). Coating of modified ZnO nanoparticles on cotton fabrics for enhanced functional characteristics. *Journal of coatings technology and research*, 19, 1-9.

Noman, M. T., Petru, M., Amor, N., & Louda, P. (2020). Thermophysiological comfort of zinc oxide nanoparticles coated woven fabrics. *Scientific reports*, 10(1), 21080.

Parvathiraja, C., & Shailajha, S. (2021). Bioproduction of CuO and Ag/CuO heterogeneous photocatalysis-photocatalytic dye degradation and biological activities. *Applied nanoscience*, 11, 1411-1425.

Paszkiewicz, M., Gołąbiewska, A., Rajski, Ł., Kowal, E., Sajdak, A., & Zaleska-Medynska, A. (2016). The antibacterial and antifungal textile properties functionalized by bimetallic nanoparticles of Ag/Cu with different structures. *Journal of nanomaterials*, *2016*.

Paul, D., & Neogi, S. (2019). Synthesis, characterization and a comparative antibacterial study of CuO, NiO and CuO-NiO mixed metal oxide. *Materials research express*, 6(5), 055004.

Perevedentseva, E., Lin, Y. C., Karmenyan, A., Wu, K. T., Lugovtsov, A., Shirshin, E., & Cheng, C. L. (2021). Raman spectroscopic study of TiO_2 nanoparticles' effects on the

Hemoglobin state in individual red blood cells. *Materials*, 14(20), 5920.

Perelshtein, I., Lipovsky, A., Perkas, N., Tzanov, T., Arguirova, M., Leseva, M., & Gedanken, A. (2015). Making the hospital a safer place by sonochemical coating of all its textiles with antibacterial nanoparticles. *Ultrasonics sonochemistry*, 25, 82-88.

Petkova, P., Francesko, A., Perelshtein, I., Gedanken, A., & Tzanov, T. (2016). Simultaneous sonochemical-enzymatic coating of medical textiles with antibacterial ZnO nanoparticles. *Ultrasonics sonochemistry*, 29, 244-250.

Porrawatkul, P., Pimsen, R., Kuyyogsuy, A., Teppaya, N., Noypha, A., Chanthai, S., & Nuengmatcha, P. (2022). Microwave-assisted synthesis of Ag/ZnO nanoparticles using Averrhoa carambola fruit extract as the reducing agent and their application in cotton fabrics with antibacterial and UV-protection properties. *RSC advances*, 12(24), 15008-15019.

Rabbi, M. A., Rahman, M. M., Minami, H., Rahman, M. A., Hoque, S. M., & Ahmad, H. (2019). Biocomposites of synthetic polymer modified microcrystalline jute cellulose particles and their hemolytic behavior. *Cellulose*, 26, 8713-8727.

Radetić, M., & Marković, D. (2019). Nano-finishing of cellulose textile materials with copper and copper oxide nanoparticles. *Cellulose*, 26, 8971-8991.

Rai, M. K., Deshmukh, S. D., Ingle, A. P., & Gade, A. K. (2012). Silver nanoparticles: the powerful nanoweapon against multidrug-resistant bacteria. *Journal of applied microbiology*, 112(5), 841-852.

Rajaboopathi, S., & Thambidurai, S. (2018). Evaluation of UPF and antibacterial activity of cotton fabric coated with colloidal seaweed extract functionalized silver nanoparticles. *Journal of photochemistry and photobiology B: biology*, 183, 75-87.

Rasheed, N. A., & Hussein, N. R. (2021). Staphylococcus aureus: an overview of discovery, characteristics, epidemiology, virulence factors and antimicrobial sensitivity. *European journal of molecular and clinical medicine*, 8(3), 1160-1183.

Rasmussen, J. W., Martinez, E., Louka, P., & Wingett, D. G. (2010). Zinc oxide nanoparticles for selective destruction of tumor cells and potential for drug delivery applications. *Expert opinion on drug delivery*, 7(9), 1063-1077.

Raut, S. B., Vasavada, D. A., & Chaudhari, S. B. (2010). Nano particles-Application in

textile finishing. *Man-made textiles in India*, 53(12), 7-12.

Rehan, M., Barhoum, A., Van Assche, G., Dufresne, A., Gätjen, L., & Wilken, R. (2017). Towards multifunctional cellulosic fabric: UV photo-reduction and in-situ synthesis of silver nanoparticles into cellulose fabrics. *International journal of biological macromolecules*, 98, 877-886.

Rezaie, A. B., Montazer, M., & Rad, M. M. (2017). Photo and biocatalytic activities along with UV protection properties on polyester fabric through green in-situ synthesis of cauliflower-like CuO nanoparticles. *Journal of photochemistry and photobiology B: biology*, 176, 100-111.

Rochford, C., Sridhar, D., Woods, N., Saleh, Z., Hartenstein, L., Ahlawat, H., & Davies, S. (2018). Global governance of antimicrobial resistance. *The Lancet*, 391(10134), 1976-1978.

Rodrigues, A. G., Romano de Oliveira Gonçalves, P. J., Ottoni, C. A., de Cássia Ruiz, R., Morgano, M. A., de Araújo, W. L., & De Souza, A. O. (2019). Functional textiles impregnated with biogenic silver nanoparticles from Bionectria ochroleuca and its antimicrobial activity. *Biomedical microdevices*, 21, 1-10.

Roque-Ruiz, J. H., Castillo-Ramírez, D., de Jesús Ruíz-Baltazar, Á., Espinosa-Cristóbal, L. F., & Reyes-López, S. Y. (2018). Preparation of silver-doped alumina spherical beads with antimicrobial properties. *Journal of nanomaterials*, *2018(1)*, 7127843.

Rotaru, R., Savin, M., Tudorachi, N., Peptu, C., Samoila, P., Sacarescu, L., & Harabagiu, V. (2018). Ferromagnetic iron oxide–cellulose nanocomposites prepared by ultrasonication. *Polymer chemistry*, 9(7), 860-868.

Saafan, A. A., & Habib, A. M. (1987). Influence of changes in fine structure on thermal properties of cotton fibres. *Journal of thermal analysis*, 32, 1511-1519.

Sahoo, S. K., Parveen, S., & Panda, J. J. (2017). The present and future of nanotechnology in human health care. *Nanomedicine in cancer*, 775-806.

Santo, C. E., Taudte, N., Nies, D. H., & Grass, G. (2008). Contribution of copper ion resistance to survival of Escherichia coli on metallic copper surfaces. *Applied and environmental microbiology*, *74*(4), 977-986.

Salat, M., Petkova, P., Hoyo, J., Perelshtein, I., Gedanken, A., & Tzanov, T. (2018). Durable

antimicrobial cotton textiles coated sonochemically with ZnO nanoparticles embedded in an in-situ enzymatically generated bioadhesive. *Carbohydrate polymers*, *189*, 198-203.

Salem, S. S., & Fouda, A. (2021). Green synthesis of metallic nanoparticles and their prospective biotechnological applications: an overview. *Biological trace element research*, *199*, 344-370.

Sánchez-López, E., Gomes, D., Esteruelas, G., Bonilla, L., Lopez-Machado, A. L., Galindo, R., & Souto, E. B. (2020). Metal-based nanoparticles as antimicrobial agents: an overview. *Nanomaterials*, *10*(2), 292.

Sasahara, T., Hayashi, S., Morisawa, Y., Sakihama, T., Yoshimura, A., & Hirai, Y. (2011). Bacillus cereus bacteremia outbreak due to contaminated hospital linens. *European journal of clinical microbiology and infectious diseases*, *30*, 219-226.

Satyanarayana, K. G., Guimarães, J. L., & Wypych, F. E. R. N. A. N. D. O. (2007). Studies on lignocellulosic fibers of Brazil. Part I: Source, production, morphology, properties and applications. *Composites Part A: applied science and manufacturing*, 38(7), 1694-1709.

Shaheen, T. I., & Abd El Aty, A. A. (2018). In-situ green myco-synthesis of silver nanoparticles onto cotton fabrics for broad spectrum antimicrobial activity. *International journal of biological macromolecules*, 118, 2121-2130.

Shaheen, T. I., Fouda, A., & Salem, S. S. (2021). Integration of cotton fabrics with biosynthesized CuO nanoparticles for bactericidal activity in the terms of their cytotoxicity assessment. *Industrial and engineering chemistry research*, 60(4), 1553-1563.

Shahidi, S., Jamali, A., Dalal Sharifi, S., & Ghomi, H. (2018). In-situ synthesis of CuO nanoparticles on cotton fabrics using spark discharge method to fabricate antibacterial textile. *Journal of natural fibers*, 15(6), 870-881.

Shaikh, S. F., Mane, R. S., Min, B. K., Hwang, Y. J., & Joo, O. S. (2016). D-sorbitol-induced phase control of TiO_2 nanoparticles and its application for dye-sensitized solar cells. *Scientific reports*, 6(1), 20103.

Shao, D., Gao, Y., Cao, K., & Wei, Q. (2017). Rapid surface functionalization of cotton

fabrics by modified hydrothermal synthesis of ZnO. *The Journal of the textile institute*, 108(8), 1391-1397.

Siddiqui, H., Parra, M. R., Pandey, P., Qureshi, M. S., & Haque, F. Z. (2020). Utility of copper oxide nanoparticles (CuO-NPs) as efficient electron donor material in bulk-heterojunction solar cells with enhanced power conversion efficiency. *Journal of Science: Advanced materials and devices*, 5(1), 104-110.

Singh, G., Joyce, E. M., Beddow, J., & Mason, T. J. (2012). Evaluation of antibacterial activity of ZnO nanoparticles coated sonochemically onto textile fabrics. *Journal of microbiology, biotechnology and food sciences*, 2(1), 106-120.

Singh, P., Garg, A., Pandit, S., Mokkapati, V. R. S. S., & Mijakovic, I. (2018). Antimicrobial effects of biogenic nanoparticles. *Nanomaterials*, 8(12), 1009.

Sivaranjana, P., Nagarajan, E. R., Rajini, N., Ayrilmis, N., Rajulu, A. V., & Siengchin, S. (2021). Preparation and characterization studies of modified cellulosic textile fabric composite with in situ-generated AgNPs coating. *Journal of industrial textiles*, 50(7), 1111-1126.

Sizeland, K. H., Hofman, K. A., Hallett, I. C., Martin, D. E., Potgieter, J., Kirby, N. M., & Cumming, M. H. (2018). Nanostructure of electrospun collagen: Do electrospun collagen fibers form native structures. *Materialia*, 3, 90-96.

Slavin, Y. N., Asnis, J., Hńfeli, U. O., & Bach, H. (2017). Metal nanoparticles: understanding the mechanisms behind antibacterial activity. *Journal of nanobiotechnology*, 15, 1-20.

Sood, A., Granick, M. S., & Tomaselli, N. L. (2014). Wound dressings and comparative effectiveness data. *Advances in wound care*, 3(8), 511-529.

Sportelli, M. C., Izzi, M., Kukushkina, E. A., Hossain, S. I., Picca, R. A., Ditaranto, N., & Cioffi, N. (2020). Can nanotechnology and materials science help the fight against SARS-CoV-2?. *Nanomaterials*, 10(4), 802.

Stan, M. S., Nica, I. C., Popa, M., Chifiriuc, M. C., Iordache, O., Dumitrescu, I., & Dinischiotu, A. (2019). Reduced graphene oxide/TiO_2 nanocomposites coating of cotton fabrics with antibacterial and self-cleaning properties. *Journal of industrial textiles*, 49(3), 277-293.

Sun, C., Li, Y., Li, Z., Su, Q., Wang, Y., & Liu, X. (2018). Durable and washable antibacterial copper nanoparticles bridged by surface grafting polymer brushes on cotton and polymeric materials. *Journal of nanomaterials*, 2018 (1), 6546193.

Tabah, A., Koulenti, D., Laupland, K., Misset, B., Valles, J., Bruzzi de Carvalho, F., & Timsit, J. F. (2012). Characteristics and determinants of outcome of hospital-acquired bloodstream infections in intensive care units: the EUROBACT International Cohort Study. *Intensive care medicine*, 38, 1930-1945.

Taheri, M., Montazer, M., & Rezaie, A. B. (2021). A Cleaner affordable method for production of bactericidal textile substrates by in situ deposition of ZnO/Ag nanoparticles. *Fibers and polymers*, 22(10), 2792-2802.

Takahashi, A., Yomoda, S., Tanimoto, K., Kanda, T., Kobayashi, I., & Ike, Y. (1998). Streptococcus pyogenes hospital-acquired infection within a dermatological ward. *Journal of hospital infection*, 40(2), 135-140.

Tamire, T., Eticha, T., & Gelgelu, T. B. (2021). Methicillin-Resistant Staphylococcus aureus: The Magnitude and Risk Factors among Patients Admitted to Tikur Anbessa Specialized Hospital, Addis Ababa, Ethiopia. *International journal of microbiology*, 2021(1), 9933926.

Tassios, P. T., Gennimata, V., Spaliara-Kalogeropoulou, L., Koutsia, C., Vatopoulos, A. C., Legakis, N. J., & Kairis, D. (1997). Multiresistant Pseudomonas aeruginosa serogroup O: 11 outbreak in an intensive care unit. *Clinical microbiology and infection*, 3(6), 621-628.

Tatlıdil, İ., Sökmen, M., Breen, C., Clegg, F., Buruk, C. K., & Bacaksız, E. (2011). Degradation of C andida albicans on TiO 2 and Ag-TiO 2 thin films prepared by sol–gel and nanosuspensions. *Journal of sol-gel science and technology*, 60, 23-32.

Thampi, V. A., Thanka Rajan, S., Anupriya, K., & Subramanian, B. (2015). Functionalization of fabrics with PANI/CuO nanoparticles by precipitation route for anti-bacterial applications. *Journal of nanoparticle research*, *17*, 1-12.

Tolera, M., Abate, D., Dheresa, M., & Marami, D. (2018). Bacterial nosocomial infections and antimicrobial susceptibility pattern among patients admitted at Hiwot Fana Specialized University Hospital, Eastern Ethiopia. *Advances in medicine*, 2018(1)

2127814.

Tomczak, F., Satyanarayana, K. G., & Sydenstricker, T. H. D. (2007). Studies on lignocellulosic fibers of Brazil: Part III–Morphology and properties of Brazilian curauá fibers. *Composites Part A: Applied science and manufacturing*, 38(10), 2227-2236.

Topalovic, T., Nierstrasz, V. A., Bautista, L., Jocic, D., Navarro, A., & Warmoeskerken, M. M. (2007). XPS and contact angle study of cotton surface oxidation by catalytic bleaching. *Colloids and surfaces A: physicochemical and engineering aspects*, 296(1-3), 76-85.

Toval, F., Köhler, C. D., Vogel, U., Wagenlehner, F., Mellmann, A., Fruth, A., & Dobrindt, U. (2014). Characterization of Escherichia coli isolates from hospital inpatients or outpatients with urinary tract infection. *Journal of clinical microbiology*, 52(2), 407-418.

Tremiliosi, G. C., Simoes, L. G. P., Minozzi, D. T., Santos, R. I., Vilela, D. C., Durigon, E. L., & Freitas-Junior, L. H. (2020). Ag nanoparticles-based antimicrobial polycotton fabrics to prevent the transmission and spread of SARS-CoV-2. *Bio archive*, 11, 2020-06.

Tripathi, R., Narayan, A., Bramhecha, I., & Sheikh, J. (2019). Development of multifunctional linen fabric using chitosan film as a template for immobilization of in-situ generated CeO_2 nanoparticles. *International journal of biological macromolecules*, 121, 1154-1159.

Usman, M. S., Zowalaty, M. E. E., Shameli, K., Zainuddin, N., Salama, M., & Ibrahim, N. A. (2013). Synthesis, characterization, and antimicrobial properties of copper nanoparticles. *International journal of nanomedicine*, 8, 4467-4479.

Verma, V., Al-Dossari, M., Singh, J., Rawat, M., Kordy, M. G., & Shaban, M. (2022). A review on green synthesis of TiO2 NPs: photocatalysis and antimicrobial applications. *Polymers*, 14(7), 1444.

Vigneshwaran, N., Kathe, A. A., Varadarajan, P. V., Nachane, R. P., & Balasubramanya, R. H. (2007). Functional finishing of cotton fabrics using silver nanoparticles. *Journal of nanoscience and nanotechnology*, 7(6), 1893-1897.

Walker, M. J., Barnett, T. C., McArthur, J. D., Cole, J. N., Gillen, C. M., Henningham, A.,

& Nizet, V. (2014). Disease manifestations and pathogenic mechanisms of group A Streptococcus. *Clinical microbiology reviews*, 27(2), 264-301.

Wang, L., Hu, C., & Shao, L. (2017). The antimicrobial activity of nanoparticles: present situation and prospects for the future. *International journal of nanomedicine*, 12, 1227-1249.

Wang, X., Wang, Z., Zhang, M., Jiang, X., Wang, Y., Lv, J., & Sun, Z. (2017). Three-dimensional hierarchical anatase@ rutile TiO_2 nanotree array films decorated by silver nanoparticles as ultrasensitive recyclable surface-enhanced Raman scattering substrates. *Journal of alloys and compounds*, *725*, 1166-1174.

Wang, W., Liu, Z., Liu, Y., Xu, C., Zheng, C., & Wang, G. (2003). A simple wet-chemical synthesis and characterization of CuO nanorods. *Applied physics A*, *76*, 417-420.

Was-Gubala, J., & Machnowski, W. (2014). Application of Raman spectroscopy for differentiation among cotton and viscose fibers dyed with several dye classes. *Spectroscopy letters*, 47(7), 527-535.

Wu, Y., Yang, Y., Zhang, Z., Wang, Z., Zhao, Y., & Sun, L. (2019). Fabrication of cotton fabrics with durable antibacterial activities finishing by Ag nanoparticles. *Textile research journal*, 89(5), 867-880.

Xin, J. H., Daoud, W. A., & Kong, Y. Y. (2004). A new approach to UV-blocking treatment for cotton fabrics. *Textile research journal*, 74(2), 97-100.

Xu, B., & Cai, Z. (2008). Trial-manufacture and UV-blocking property of ZnO nanorods on cotton fabrics. *Journal of applied polymer science*, 108(6), 3781-3786.

Xu, Q., Wu, Y., Zhang, Y., Fu, F., & Liu, X. (2016). Durable antibacterial cotton modified by silver nanoparticles and chitosan derivative binder. *Fibers and polymers*, 17, 1782-1789.

Xu, Q., Wang, P., Zhang, Y., & Li, C. (2021). Durable antibacterial and UV protective properties of cotton fabric coated with carboxymethyl chitosan and Ag/TiO_2 composite nanoparticles. *Fibers and polymers*, 23, 1-10.

Xu, Q., Ke, X., Shen, L., Ge, N., Zhang, Y., Fu, F., & Liu, X. (2018). Surface modification by

carboxymethy chitosan via pad-dry-cure method for binding Ag NPs onto cotton fabric. *International Journal of biological macromolecules*, 111, 796-803.

Xu, Q., Xie, L., Diao, H., Li, F., Zhang, Y., Fu, F., & Liu, X. (2017). Antibacterial cotton fabric with enhanced durability prepared using silver nanoparticles and carboxymethyl chitosan. *Carbohydrate polymers*, 177, 187-193.

Yang, J. J., Huang, Y. C., Chuang, T. H., Herr, D. R., Hsieh, M. F., Huang, C. J., & Huang, C. M. (2020). Cysteine-capped hydrogels incorporating copper as effective antimicrobial materials against methicillin-resistant staphylococcus aureus. *Microorganisms*, 8(2), 149.

Yucelen, G. I., Connell, R. E., Terbush, J. R., Westenberg, D. J., & Dogan, F. (2015). Synthesis and immobilization of silver nanoparticles on aluminosilicate nanotubes and their antibacterial properties. *Applied nanoscience*, *6*, 607-614.

Yusof, N. A. A., Zain, N. M., & Pauzi, N. (2019). Synthesis of ZnO nanoparticles with chitosan as stabilizing agent and their antibacterial properties against Gram-positive and Gram-negative bacteria. *International journal of biological macromolecules*, 124, 1132-1136.

Zaborina, O., Holbrook, C., Chen, Y., Long, J., Zaborin, A., Morozova, I., & Alverdy, J. C. (2008). Structure–function aspects of PstS in multi-drug–resistant Pseudomonas aeruginosa. *Public library of science pathogens*, *4*(2), e43.

Zahid, M., Papadopoulou, E. L., Suarato, G., Binas, V. D., Kiriakidis, G., Gounaki, I.,& Athanassiou, A. (2018). Fabrication of visible light-induced antibacterial and self-cleaning cotton fabrics using manganese doped TiO_2 nanoparticles. *ACS applied bio materials*, 1(4), 1154-1164.

Zeleke, M., Adem, M., Aynalem, M., & Mossie, H. (2019). Cotton production and marketing trend in Ethiopia: A review. *Cogent food and agriculture*, 5(1), 1691812.

Zhang, G., Wang, D., Yan, J., Xiao, Y., Gu, W., & Zang, C. (2019). Study on the photocatalytic and antibacterial properties of TiO_2 nanoparticles-coated cotton fabrics. *Materials*, 12(12), 2010.

Zhang, Y., Xu, Q., Fu, F., & Liu, X. (2016). Durable antimicrobial cotton textiles modified with inorganic nanoparticles. *Cellulose*, 23, 2791-2808.

Zhao, W., Xiao, X., Pan, G., & Ye, Z. (2020). Fabrication of Cu species functionalized cotton fabric with oil/water separating reusability by in-situ reduction process. *Surface and coatings technology*, 385, 125405.

Zhou, J., Hu, X., Zhu, Y., Lyu, H., Zhang, L., Fu, F., & Liu, X. (2019). A hybrid binder of carboxymethyl chitosan and l-methionine enables a slight amount of Ag NPs to be durably effective on antibacterial cotton fabrics. *Cellulose*, 26, 9323-9333.

Zhu, J., Li, H., Wang, Y., Wang, Y., & Yan, J. (2021). Preparation of Ag NPs and its multifunctional finishing for cotton fabric. *Polymers*, 13(8), 1338.

Zille, A., Almeida, L., Amorim, T., Carneiro, N., Esteves, M. F., Silva, C. J., & Souto, A. P. (2014). Application of nanotechnology in antimicrobial finishing of biomedical textiles. *Materials research express*, 1(3), 032003.

Appendix

Table 1: Eλ, Tλ, and Sλ values from 290-400 nm for AmCot.

AmCot			
Wavelength (nm)	Eλ	Tλ	Sλ
290	1	26.002	7.57E-05
295	1	26.243	1.34E-03
300	0.649	26.607	1.36E-02
305	0.22	27.227	7.67E-02
310	7.45E-02	28.054	0.172
315	2.51E-02	29.04	0.282
320	8.60E-03	29.717	0.375
325	2.90E-03	30.339	0.494
330	1.36E-03	30.974	0.629
335	1.15E-03	31.623	0.602
340	9.70E-04	32.285	0.675
345	8.10E-04	32.584	0.65
350	6.80E-04	32.961	0.692
355	5.80E-04	33.189	0.743
360	4.80E-04	33.496	0.674
365	4.10E-04	33.651	0.849
370	3.40E-04	33.651	0.876
375	2.90E-04	33.806	0.78
380	2.43E-04	33.806	0.902
385	2.04E-04	33.962	0.693
390	1.72E-04	34.197	0.897
395	1.45E-04	34.514	0.693
400	1.22E-04	34.754	1.18

Table 2: Eλ, Tλ, and Sλ values from 290-400 nm for AmCot+Ag

AmCot+Ag			
Wavelength (nm)	Eλ	Tλ	Sλ
290	1	11.857	7.57E-05
295	1	11.995	1.34E-03
300	0.649	12.07814	1.36E-02
305	0.22	12.078	7.67E-02
310	7.45E-02	12.794	0.172
315	2.51E-02	13.803	0.282
320	8.60E-03	14.55	0.375
325	2.90E-03	14.757	0.494
330	1.36E-03	14.689	0.629
335	1.15E-03	14.554	0.602
340	9.70E-04	14.554	0.675
345	8.10E-04	14.421	0.65
350	6.80E-04	14.355	0.692
355	5.80E-04	14.322	0.743
360	4.80E-04	14.256	0.674
365	4.10E-04	14.256	0.849
370	3.40E-04	14.19	0.876
375	2.90E-04	14.125	0.78
380	2.43E-04	14.093	0.902
385	2.04E-04	14.093	0.693
390	1.72E-04	14.06	0.897
395	1.45E-04	14.028	0.693
400	1.22E-04	13.995	1.18

Table 3: Eλ, Tλ, and Sλ values from 290-400 nm for AmCot+CuO

AmCot+CuO			
Wavelength (nm)	Eλ	Tλ	Sλ
290	1	4.246196	7.57E-05
295	1	4.265795	1.34E-03
300	0.649	4.265795	1.36E-02
305	0.22	4.285485	7.67E-02
310	7.45E-02	4.477133	0.172
315	2.51E-02	4.786301	0.282
320	8.60E-03	4.954502	0.375
325	2.90E-03	5.000345	0.494
330	1.36E-03	5.035006	0.629
335	1.15E-03	5.069907	0.602
340	9.70E-04	5.093309	0.675
345	8.10E-04	5.128614	0.65
350	6.80E-04	5.164164	0.692
355	5.80E-04	5.248075	0.743
360	4.80E-04	5.272299	0.674
365	4.10E-04	5.308844	0.849
370	3.40E-04	5.382698	0.876
375	2.90E-04	5.407543	0.78
380	2.43E-04	5.457579	0.902
385	2.04E-04	5.508077	0.693
390	1.72E-04	5.571857	0.897
395	1.45E-04	5.61048	0.693
400	1.22E-04	5.64937	1.18

Table 4: Eλ, Tλ, and Sλ values from 290-400 nm for AmCot+TiO_2

AmCot+TiO_2			
Wavelength (nm)	Eλ	Tλ	Sλ
290	1	6.426877	7.57E-05
295	1	6.426877	1.34E-03
300	0.649	6.456542	1.36E-02
305	0.22	6.516284	7.67E-02
310	7.45E-02	6.714289	0.172
315	2.51E-02	7.095778	0.282
320	8.60E-03	7.498942	0.375
325	2.90E-03	7.780366	0.494
330	1.36E-03	8.109611	0.629
335	1.15E-03	8.413951	0.602
340	9.70E-04	8.810489	0.675
345	8.10E-04	9.141132	0.65
350	6.80E-04	9.527962	0.692
355	5.80E-04	9.862795	0.743
360	4.80E-04	10.20939	0.674
365	4.10E-04	10.51962	0.849
370	3.40E-04	10.78947	0.876
375	2.90E-04	11.01539	0.78
380	2.43E-04	11.22018	0.902
385	2.04E-04	11.45513	0.693
390	1.72E-04	11.61449	0.897
395	1.45E-04	11.83042	0.693
400	1.22E-04	11.99499	1.18

Table 5: Eλ, Tλ, and Sλ values from 290-400 nm for AmCot+ZnO

AmCot+ZnO			
Wavelength (nm)	Eλ	Tλ	Sλ
290	1	8.79	7.57E-05
295	1	8.77	1.34E-03
300	0.649	8.716	1.36E-02
305	0.22	8.67	7.67E-02
310	7.45E-02	9.099	0.172
315	2.51E-02	9.794	0.282
320	8.60E-03	10.447	0.375
325	2.90E-03	10.739	0.494
330	1.36E-03	10.914	0.629
335	1.15E-03	11.168	0.602
340	9.70E-04	11.35	0.675
345	8.10E-04	11.56	0.65
350	6.80E-04	11.776	0.692
355	5.80E-04	12.106	0.743
360	4.80E-04	12.705	0.674
365	4.10E-04	13.804	0.849
370	3.40E-04	15.595	0.876
375	2.90E-04	17.66	0.78
380	2.43E-04	19.408	0.902
385	2.04E-04	20.23	0.693
390	1.72E-04	20.89	0.897
395	1.45E-04	21.442	0.693
400	1.22E-04	21.928	1.18

Table 6: Eλ, Tλ, and Sλ values from 290-400 nm for AmCot+Ag-CuO

AmCot+Ag-CuO			
Wavelength (nm)	Eλ	Tλ	Sλ
290	1	9.931	7.57E-05
295	1	9.931	1.34E-03
300	0.649	9.977	1.36E-02
305	0.22	10.092	7.67E-02
310	7.45E-02	10.665	0.172
315	2.51E-02	11.668	0.282
320	8.60E-03	12.359	0.375
325	2.90E-03	12.56	0.494
330	1.36E-03	12.647	0.629
335	1.15E-03	12.735	0.602
340	9.70E-04	12.823	0.675
345	8.10E-04	12.794	0.65
350	6.80E-04	12.853	0.692
355	5.80E-04	12.912	0.743
360	4.80E-04	13.032	0.674
365	4.10E-04	13.092	0.849
370	3.40E-04	13.181	0.876
375	2.90E-04	13.243	0.78
380	2.43E-04	13.274	0.902
385	2.04E-04	13.365	0.693
390	1.72E-04	13.427	0.897
395	1.45E-04	13.521	0.693
400	1.22E-04	13.552	1.18

Table 7: Eλ, Tλ, and Sλ values from 290-400 nm for AmCot+Ag-ZnO

AmCot+Ag-ZnO			
Wavelength (nm)	Eλ	Tλ	Sλ
290	1	6.367	7.57E-05
295	1	6.368	1.34E-03
300	0.649	6.412	1.36E-02
305	0.22	6.412	7.67E-02
310	7.45E-02	6.412	0.172
315	2.51E-02	6.622	0.282
320	8.60E-03	7.014	0.375
325	2.90E-03	7.244	0.494
330	1.36E-03	7.328	0.629
335	1.15E-03	7.294	0.602
340	9.70E-04	7.294	0.675
345	8.10E-04	7.244	0.65
350	6.80E-04	7.211	0.692
355	5.80E-04	7.178	0.743
360	4.80E-04	7.178	0.674
365	4.10E-04	7.178	0.849
370	3.40E-04	7.178	0.876
375	2.90E-04	7.211	0.78
380	2.43E-04	7.244	0.902
385	2.04E-04	7.211	0.693
390	1.72E-04	7.211	0.897
395	1.45E-04	7.194	0.693
400	1.22E-04	7.178	1.18

Table 8: Eλ, Tλ, and Sλ values from 290-400 nm for AmCot+Ag-TiO_2

AmCot+Ag-TiO_2			
Wavelength (nm)	Eλ	Tλ	Sλ
290	1	7.925013	7.57E-05
295	1	7.998343	1.34E-03
300	0.649	8.109611	1.36E-02
305	0.22	8.203515	7.67E-02
310	7.45E-02	8.472274	0.172
315	2.51E-02	8.810489	0.282
320	8.60E-03	9.057326	0.375
325	2.90E-03	9.418896	0.494
330	1.36E-03	9.840111	0.629
335	1.15E-03	10.35142	0.602
340	9.70E-04	10.83927	0.675
345	8.10E-04	11.35011	0.65
350	6.80E-04	11.85769	0.692
355	5.80E-04	12.38797	0.743
360	4.80E-04	12.79381	0.674
365	4.10E-04	13.21296	0.849
370	3.40E-04	13.61445	0.876
375	2.90E-04	13.86756	0.78
380	2.43E-04	14.09289	0.902
385	2.04E-04	14.32188	0.693
390	1.72E-04	14.55459	0.897
395	1.45E-04	14.75707	0.693
400	1.22E-04	14.96236	1.18

Table 9: Eλ, Tλ, and Sλ values from 290-400 nm for AmCot+CuO-TiO_2

AmCot+CuO-TiO_2			
Wavelength (nm)	Eλ	Tλ	Sλ
290	1	8.05	7.57E-05
295	1	8.05	1.34E-03
300	0.649	8.24	1.36E-02
305	0.22	8.5	7.67E-02
310	7.45E-02	9.3	0.172
315	2.51E-02	10	0.282
320	8.60E-03	11.6	0.375
325	2.90E-03	12.3	0.494
330	1.36E-03	12.7	0.629
335	1.15E-03	13	0.602
340	9.70E-04	13.7	0.675
345	8.10E-04	14.2	0.65
350	6.80E-04	14.7	0.692
355	5.80E-04	15.3	0.743
360	4.80E-04	15.8	0.674
365	4.10E-04	16.4	0.849
370	3.40E-04	16.7	0.876
375	2.90E-04	17.3	0.78
380	2.43E-04	17.6	0.902
385	2.04E-04	18	0.693
390	1.72E-04	18.2	0.897
395	1.45E-04	18.6	0.693
400	1.22E-04	19	1.18